NASA TECHNICAL NOTE

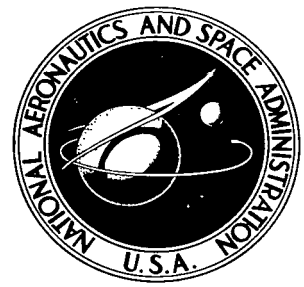

WIND-TUNNEL INVESTIGATION OF A VARIABLE CAMBER AND TWIST WING

James C. Ferris

Langley Research Center
Hampton, Va. 23665

NATIONAL AERONAUTICS AND SPACE ADMINISTRATION • WASHINGTON D. C. • AUGUST 1977

1. Report No. NASA TN D-8475	2. Government Accession No.
4. Title and Subtitle WIND-TUNNEL INVESTIGATION OF A VARIABLE CAMBER AND TWIST WING	5. Report Date August 1977
	6. Performing Organization Code
7. Author(s) James C. Ferris	8. Performing Organization Report No. L-11357
	10. Work Unit No. 505-11-16-08
9. Performing Organization Name and Address NASA Langley Research Center Hampton, VA 23665	11. Contract or Grant No.
	13. Type of Report and Period Covered Technical Note
12. Sponsoring Agency Name and Address National Aeronautics and Space Administration Washington, DC 20546	14. Sponsoring Agency Code
15. Supplementary Notes	

16. Abstract

A wind-tunnel investigation was made to determine the longitudinal aerodynamic characteristics of a 35° swept, variable camber and twist semispan wing in the presence of a body. The variable camber and twist were incorporated to allow a near optimum lift distribution over the wing for both the cruise condition and the high lift conditions for maneuverability. The wing incorporated movable leading-edge segments whose swept hinge lines provided maximum camber variations at the outboard leading edge and movable trailing-edge segments whose swept hinge lines provided maximum camber variations near the inboard trailing edge. The model was investigated at Mach numbers of 0.60, 0.80, and 0.90 through an angle-of-attack range from 0° to 10° or buffet onset.

17. Key Words (Suggested by Author(s)) Maneuverable aircraft Thin wing Variable camber Variable-camber wing Variable twist	18. Distribution Statement Unclassified - Unlimited Subject Category 02		
19. Security Classif. (of this report) Unclassified	20. Security Classif. (of this page) Unclassified	21. No. of Pages 79	22. Price* $5.00

* For sale by the National Technical Information Service, Springfield, Virginia 22161

WIND-TUNNEL INVESTIGATION OF A VARIABLE CAMBER AND TWIST WING

James C. Ferris
Langley Research Center

SUMMARY

A wind-tunnel investigation was made to determine the longitudinal aerodynamic characteristics of a 35° swept, variable camber and twist semispan wing in the presence of a body. The variable camber and twist were incorporated to allow a near optimum lift distribution over the wing for both the cruise condition and the high lift conditions for maneuverability. The wing incorporated movable leading-edge segments whose swept hinge lines provided maximum camber variations at the outboard leading edge and movable trailing-edge segments whose swept hinge lines provided maximum camber variations near the inboard trailing edge. The angle of the segments could be varied with an internal mechanism; thus, the camber and twist could be optimized for various lift coefficients.

The model was investigated at Mach numbers of 0.60, 0.80, and 0.90 at Reynolds numbers based on the mean geometric chord of 6.2×10^6, 7.4×10^6, and 7.6×10^6, respectively. The angle of attack was varied from 0° to approximately 10° or to buffet onset.

Leading-edge camber simulating elliptical camber, circular camber, and simplified camber of simple hinge and double hinge line configurations was investigated with uncambered trailing edges. The trailing-edge camber investigation included elliptical leading-edge camber with three variations of elliptical trailing-edge camber and one extensive trailing-edge camber configuration.

The results of the investigation showed that, when properly incorporated, variable camber and twist can effectively reduce the drag of a thin low-aspect-ratio wing over a wide range of lift coefficients. Compared to the uncambered wing, the wing with leading-edge camber was effective in reducing the drag in the lift-coefficient range from 0 to 0.4 while the wing with trailing-edge camber is required at lift coefficients greater than 0.5. The increase in buffet-free lift coefficient as a result of variable camber and twist relative to that of the basic uncambered and untwisted wing varied from 68 to 102 percent over the Mach number range of the investigation.

INTRODUCTION

The performance of most moderate aspect ratio, thin swept wing maneuvering aircraft is significantly degraded at high lift coefficients at high subsonic Mach numbers because of shock-induced boundary-layer separation and, at higher angles of attack, because of leading-edge separation and wing stall. The resulting degradation in handling qualities significantly reduces the combat effectiveness of these airplanes. There are several approaches to the leading-edge stall problem, including leading-edge flaps, slats, and control of the boundary layer

by suction or blowing. These approaches, along with trailing-edge flaps, have been used effectively for low-speed landing and take-off and, at higher subsonic speeds, to increase the maximum usable lift coefficient.

Camber has always been used to provide lift with low drag at cruise (a more recent example is given in ref. 1) and is used to increase the buffet-free lift coefficient (ref. 2). Leading-edge and trailing-edge flaps have been used to increase the camber for maneuvering fighters at high subsonic speeds in order to maximize the usable lift coefficient. (See refs. 3 to 8.) Twist is used to provide the desired span load distribution at cruise (ref. 9). While considerable data are available on varying the camber with flaps, very little data are available on variable twist or washout.

Low-thickness-ratio wings incorporating variable camber and twist appear to offer higher performance for fixed-wing-planform fighter aircraft since the camber can be reduced or reflexed for the supersonic mission and increased to provide high lift coefficients required for transonic and subsonic maneuverability.

The objective of this study was to determine the aerodynamic characteristics of a low-thickness-ratio fighter wing. To accomplish the variable camber function, the wing planform had four leading-edge segments and four trailing-edge segments, all with spanwise hinge lines. To accomplish the variable twist, the hinge lines of the leading-edge segments were parallel and swept more than the leading edge, and the trailing-edge segments were parallel and swept more than the trailing edge. For this hinge line layout, twist is increased as camber is increased and, thus, the variable camber and twist concept. The purpose of this paper is to present force and moment data on this configuration at Mach numbers of 0.60, 0.80, and 0.90.

SYMBOLS

The longitudinal results are referred to the stability axis system. The origin of the stability axes is at the moment reference center, located at 25 percent of the reference length $\bar{c}$ and 147.57 cm (58.09 in.) from the fuselage apex.

Values are given in both SI and U.S. Customary Units. The measurements and calculations were made in U.S. Customary Units.

$b/2$ exposed semispan, 106.68 cm (42 in.)

C_A axial-force coefficient, $\frac{\text{Axial force}}{qS}$

C_{acc} wing-tip accelerometer output, g units

$C_{b,rms}$ wing root-mean-square bending-moment coefficient, $2\frac{\text{rms Bending moment}}{qS(b/2)}$

C_D drag coefficient, $\frac{\text{Drag}}{qS}$

C_L lift coefficient, $\frac{\text{Lift}}{qS}$

C_m pitching-moment coefficient, $\frac{\text{Pitching moment}}{qS\bar{c}}$

c chord, cm (in.)

$\bar{c}$ mean geometric chord, 59.59 cm (23.46 in.)

i_s incidence of airfoil section, deg

L leading edge

L/D lift-drag ratio

$(L/D)_{max}$ maximum lift-drag ratio

M free-stream Mach number

q free-stream dynamic pressure, Pa (lbf/ft^2)

$R_{\bar{c}}$ Reynolds number, based on $\bar{c}$

S exposed wing area, 0.599 m^2 (6.447 ft^2)

T trailing edge

x longitudinal distance, cm (in.)

y spanwise distance from root chord, cm (in.)

z ordinate normal to airfoil reference line, cm (in.)

α angle of attack, deg

$\Delta\delta_n$ incremental deflection angle of variable camber segments, deg (n denotes segment number, see fig. 4(b))

η wing semispan station, $2y/(b/2)$

MODEL DESCRIPTION

The general arrangement of the semispan model is shown in figure 1(a). A spacer was installed between the fuselage and the wind-tunnel wall to place the entire semispan model in the free-stream flow of the tunnel. Details of the segments of the wing planform are shown in figure 1(b), and cross sections of the fuselage are shown in figure 1(c). Photographs of the model installed in the

Langley 8-foot transonic pressure tunnel are presented as figure 2. The cross-sectional area distribution presented in figure 3 is for a three-dimensional full-span model having the same geometric characteristics as the semispan model. This area distribution was designed, according to the area-rule concept, for a Mach number of 1.0 at zero lift, and the fineness ratio was 7.52, which is representative of current fighter airplanes.

Only the wing was attached to the balance, and the nonmetric fuselage was separated from the wing by a small gap (approximately 0.32 cm (1/8 in.) wide) around the airfoil near the wing root.

The wing consisted of an NACA 65A005 airfoil at the root and an NACA 65A004 airfoil at the tip with a linear variation between them (no camber or twist in the basic wing). In addition, the airfoils were modified to have finite thickness at the trailing edge to improve the structural characteristics and to provide increased thickness in the aft part of the airfoil for the variable camber and twist mechanism. This trailing-edge modification was small and varied linearly from 0.00375c at the root to 0.00300c at the tip. Coordinates of the airfoil sections are given in table I.

The hinge lines of the leading-edge segments were swept 40.1° (5.1° greater than the leading edge) and were parallel, thus providing a cylindrical camber. The hinge lines of the trailing-edge segments were swept 25.4° (11.4° greater than the trailing edge), and they were also parallel, providing cylindrical camber. As camber is applied to a wing with this arrangement, twist or washout also results.

The wing planform with the segments numbered is shown in figure 4(a); the semispan locations selected for the camber and twist computations and the cross section near the root and tip of the wing planform are also shown.

The incremental deflection angles of the variable camber segments are shown in the schematic drawing in figure 4(b). As shown in the small drawing at the top, all of the leading-edge segment deflection angles are measured in a plane normal to the hinge lines of the leading-edge segments, and the trailing-edge segment deflection angles are measured in a plane normal to the hinge lines of the trailing-edge segments. Each of the segments could be deflected through an angle range from 2° up to 12° down. The incremental deflection angles (in deg) of the leading-edge segments are referenced to their aft adjacent segments (that is, for segment 1 $\Delta\delta_1$ is referenced to segment 2 and for segment 2 $\Delta\delta_2$ is referenced to segment 3, etc.). The incremental deflection angles of the trailing-edge segments are referenced to their forward adjacent segments (that is, for segment 5 $\Delta\delta_5$ is referenced to the main wing box and for segment 6 $\Delta\delta_6$ is referenced to segment 5, etc.). All of the angles from leading edge to trailing edge at any wing station represent the mean line of the airfoil at that station. The incremental angles, however, must be converted to their streamwise orientation to obtain the mean line of the streamwise section.

A typical cambered configuration (L_6T_{15}) is shown in figure 4(c). The schematic diagram shows the shape of the mean camber line at inboard and outboard stations when camber and twist are applied to the wing panel by deflecting the leading-edge and trailing-edge segments. The trailing-edge segments

increase the incidence of the inboard part of the wing panel, and the leading-edge segments reduce the incidence of the outboard panels; thus, the original uncambered wing can have an effective twist of approximately 8° for the configuration shown. The new chord lines and the position of maximum camber are also shown for the two semispan stations.

Five types of camber were investigated with the present variable camber model. The streamwise variation of maximum camber and section incidence i_s as a function of the semispan are shown in figures 5(a) to 5(d). Three of these types involved the leading-edge variable segments only. They include an elliptical-type camber (the mean line of the forward portion of the airfoil was shaped to approximate an ellipse, the configurations so cambered being designated L_5T_0 and L_6T_0), a circular-type camber (the mean line of the airfoil was shaped to approximate a circle, the configurations so cambered being designated $L_{24}T_0$ and L_8T_0), and a third type in which the number of movable segments was reduced to simplify the camber actuation system (these were designated $L_{25}T_0$ and $L_{28}T_0$ for two-segment configurations and $L_{29}T_0$ for the one-segment configuration). The L_6T_0 configuration with an elliptical leading edge was used with the trailing-edge camber variations. The trailing-edge camber was of two types, a systematic variation of increasing elliptical camber (L_6T_{11}, L_6T_1, and L_6T_{10}) and an attempt with a single configuration to increase the lift coefficient to 1.0 at $M = 0.90$ by a selective increase in the trailing-edge camber (L_6T_{15}).

The mechanism for changing the camber was located within the wing, and the adjustments were made through the hinge lines on the lower surface. The protractors for measuring and setting the segment angles had magnetic bases designed to fit the upper surface of the wing; the protractors for leading-edge segments 1 and 3 and trailing-edge segments 6 and 8 are shown in position in figure 2(b). The hinge lines were filled and smoothed to contour with a silicone material to prevent air flow from the lower surface to the upper surface. Aluminum tape was also applied to the lower-surface hinge lines after each camber adjustment as a further precaution against flow through the hinge lines.

APPARATUS AND PROCEDURES

Test Facility

The investigation was conducted in the Langley 8-foot transonic pressure tunnel. This facility is a continuous-flow single-return rectangular slotted-throat tunnel having controls that allow for independent variation of Mach number, density, stagnation temperature, and dewpoint temperature. The test section is approximately 2.2 m (7.1 ft) square. The cross-sectional area is the same as that of a circle with a 2.4-m (8-ft) diameter. The upper and lower walls are axially slotted to permit the test-section Mach number to be changed continuously throughout the transonic speed range. The slotted top and bottom walls each have an average open ratio of approximately 0.06. The stagnation pressure in the tunnel can be varied from a minimum of about 0.25 atm (1 atm = 0.101 MPa) at all Mach numbers to a maximum of approximately 2.00 atm at Mach numbers less than 0.40. At transonic Mach numbers, however, the maximum stagnation pressure that can be obtained is about 1.5 atm.

Boundary-Layer Transition

Boundary-layer transition was fixed at 5 percent of the local chord on the wing by the addition of a 0.25-cm (0.64-in.) wide (streamwise) strip of No. 100 carborundum grains and on the fuselage by a strip of No. 80 carborundum grains located 6.4 cm (16.3 in.) aft of the nose apex.

Instrumentation

Five-component static aerodynamic force and moment data were obtained for the wing using a wall-mounted strain-gage balance to which the model wing was attached. The fuselage, which was nonmetric, was mounted on a turntable that moved with the balance and wing and therefore remained at the same angle of attack as the wing. The angle of attack of the wing was measured with an accelerometer located in the wing attachment block.

Strain gages were mounted inboard in the wing upper and lower surface at $\eta = 0.15$, and an accelerometer was installed at $\eta = 0.93$ as shown in figure 1(b). The root-mean-square output from these instruments was integrated for 45 sec, and coefficients were computed to determine the buffet characteristics of the wing.

Test Conditions and Data Reduction

Tests were made at angles of attack from 0° to 10° or buffet onset at Mach numbers of 0.60, 0.80, and 0.90 for Reynolds numbers based on the mean geometric chord of 6.2×10^6, 7.4×10^6, and 7.6×10^6, respectively. The basic uncambered configuration was also investigated at $R_{\bar{c}}$ of 5.9×10^6 and 9.8×10^6 at $M = 0.80$. The maximum camber configuration L_6T_{15} of the investigation was also run at $R_{\bar{c}} = 5.9 \times 10^6$.

The constants for reducing the data were based on the exposed area and linear dimensions of the semispan wing panel.

PRESENTATION OF RESULTS

The results of the investigation of the longitudinal aerodynamic and buffet characteristics of the variable camber and twist wing are presented in the following figures:

DISCUSSION

The following discussion pertains to force and moment data obtained on the wing only since the fuselage of the model was nonmetric. The data from the results of this investigation are presented and analyzed in regard to increments in the forces and moments obtained from camber and twist of the wing alone and are not directly comparable with three-dimensional wing and body configurations.

Basic Longitudinal Data

As shown in figure 6, increasing the Reynolds number caused a slight decrease in drag resulting in a 6-percent increase in $(L/D)_{max}$.

Leading-Edge Camber

The camber and twist distributions across the semispan for the various leading-edge configurations are presented in figures 5(a) and 5(b), respectively. The effect of elliptical leading-edge camber (L_5T_0 and L_6T_0) is shown in figure 7 for the model without trailing-edge camber. This type of camber reduced the drag over much of the lift-coefficient range of the investigation and, as a result, the maximum lift-drag ratio $(L/D)_{max}$ and the lift coefficient at $(L/D)_{max}$ are increased at all Mach numbers for these configurations. The L_6T_0 leading-edge configuration had incremental deflection angles of 12.8°, 4.7°, 2.8°, and 1.2° for leading-edge segments 1 to 4, respectively, and is the basic leading edge used in this investigation. It is evident (fig. 7(c)) that this camber is excessive for $M = 0.90$ at lift coefficients up to 0.3 as the L_5T_0 configuration with less camber has higher lift-drag ratios for these conditions.

The effect of circular leading-edge camber ($L_{24}T_0$ and L_8T_0) is shown compared to that of the elliptical leading-edge camber (L_6T_0) in figure 8. The circular-camber configuration ($L_{24}T_0$) shows the best improvement in drag of the three leading-edge configurations; it also shows, at Mach 0.80, an increase in $(L/D)_{max}$ and C_L at $(L/D)_{max}$ although at Mach 0.90, it shows a loss in $(L/D)_{max}$.

In an effort to determine if the camber-changing mechanism could be simplified by reducing the number of movable segments, one-segment and two-segment configurations of the leading edge were investigated. The one-segment configuration $L_{29}T_0$ was obtained by a 7.7° deflection of segment 3 while the other segments were left at zero angle. As shown in figures 5(a) and 5(b), this configu-

ration had the least amount of camber and twist at the wing-tip station, but the distribution of camber and twist over the semispan was similar to the L_6T_0 elliptical leading edge. The two-segment configurations, $L_{25}T_0$ and $L_{28}T_0$, were obtained by deflecting the second and third segments and leaving segments 1 and 4 at zero angle. The two-segment configuration $L_{25}T_0$ had a low camber and twist similar to the one-segment $L_{29}T_0$ and L_6T_0 configurations. The high camber and twist two-segment configuration $L_{28}T_0$ had a camber distribution similar to the circular configuration $L_{24}T_0$ with somewhat more camber in the outboard part of the semispan. The results are presented in figure 9, and the single-segment configuration appears to compare favorably with the elliptical-camber configurations at all Mach numbers of the investigation. The two-segment configuration $L_{28}T_0$ had significantly better aerodynamic characteristics at $M = 0.60$ than the other leading-edge camber configurations at lift coefficients greater than 0.4.

In general, the leading-edge camber reduced the values of lift coefficient by small amounts over the angle-of-attack range, the reduction being greater at $M = 0.90$ where the increment was approximately 0.05. (Compare the L_0T_0 curve of fig. 7(c) with the L_8T_0 circular-camber curve of fig. 8(c) and the $L_{28}T_0$ two-segment curve of fig. 9(c).) It should be noted that the leading-edge camber configurations cause a washout in the wing panel (see fig. 4(c)) because of the hinge line sweep, and the reductions in lift are at the outboard region of the wing panel. The camber and washout improve the span loading on the wing panel and cause a reduction in drag of approximately 28 to 40 percent compared to that of the uncambered wing at Mach numbers of 0.60 and 0.80 and 20 percent at a Mach number of 0.90, in the moderate lift-coefficient range from 0.35 to 0.45. The favorable influence of the leading-edge camber on the drag provides increases in $(L/D)_{max}$ of approximately 19 percent with the $L_{25}T_0$ configuration at Mach numbers of 0.60 and 0.80, and the increase was the same with the L_5T_0 configuration at $M = 0.90$.

The leading-edge camber (see figs. 7, 8, and 9) generally caused a reduction in the pitching-moment coefficients. The elliptical-type camber also had a small destabilizing trend at Mach numbers of 0.60 and 0.80, whereas the circular type had a stabilizing trend at these same Mach numbers. At $M = 0.90$ the circular camber L_8T_0 and the two-segment $L_{28}T_0$ increase the stability over the lift-coefficient range from 0 to 0.35 and decreased the stability at C_L greater than 0.35.

Trailing-Edge Camber

The camber and twist distribution across the semispan for the trailing-edge camber configurations is shown in figures 5(c) and 5(d), respectively. The L_6T_0 leading-edge camber is used with all of the trailing-edge configurations. The L_6T_{11}, L_6T_1, and L_6T_{10} configurations show systematic increases in an elliptical-type trailing-edge camber. For the L_6T_{15} configuration, the camber in the inboard 60 percent of the wing was increased substantially in an attempt to increase the wing lift coefficient to 1.0. The effect of the elliptical trailing-edge camber is shown in figure 10. As would be expected, increases in the trailing-edge camber caused large increases in the lift coefficient C_L over the angle-of-attack range at all Mach numbers of the investigation.

The drag is reduced an additional amount by the trailing-edge camber. Comparing the L_6T_0 configuration to the L_6T_{10} configuration in figure 10, this reduction amounts to 34 percent at $C_L = 0.65$ (highest C_L obtained for L_6T_0 at $M = 0.80$) at Mach numbers of 0.60 and 0.80 and 27 percent at a Mach number of 0.90. If higher lift coefficients are selected, another 5-percent reduction in drag is evident. For example, at $M = 0.60$ and $C_L = 0.7$ the reduction is 39 percent, and at $M = 0.90$ and $C_L = 0.75$ (the values for L_6T_0 are extrapolated from $L_{29}T_0$ in fig. 9(c)) the reduction is 32 percent.

More camber was added to the trailing-edge segments L_6T_{15} in an effort to increase C_L at buffet onset. The results are shown compared to the zero camber configuration and the elliptical trailing-edge camber configuration L_6T_{10} in figure 11. The lift coefficient was substantially increased at all Mach numbers of the investigation by the increased trailing-edge camber. While the lift coefficient increased to a value greater than 1.0 at $M = 0.90$ and near 1.0 at the other Mach numbers, it is not intended to suggest that this camber and twist combination is most efficient for the high Mach number and lift-coefficient range.

Drag polars, pitching-moment coefficient, and angle of attack for the basic uncambered wing compared to a best-camber polar derived from the various cambered configurations of the investigation are presented in figure 12 for all Mach numbers of the investigation. These polars are not necessarily the best camber and twist combinations for this aspect ratio and wing planform but rather the best combination obtained in this investigation. Values of C_m and C_L against α are shown for the data points on the drag polar only, with no attempt to arrive at a continuous curve for C_L, C_m, and α.

The leading-edge camber lowers the drag substantially in the low lift-coefficient range, while the trailing-edge camber is necessary for the very large improvements in the high lift-coefficient range. The trailing-edge camber causes very large increments in C_L at constant angle of attack with substantial negative shifts in pitching-moment coefficients.

Buffet Characteristics

The buffet indicators of axial-force coefficient C_A, wing-tip accelerometer C_{acc} in g units, and wing root-mean-square bending-moment coefficient $C_{b,rms}$ are presented in figures 13 to 18 as a function of the lift coefficient. Most of the buffet analysis is based on data from the wing-root bending gages, and the axial-force coefficient and wing-tip accelerometer are used for comparison purposes only. The small Reynolds number variation at $M = 0.80$ (fig. 13) had little effect on the buffet-onset characteristics of the model; however, there are some increases in intensity level as a result of the increased dynamic pressure.

The elliptical and circular leading-edge camber configurations (figs. 14 and 15, respectively) tend to extend the buffet onset to somewhat higher lift coefficients and to reduce the intensity levels.

As would be expected, the trailing-edge camber configurations provide the largest increase in buffet-free lift coefficient for the Mach numbers of this investigation. The buffet data for the elliptical trailing-edge camber variations are presented in figure 17. Buffet onset is indicated by the marks on the curves of $C_{b,rms}$ against C_L and is established at the tangent point to the curve of a line drawn at a 45° angle to the axes. The increment in lift coefficient compared to the L_6T_0 configuration at buffet onset for L_6T_0 is 60 percent and 40 percent at Mach numbers of 0.60 and 0.80, respectively. At $M = 0.90$ (fig. 17(c)) the lift-coefficient increase at buffet onset is 46 percent.

The configuration with the selective increase in trailing-edge camber L_6T_{15} is compared to the uncambered wing configuration L_0T_0 and the maximum elliptical leading-edge and trailing-edge camber configuration L_6T_{10} in figure 18. The increase in buffet-free lift coefficient for this configuration L_6T_{15} is 102 percent and 68 percent at Mach numbers of 0.60 and 0.80, respectively. Buffet onset at $M = 0.90$ for this configuration is not indicated in these data.

CONCLUDING REMARKS

The results of an investigation to determine the effects of camber and twist applied to a semispan wing in the presence of body by deflecting multiple leading-edge and trailing-edge segments indicated that all of the leading-edge camber configurations investigated were effective in reducing the drag at lift coefficients up to 0.4, the elliptical and circular camber were the most effective, and the simplified single hinge configuration was similar in performance to the more complex four-segment elliptical camber and twist that it simulated. The value of the maximum lift-drag ratio was increased approximately 18 percent over the Mach number range from 0.60 to 0.90 by the leading-edge camber. At the higher lift coefficients (0.50 and above) the combination of camber and twist applied by both leading-edge and trailing-edge camber was effective in reducing the drag and the trailing-edge camber gave large increases in the lift coefficient. The combination of leading-edge and trailing-edge camber and twist increased the lift coefficient at buffet onset from 68 percent to more than 100 percent over the Mach number range of the investigation.

Langley Research Center
National Aeronautics and Space Administration
Hampton, VA 23665
May 19, 1977

REFERENCES

1. Dollyhigh, Samuel M.: Subsonic and Supersonic Longitudinal Stability and Control Characteristics of an Aft Tail Fighter Configuration With Cambered and Uncambered Wings and Uncambered Fuselage. NASA TM X-3078, 1974.

2. Ray, Edward J.; and Taylor, Robert T.: Buffet and Static Aerodynamic Characteristics of a Systematic Series of Wings Determined From a Subsonic Wind-Tunnel Study. NASA TN D-5805, 1970.

3. Ray, Edward J.; McKinney, Linwood W.; and Carmichael, Julian G.: Maneuver and Buffet Characteristics of Fighter Aircraft. NASA TN D-7131, 1973.

4. Monaghan, Richard C.; and Friend, Edward L.: Effects of Flaps on Buffet Characteristics and Wing-Rock Onset of an F-8C Airplane at Subsonic and Transonic Speeds. NASA TM X-2873, 1973.

5. Friend, Edward L.; and Sefic, Walter J.: Flight Measurements of Buffet Characteristics of the F-104 Airplane for Selected Wing-Flap Deflections. NASA TN D-6943, 1972.

6. Fischel, Jack; and Friend, Edward L.: Preliminary Assessment of Effects of Wing Flaps on High Subsonic Flight Buffet Characteristics of Three Airplanes. NASA TM X-2011, 1970.

7. Sisk, Thomas R.; Friend, Edward L.; Carr, Peter C.; and Sakamoto, Glenn M.: Use of Maneuver Flaps To Enhance the Transonic Maneuverability of Fighter Aircraft. NASA TM X-2844, 1973.

8. Sisk, Thomas R.: A Preliminary Assessment of the Transonic Maneuvering Characteristics of Two Advanced Technology Fighter Aircraft. NASA TM X-3439, 1976.

9. Pendergraft, Odis C., Jr.: Effect of Camber and Twist on Longitudinal Aerodynamic Characteristics of a Wing-Fuselage Model at Mach Numbers up to 1.30. NASA TM X-1610, 1968.

TABLE I.- WING AIRFOIL COORDINATES ALONG STREAMWISE CHORDS

Root NACA 65A005 airfoil (modified) $\frac{\text{Leading-edge radius}}{\text{Local chord}} = 0.00150$		Tip NACA 65A004 airfoil (modified) $\frac{\text{Leading-edge radius}}{\text{Local chord}} = 0.00102$	
x/c	z/c	x/c	z/c
0.0000	0.00000	0.0000	0.00000
.0050	.00385	.0050	.00304
.0075	.00467	.0075	.00368
.0125	.00595	.0125	.00469
.0250	.00815	.0250	.00647
.0500	.01094	.0500	.00875
.0750	.01326	.0750	.01059
.1000	.01519	.1000	.01213
.1500	.01826	.1500	.01459
.2000	.02059	.2000	.01645
.2500	.02237	.2500	.01788
.3000	.02367	.3000	.01892
.3500	.02453	.3500	.01962
.4000	.02496	.4000	.01997
.4500	.02494	.4500	.01996
.5000	.02440	.5000	.01954
.5500	.02331	.5500	.01868
.6000	.02173	.6000	.01743
.6500	.01976	.6500	.01586
.7000	.01746	.7000	.01402
.7500	.01490	.7500	.01197
.8000	.01229	.8000	.00987
.8500	.00969	.8500	.00778
.9000	.00708	.9000	.00569
.9500	.00448	.9500	.00359
1.0000	.00188	1.0000	.00150

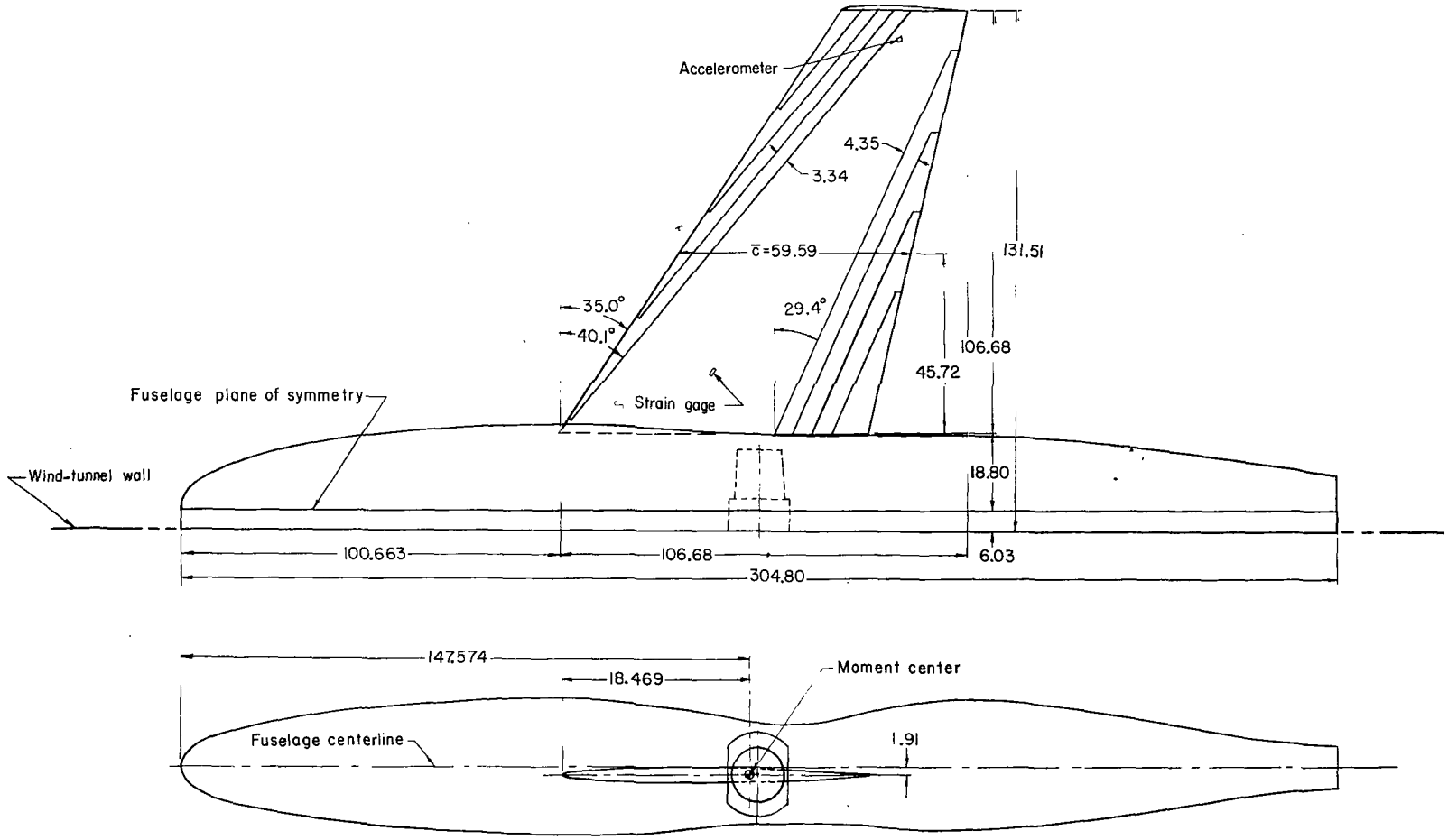

(a) General arrangement of model.

Figure 1.- Drawings of the wind-tunnel model. (Dimensions are in cm.)

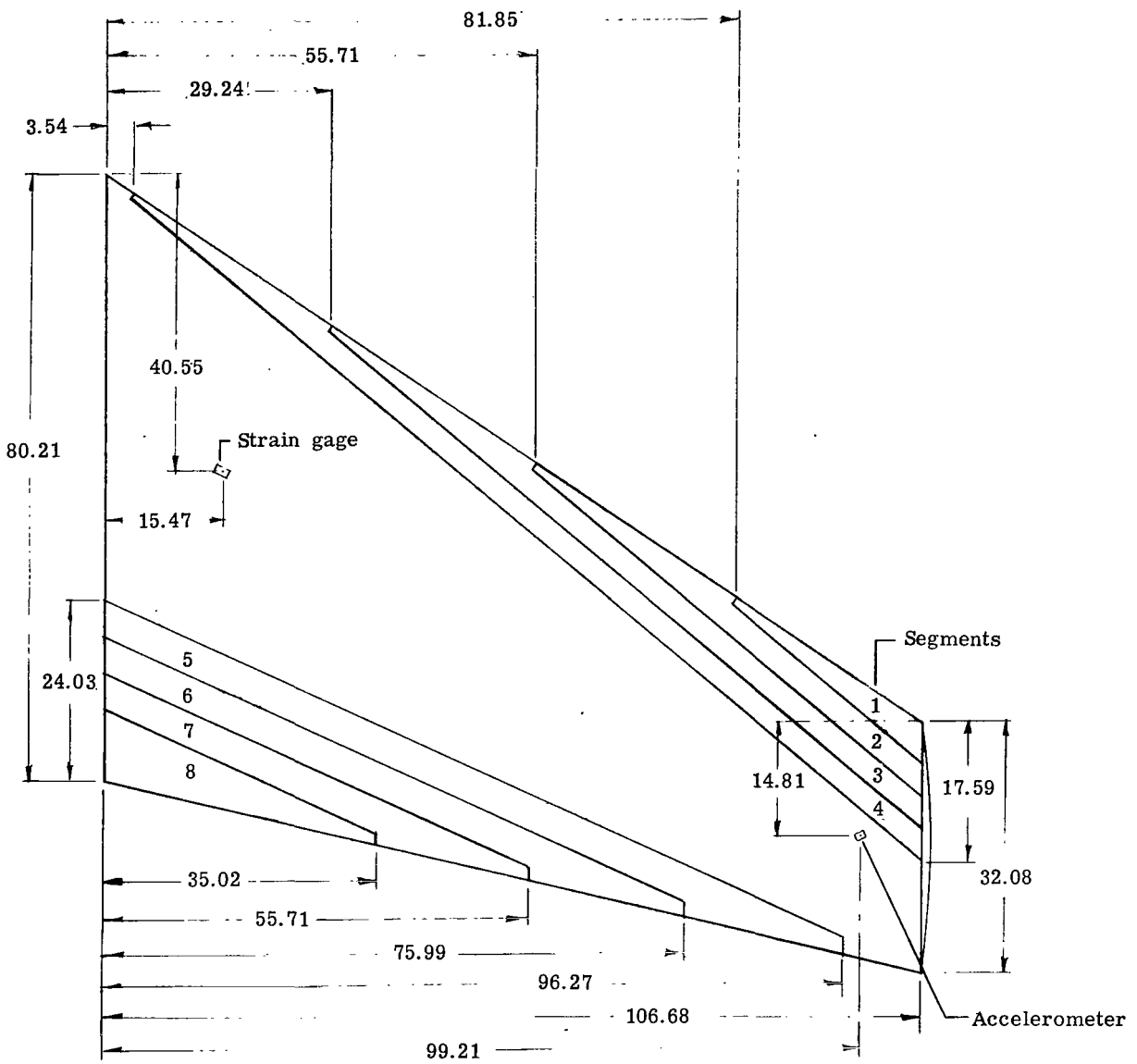

(b) Details of the wing segments and planform.

Figure 1.- Continued.

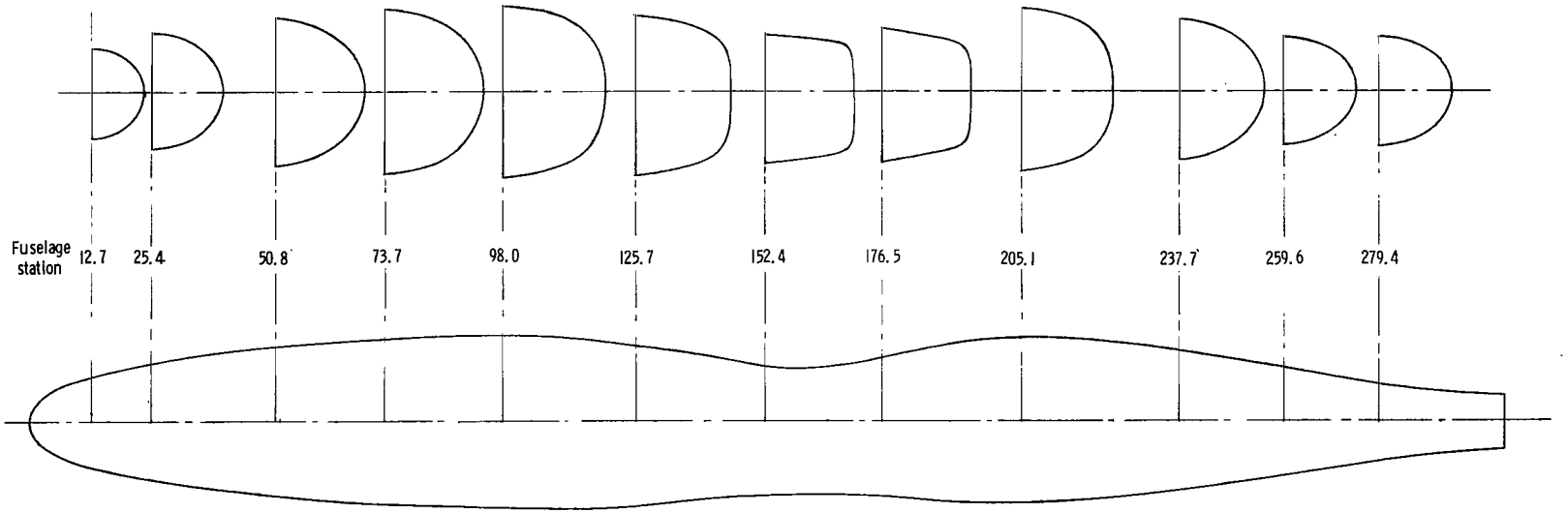

(c) Fuselage cross sections.

Figure 1.- Concluded.

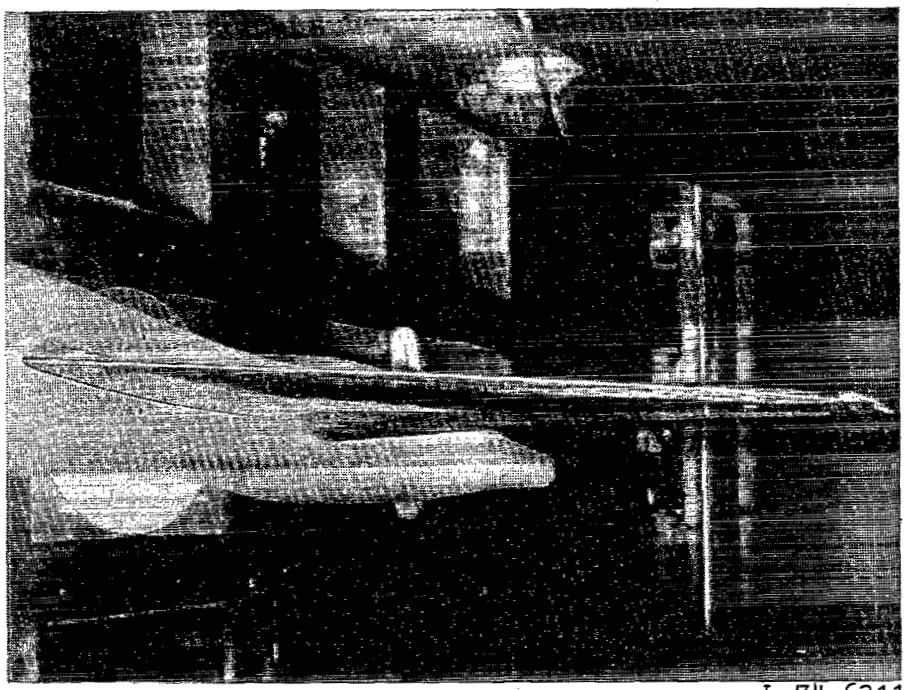

L-74-6311

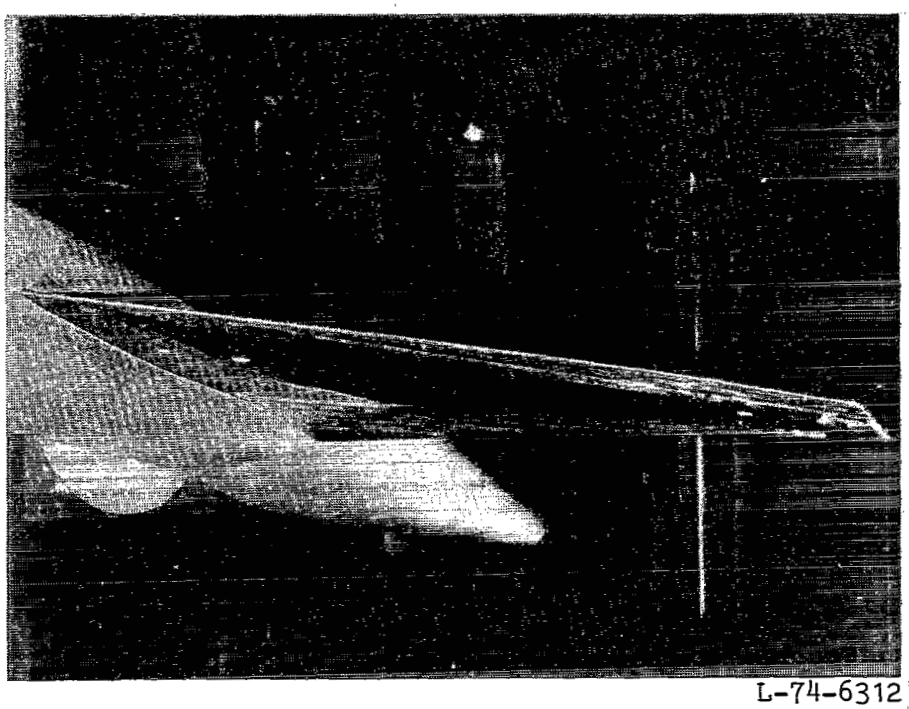

L-74-6312

(a) Front.

Figure 2.- Photographs of model installation.

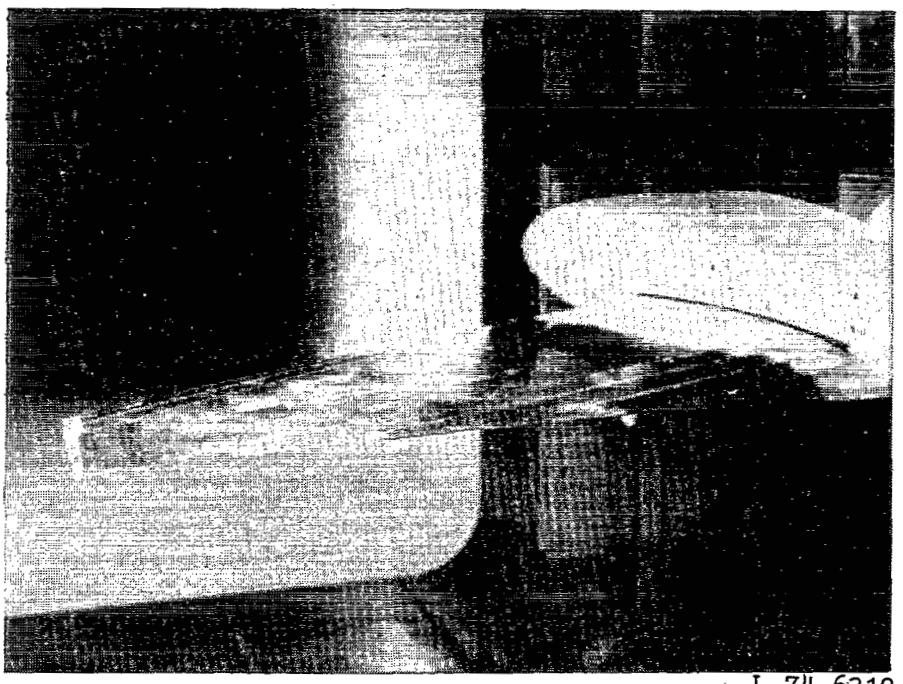

L-74-6310

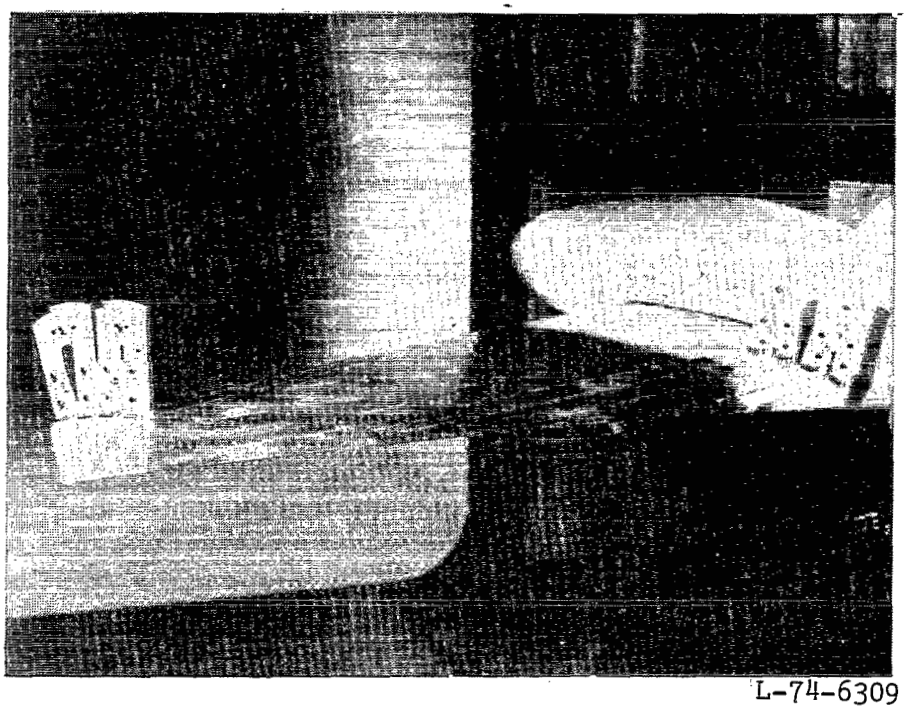

L-74-6309

(b) Rear.

Figure 2.- Concluded.

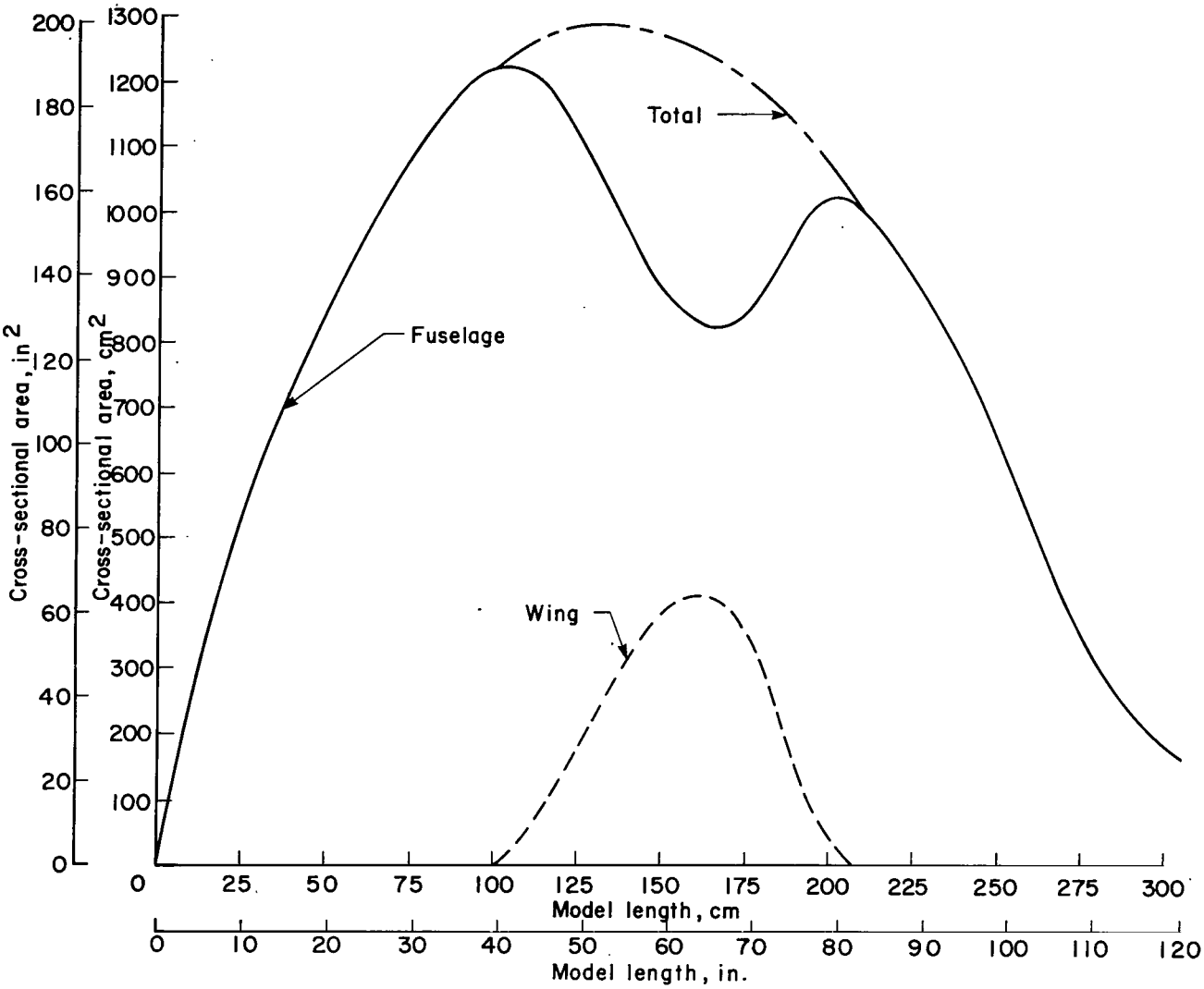

Figure 3.- Model cross-sectional area distribution.

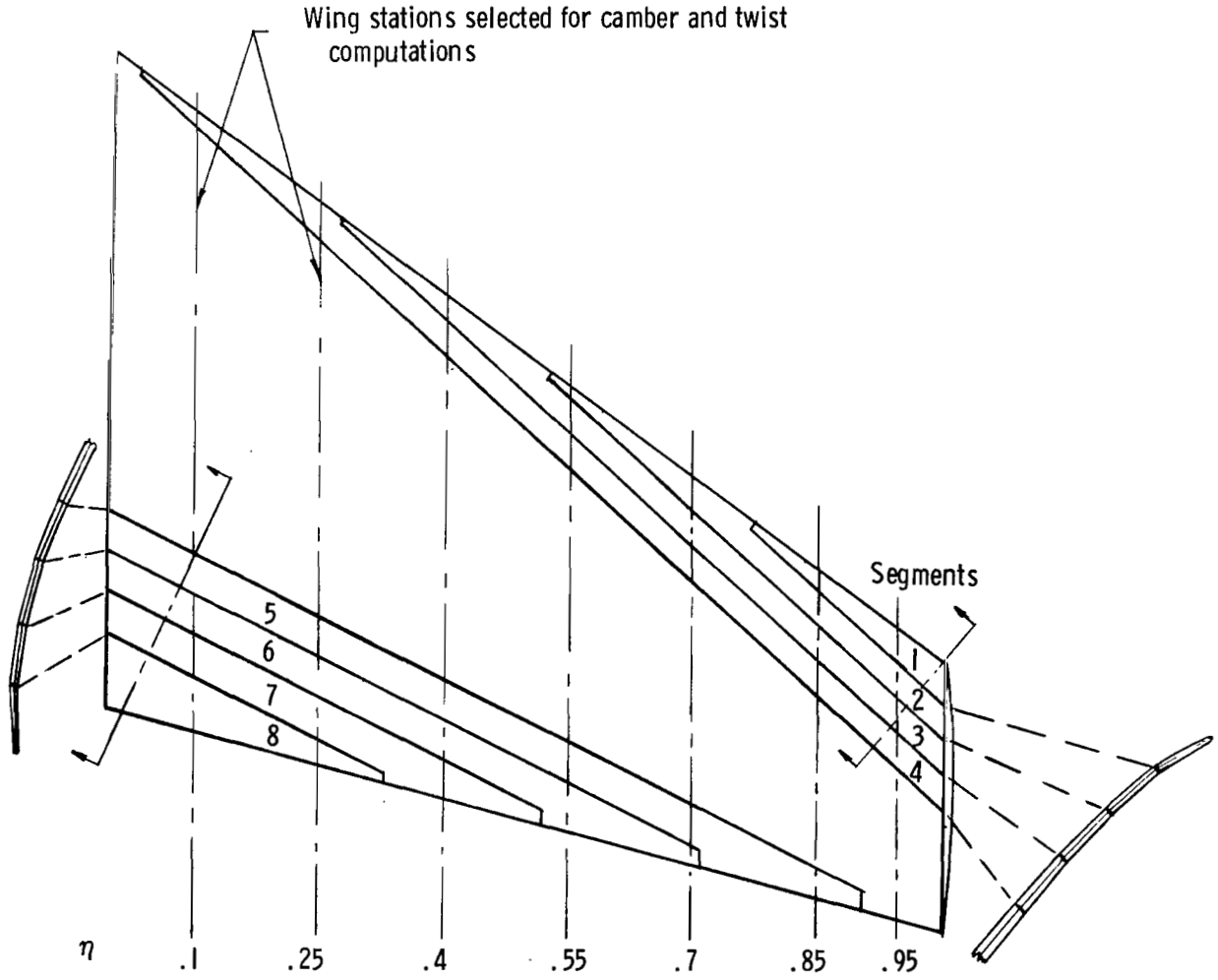

(a) Geometric arrangement of the variable camber segments of the wing panel.

Figure 4.- Details of the variable camber segments.

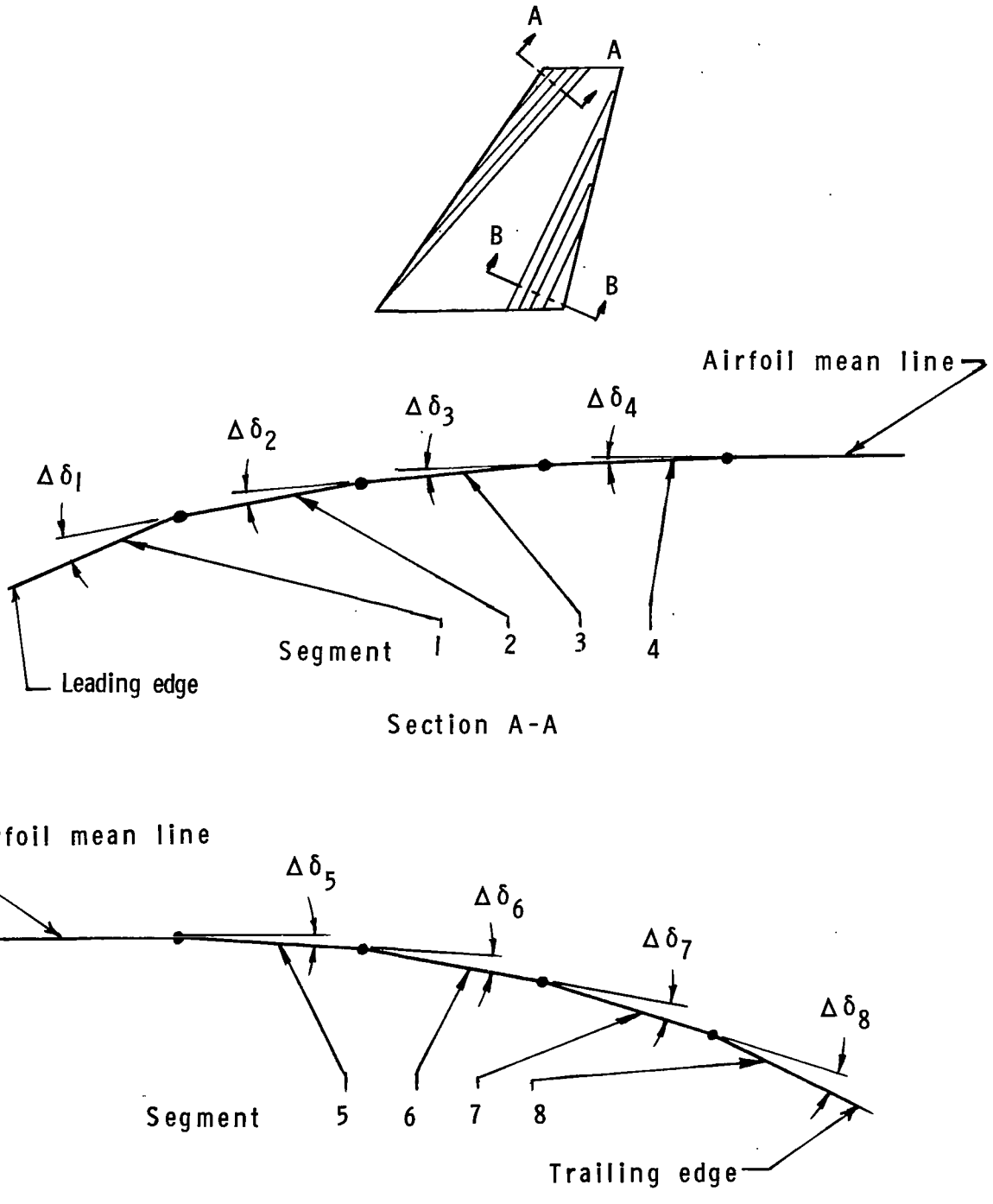

(b) Schematic drawing of the variable camber segment orientation.

Figure 4.- Continued.

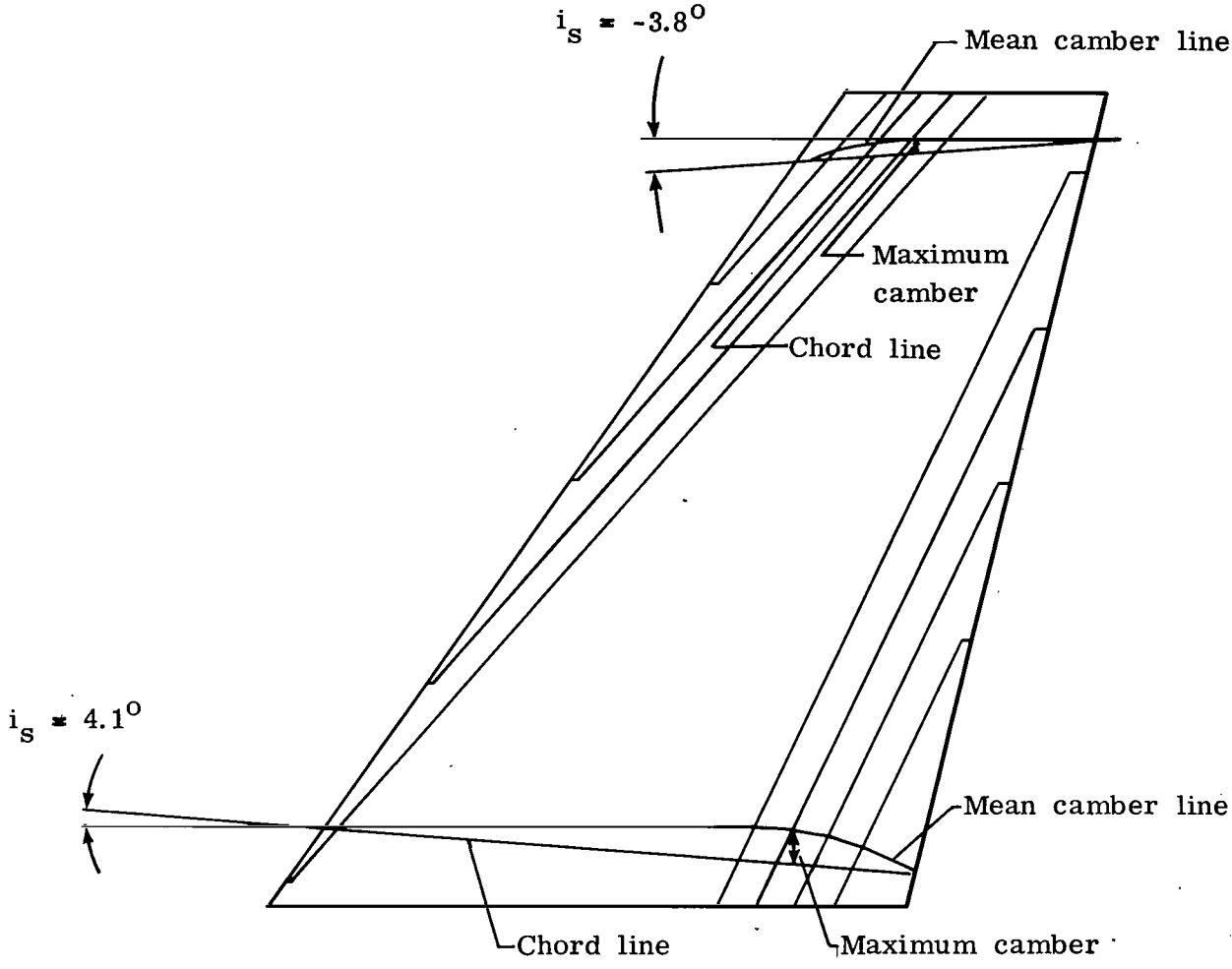

(c) Camber and twist illustration.

Figure 4.- Concluded.

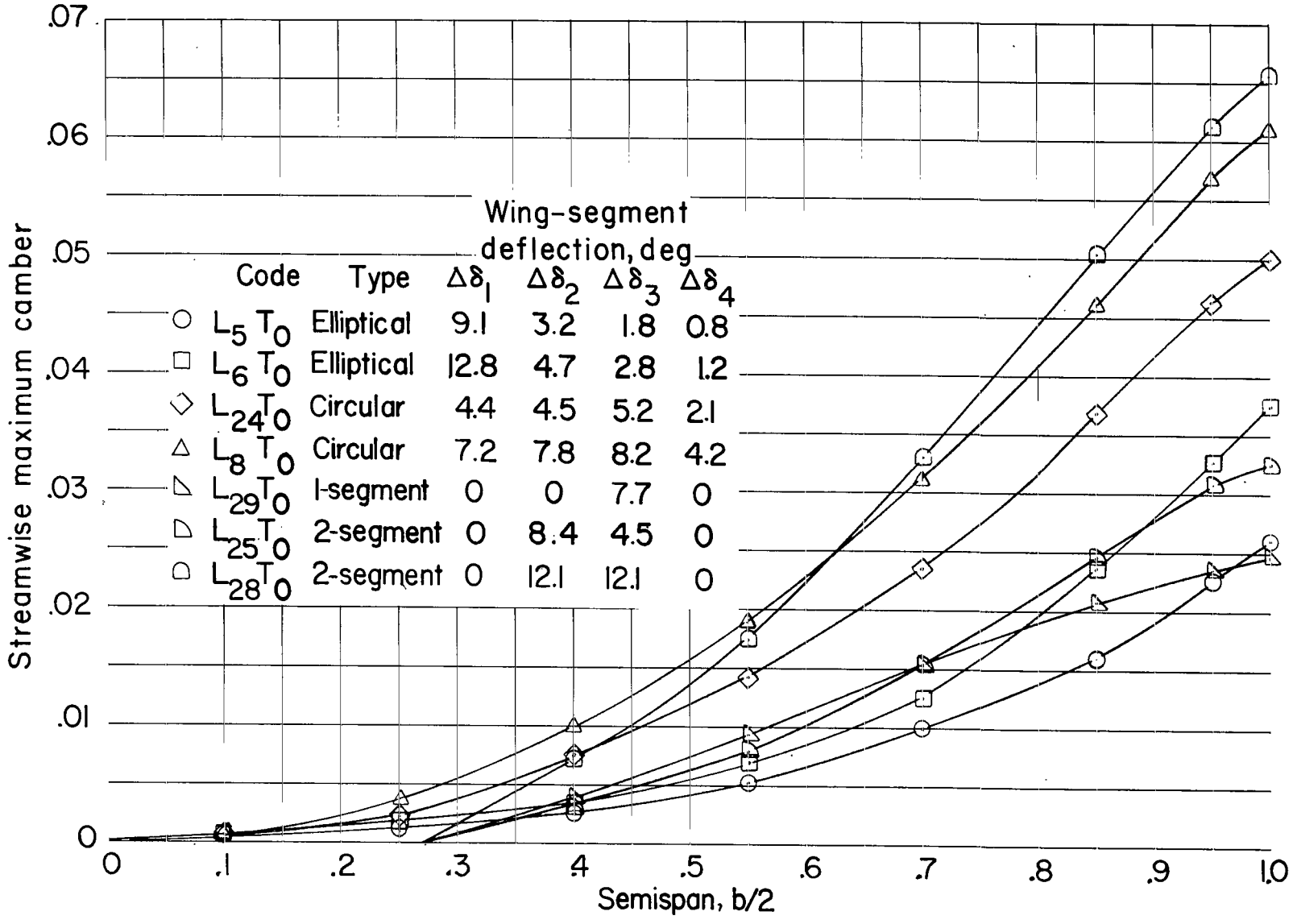

(a) Spanwise camber variation of the leading-edge configurations.

Figure 5.- Spanwise camber and twist distribution.

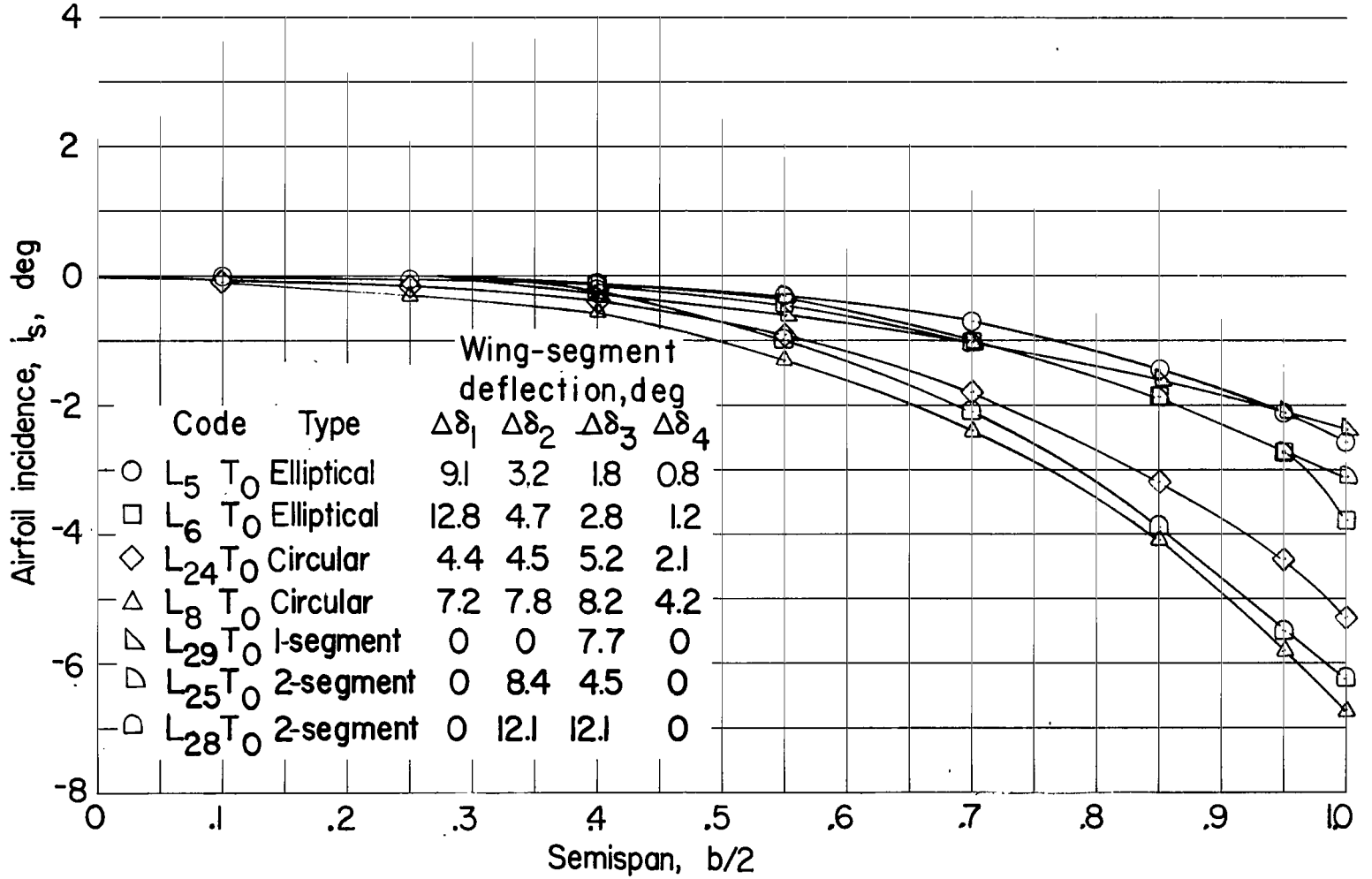

(b) Spanwise incidence variation of the leading-edge configurations.

Figure 5.- Continued.

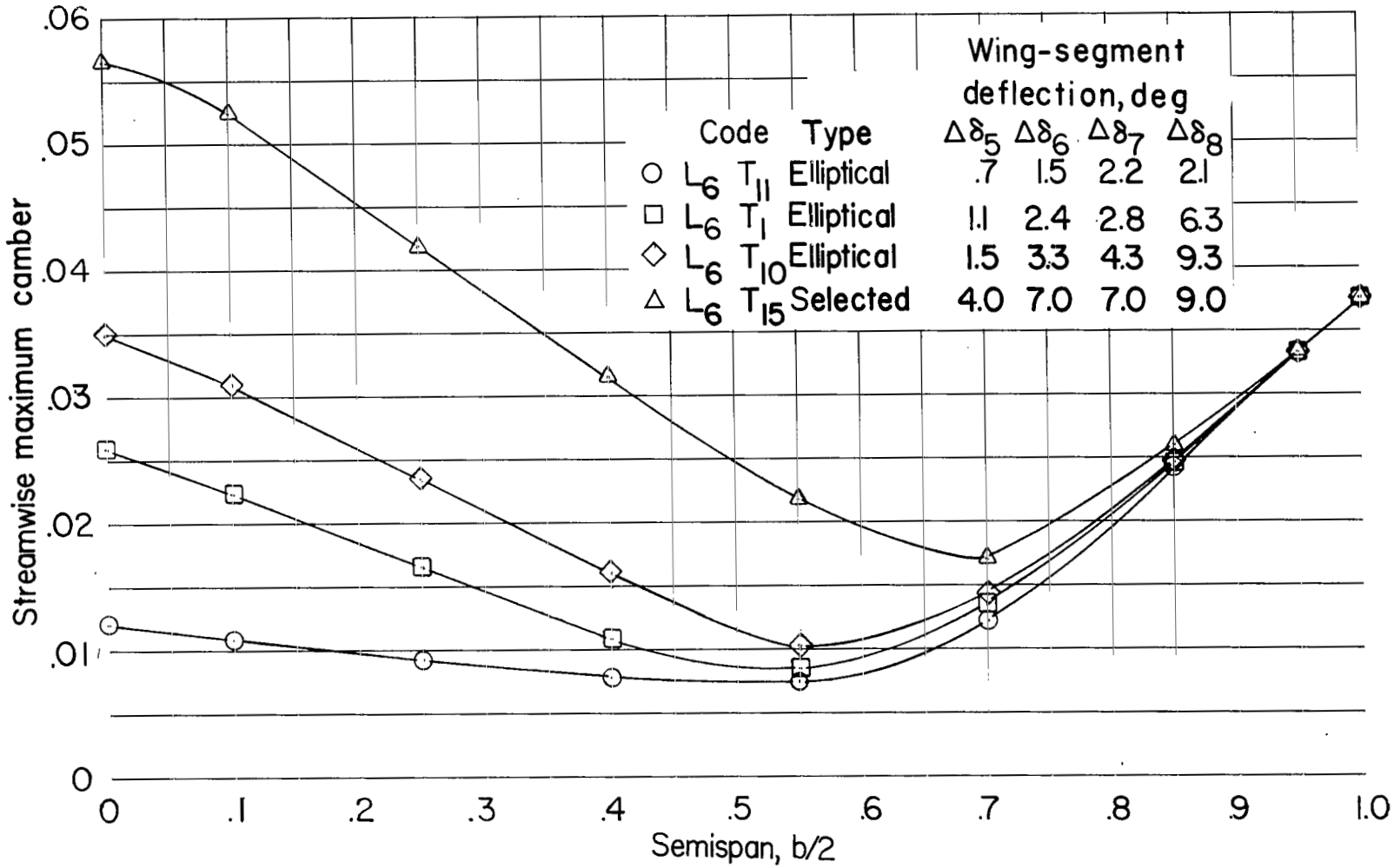

(c) Spanwise camber variation of the trailing-edge configurations.

Figure 5.- Continued.

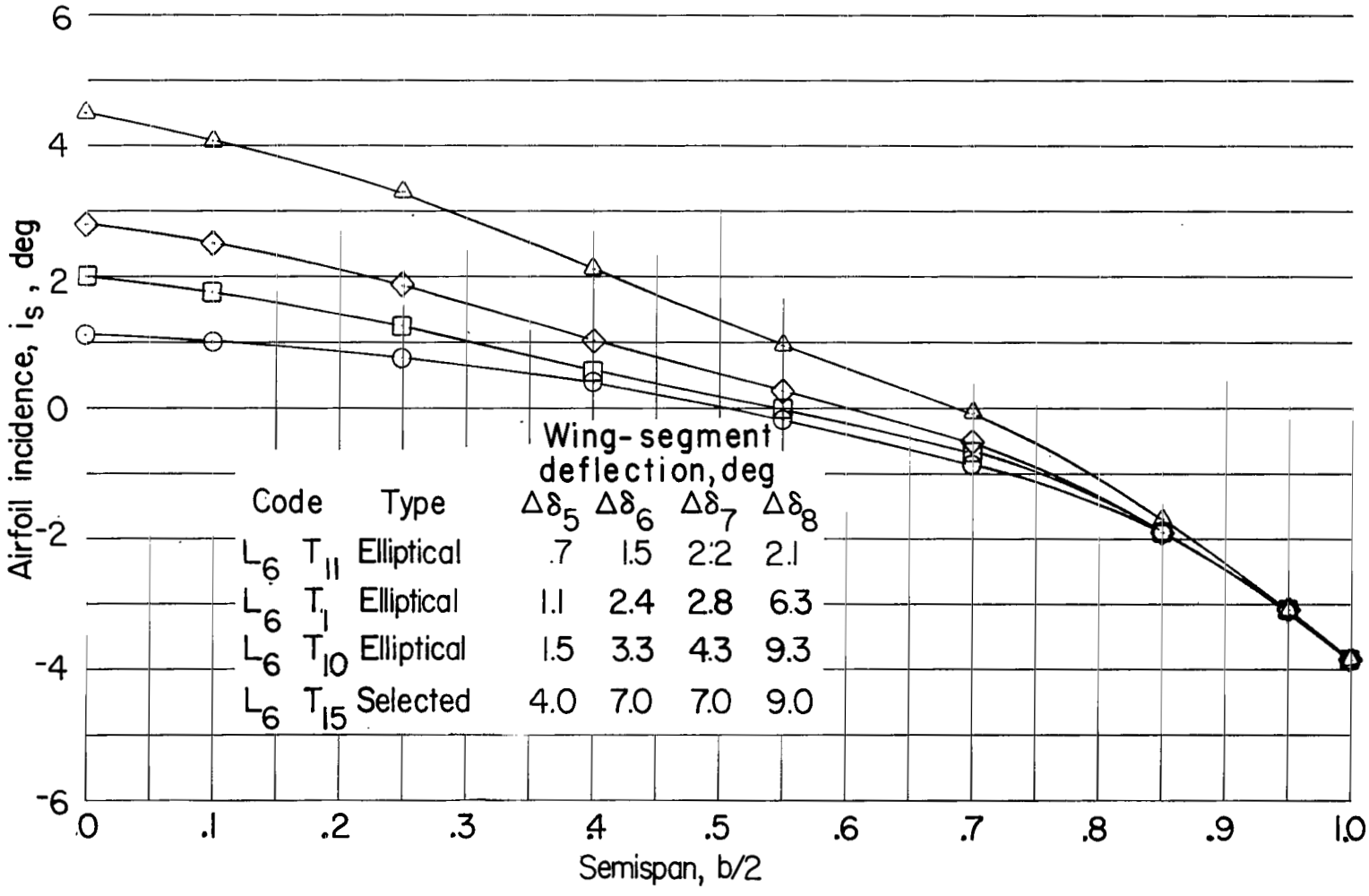

(d) Spanwise incidence variation of the trailing-edge configurations.

Figure 5.- Concluded.

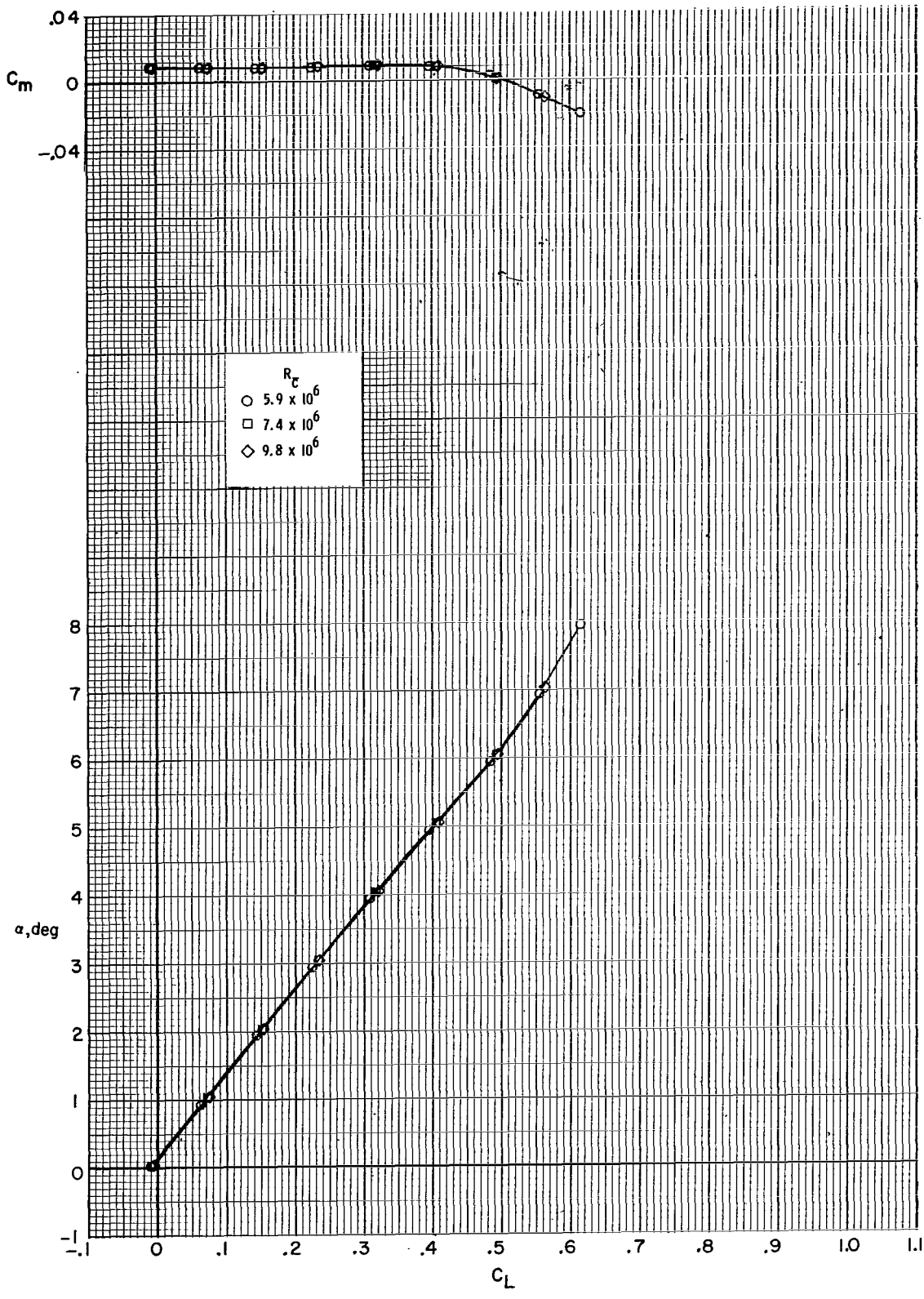

Figure 6.- Effect of Reynolds number on the longitudinal aerodynamic characteristics. M = 0.80.

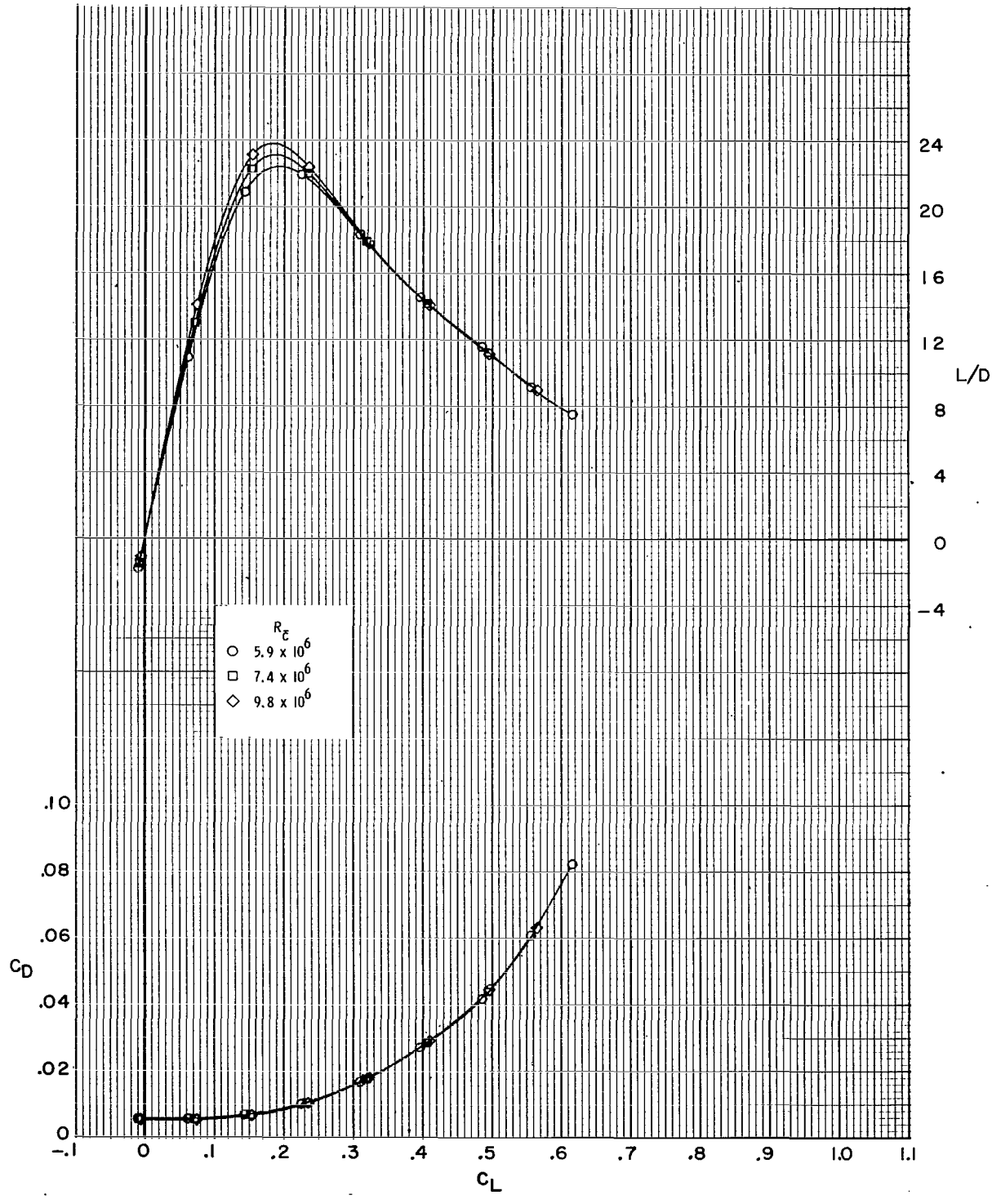

Figure 6.- Concluded.

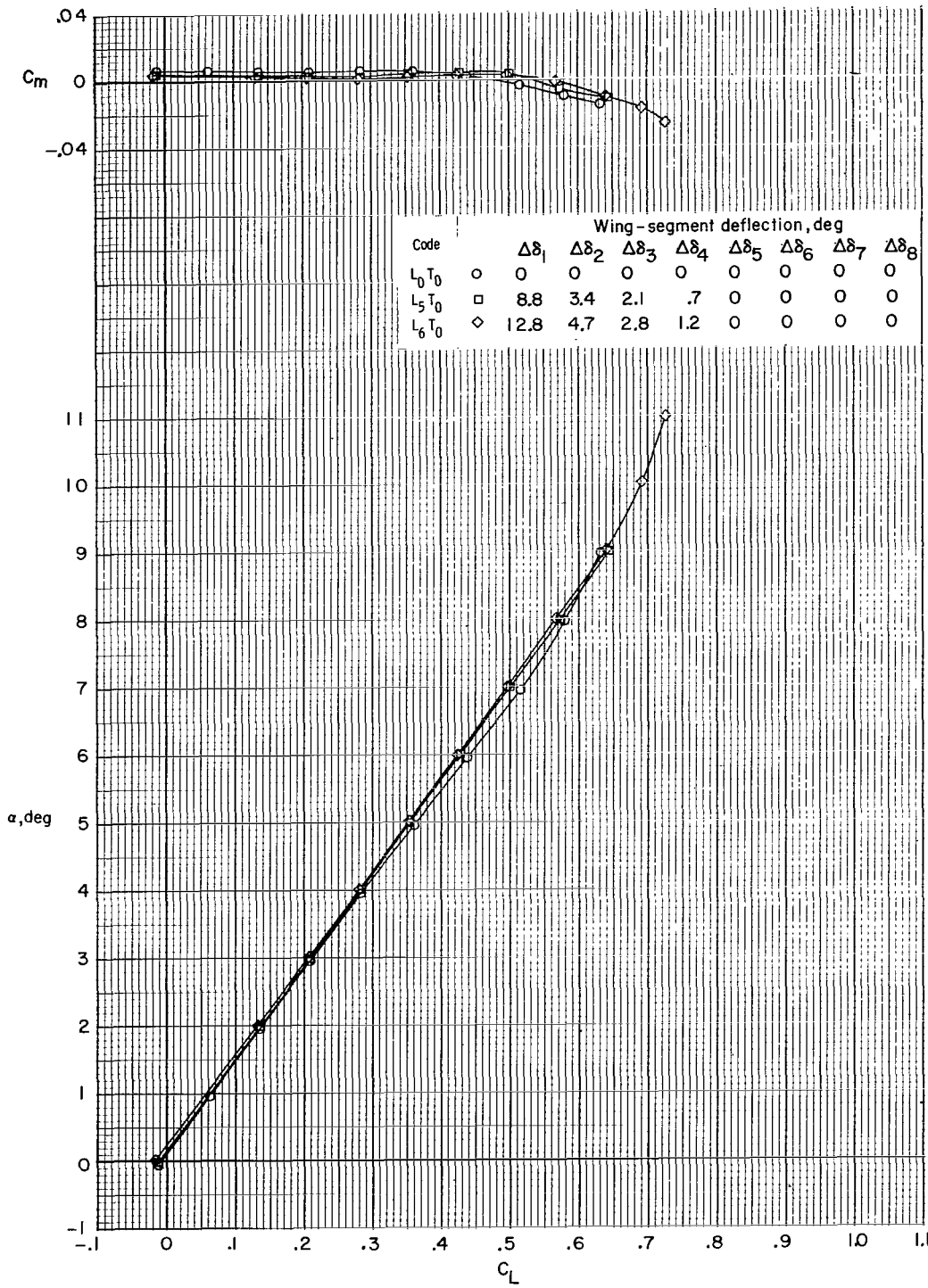

(a) M = 0.60; $R_{\bar{c}} = 6.2 \times 10^6$.

Figure 7.- Effect of elliptical leading-edge camber on the longitudinal aerodynamic characteristics.

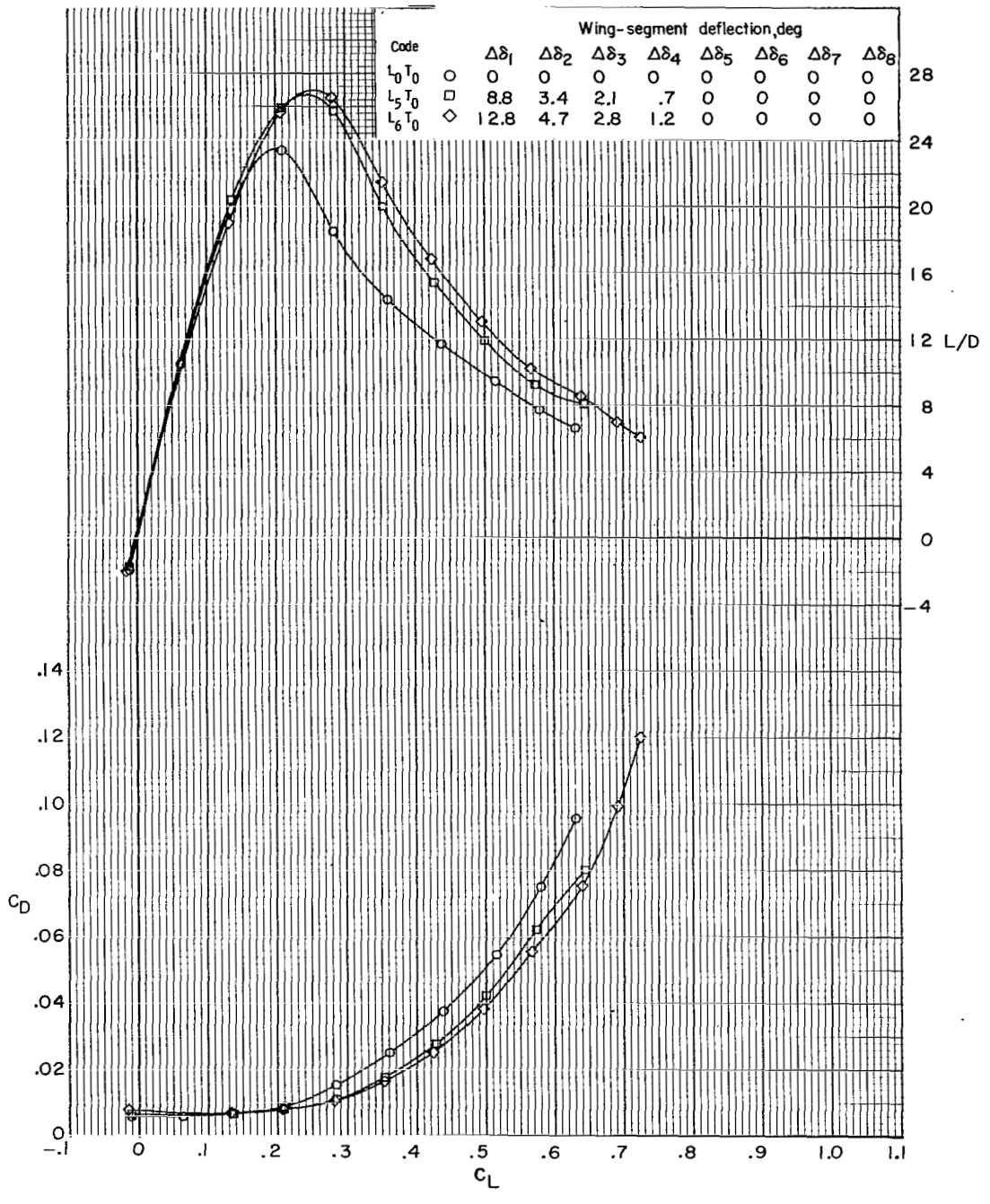

(a) Concluded.

Figure 7.- Continued.

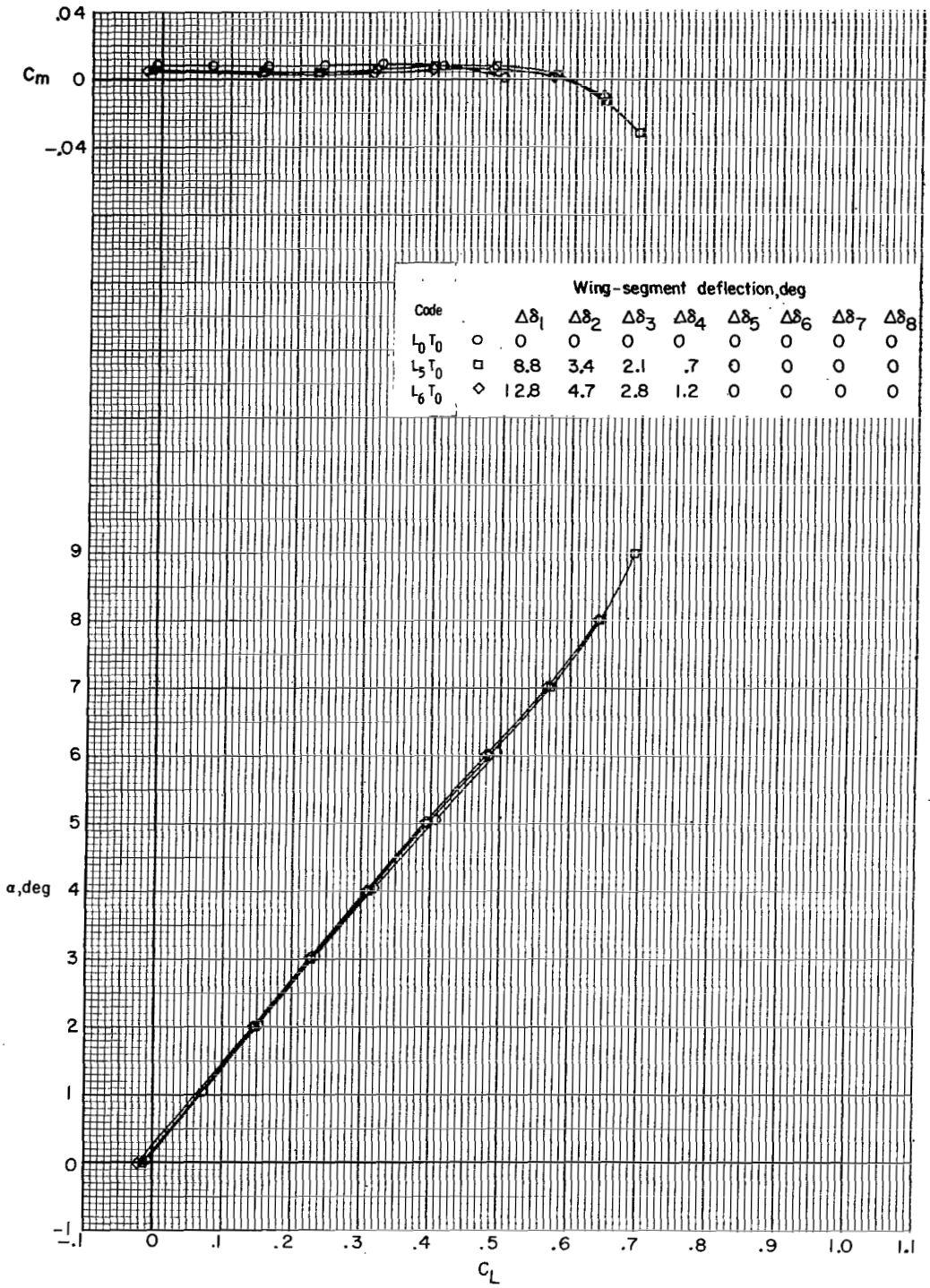

(b) M = 0.80; $R_{\bar{c}} = 7.4 \times 10^6$.

Figure 7.- Continued.

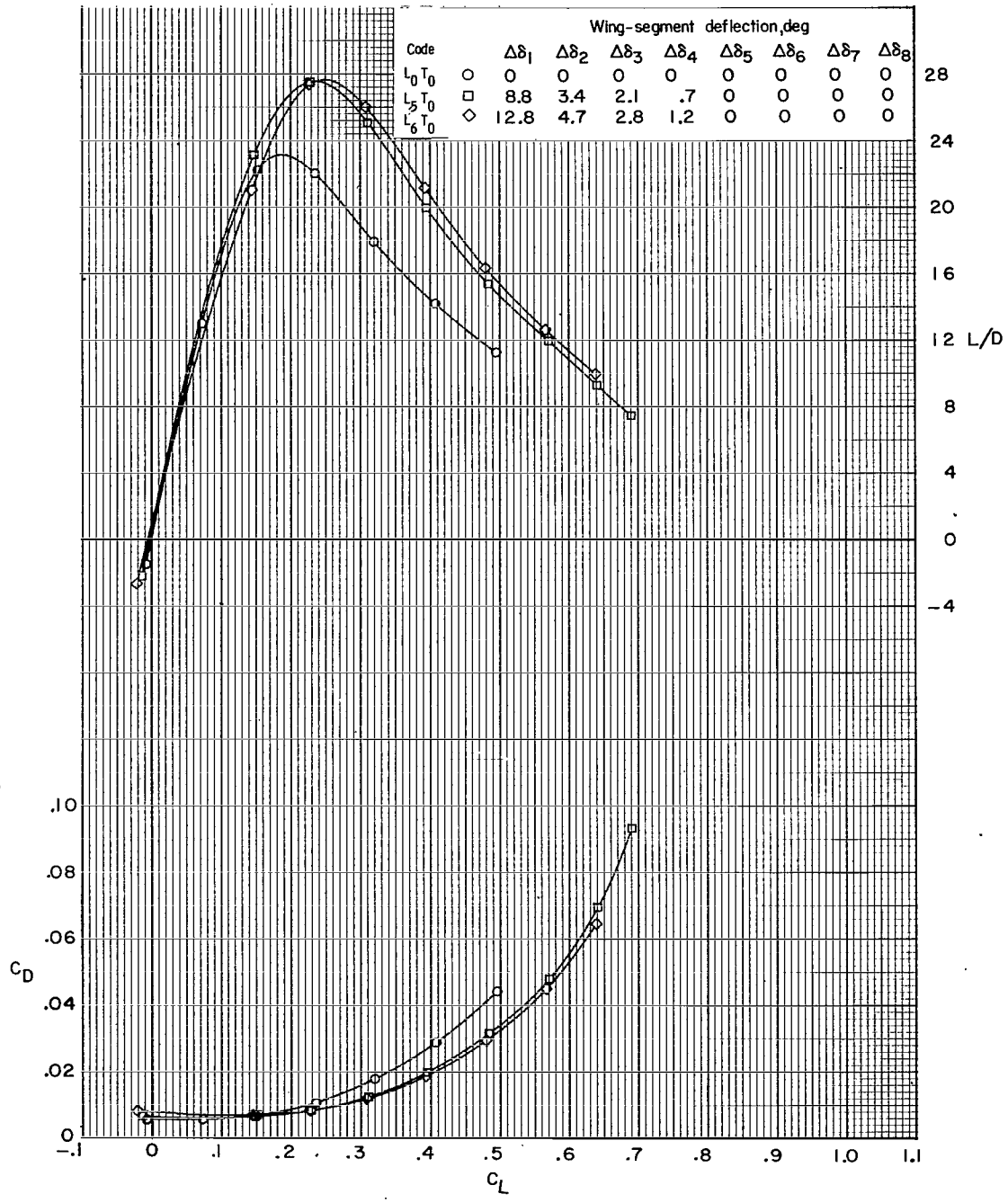

(b) Concluded.

Figure 7.- Continued.

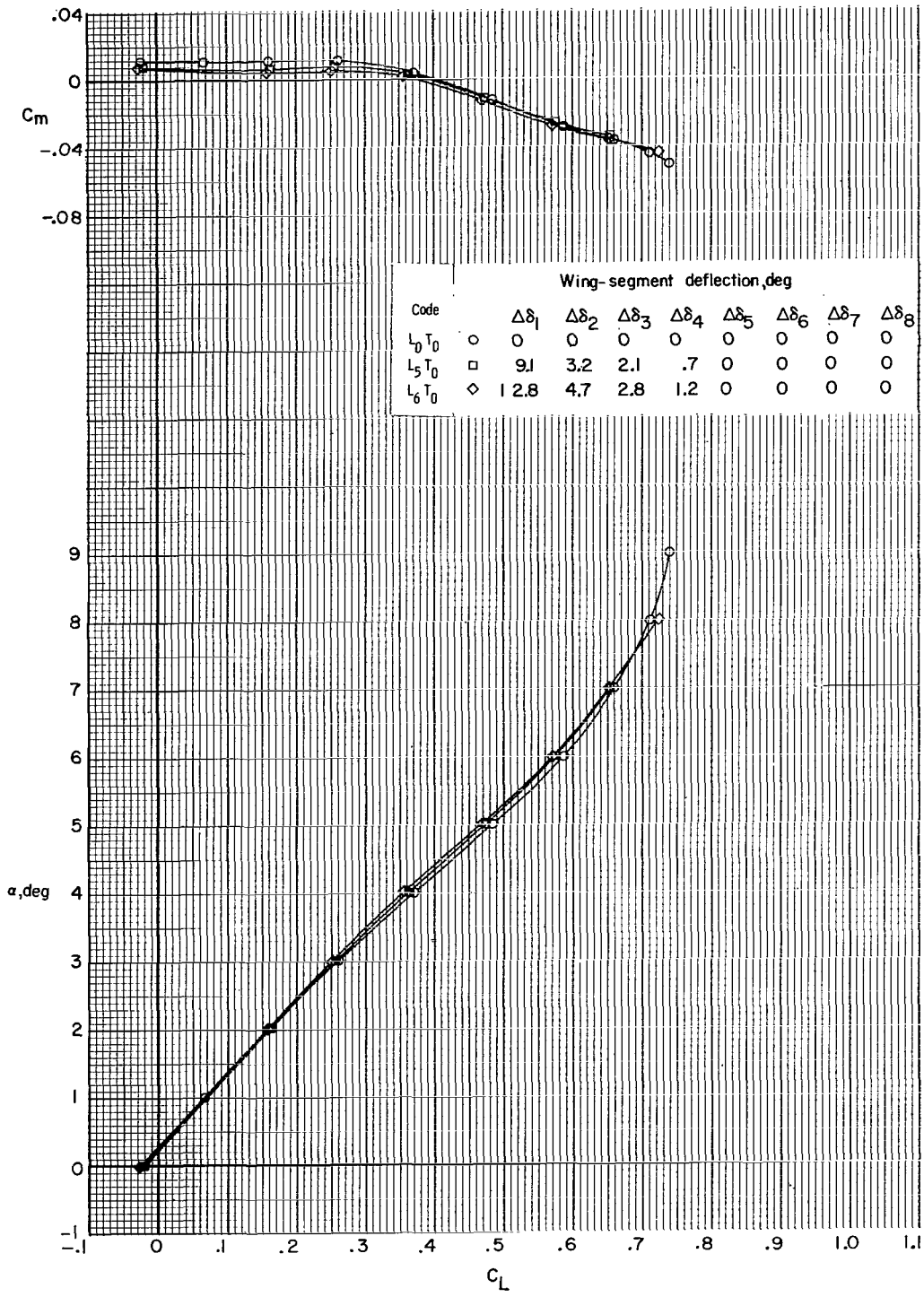

(c) M = 0.90; $R_{\bar{c}} = 7.6 \times 10^6$.

Figure 7.- Continued.

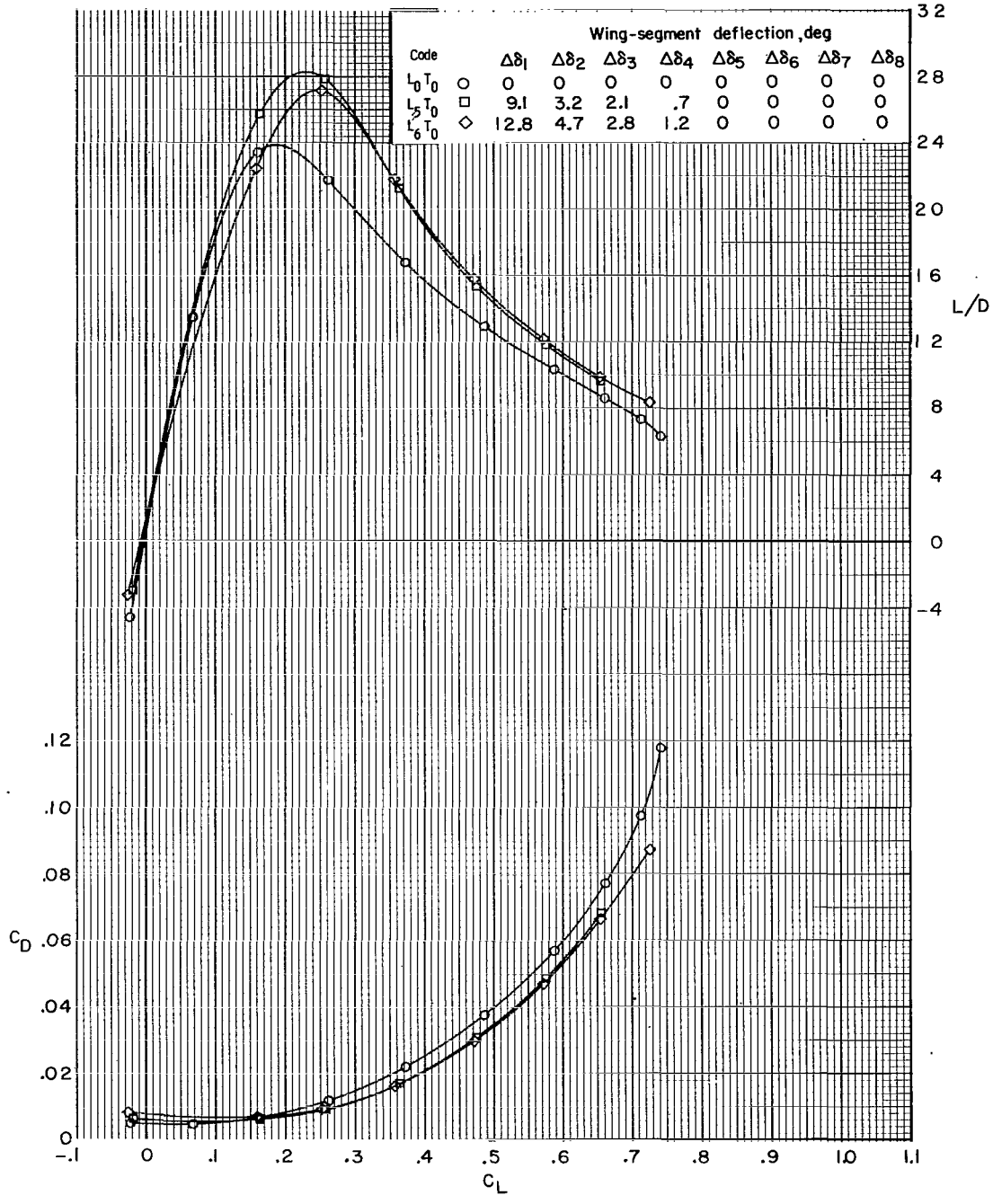

(c) Concluded.

Figure 7.- Concluded.

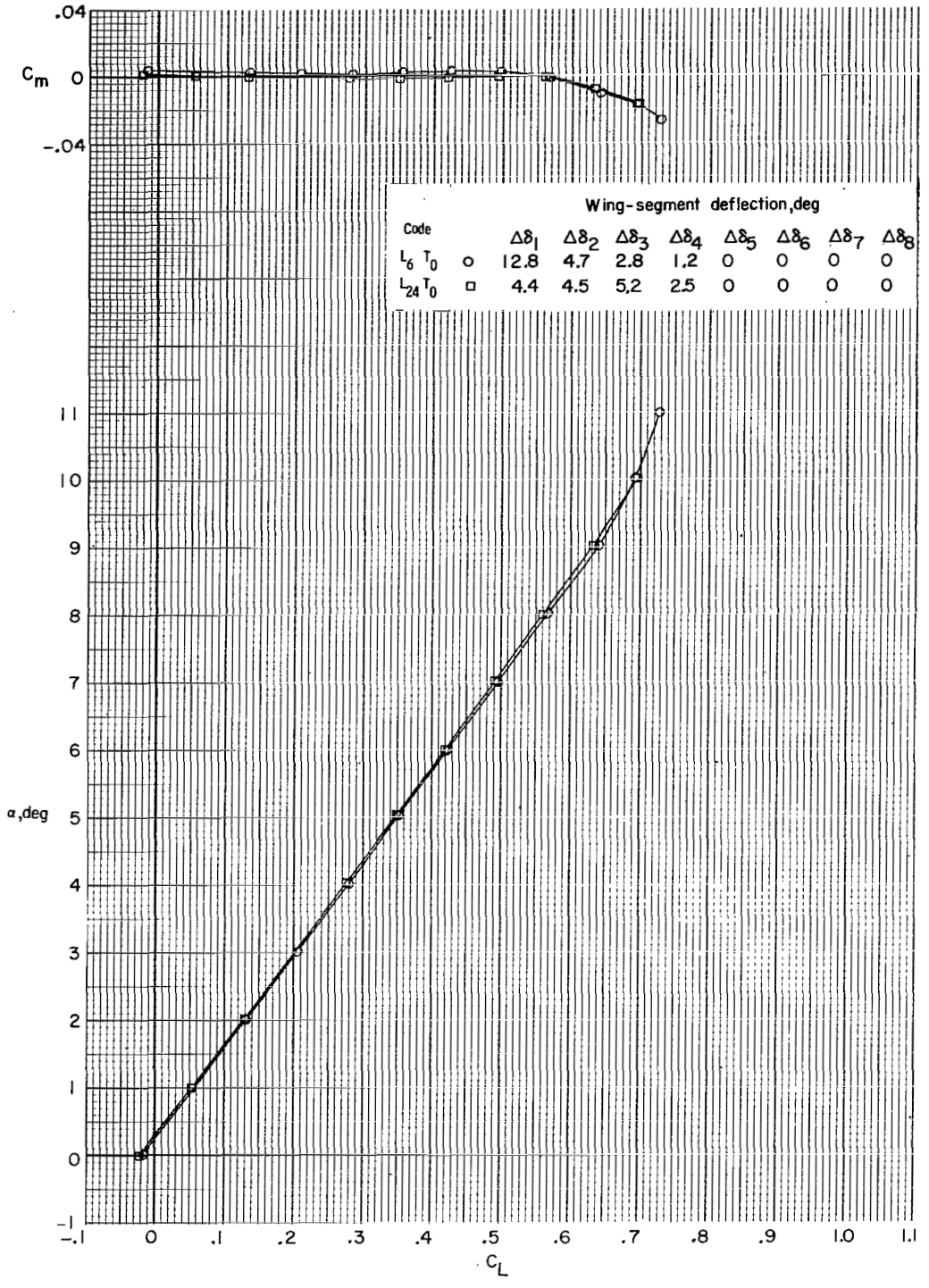

(a) $M = 0.60$; $R_{\bar{c}} = 6.2 \times 10^6$.

Figure 8.- Effect of circular leading-edge camber on the longitudinal aerodynamic characteristics.

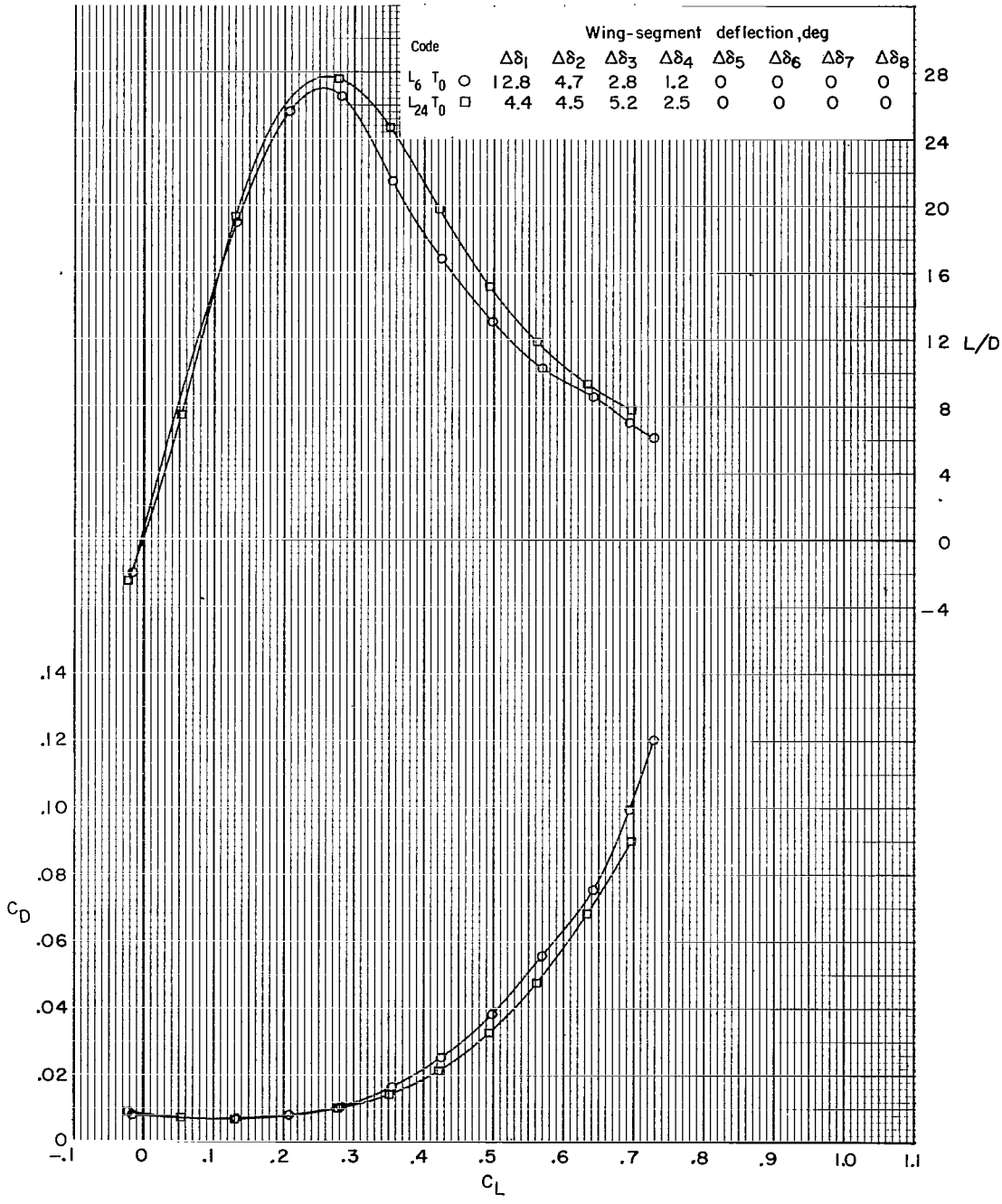

(a) Concluded.

Figure 8.- Continued.

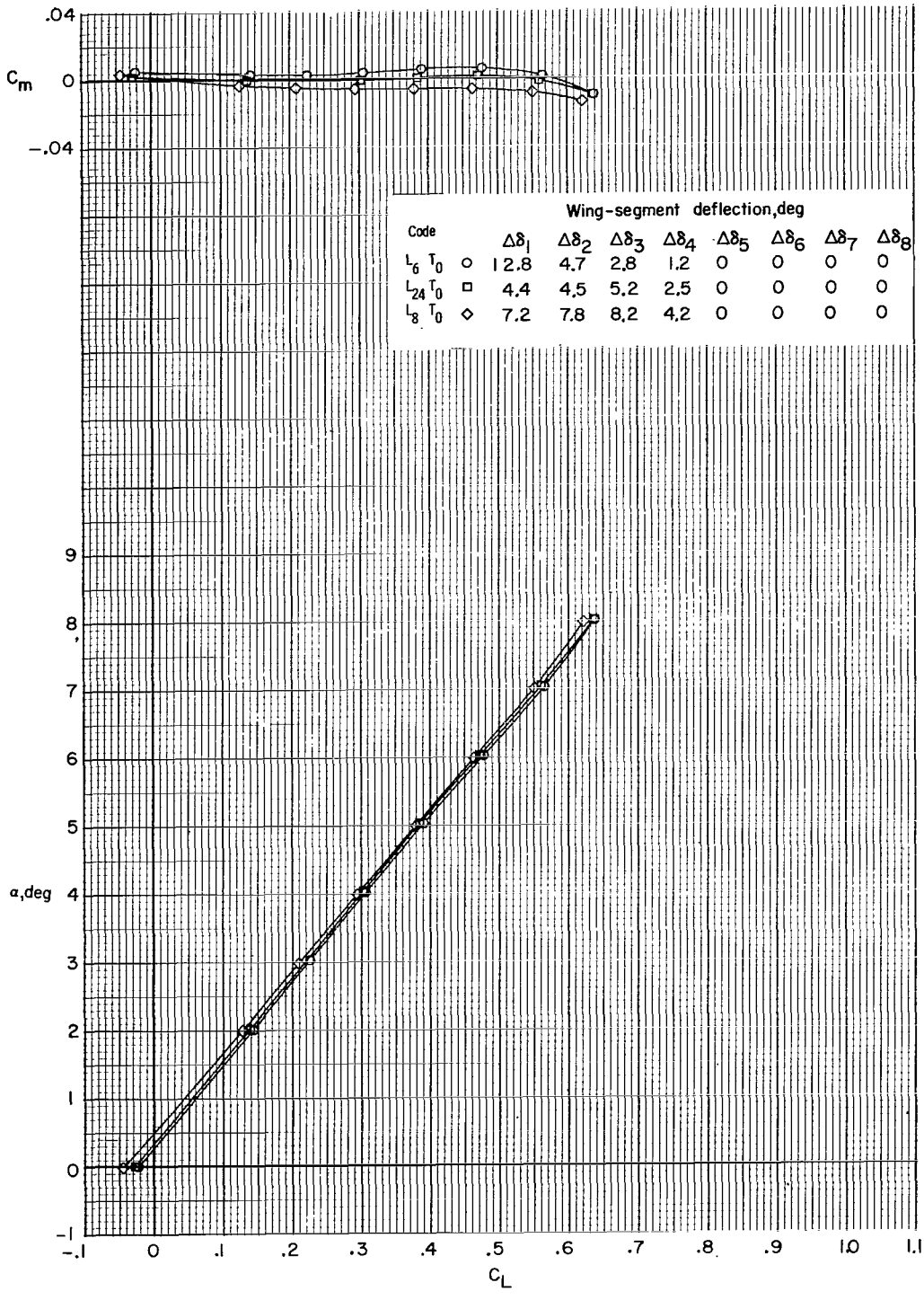

(b) M = 0.80; $R_{\bar{c}} = 7.4 \times 10^6$.

Figure 8.- Continued.

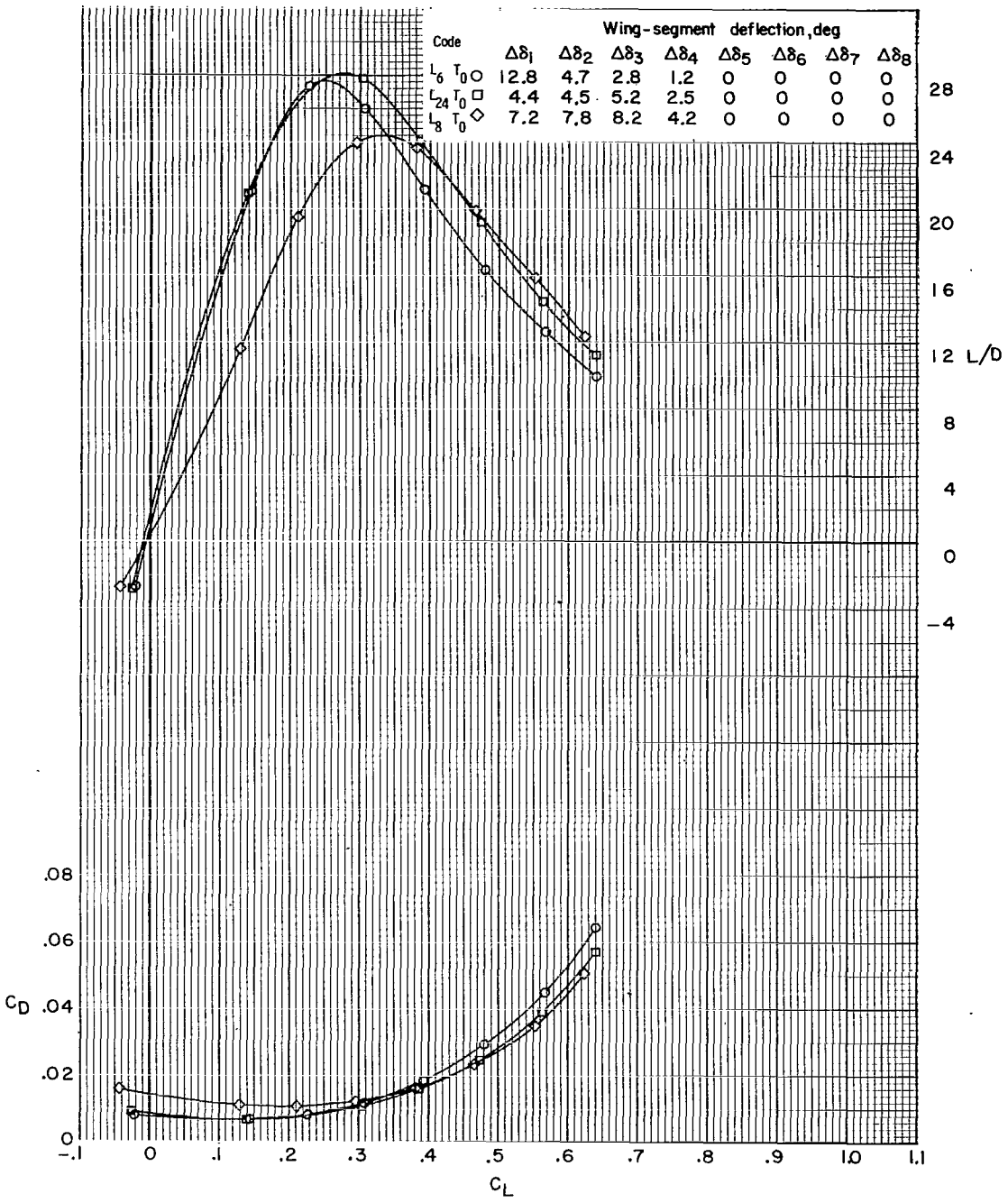

(b) Concluded.

Figure 8.- Continued.

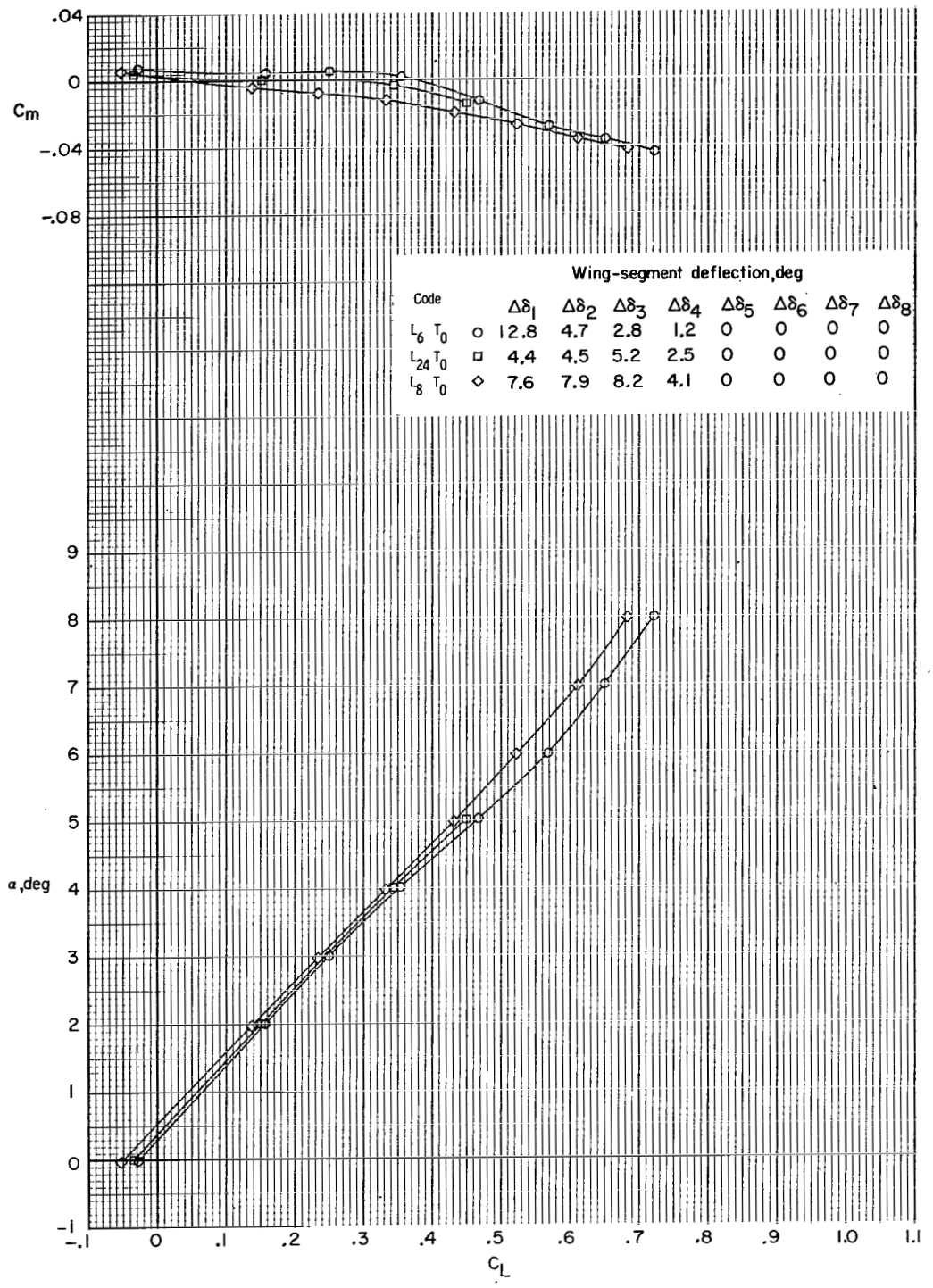

(c) M = 0.90; $R_{\bar{c}} = 7.6 \times 10^6$.

Figure 8.- Continued.

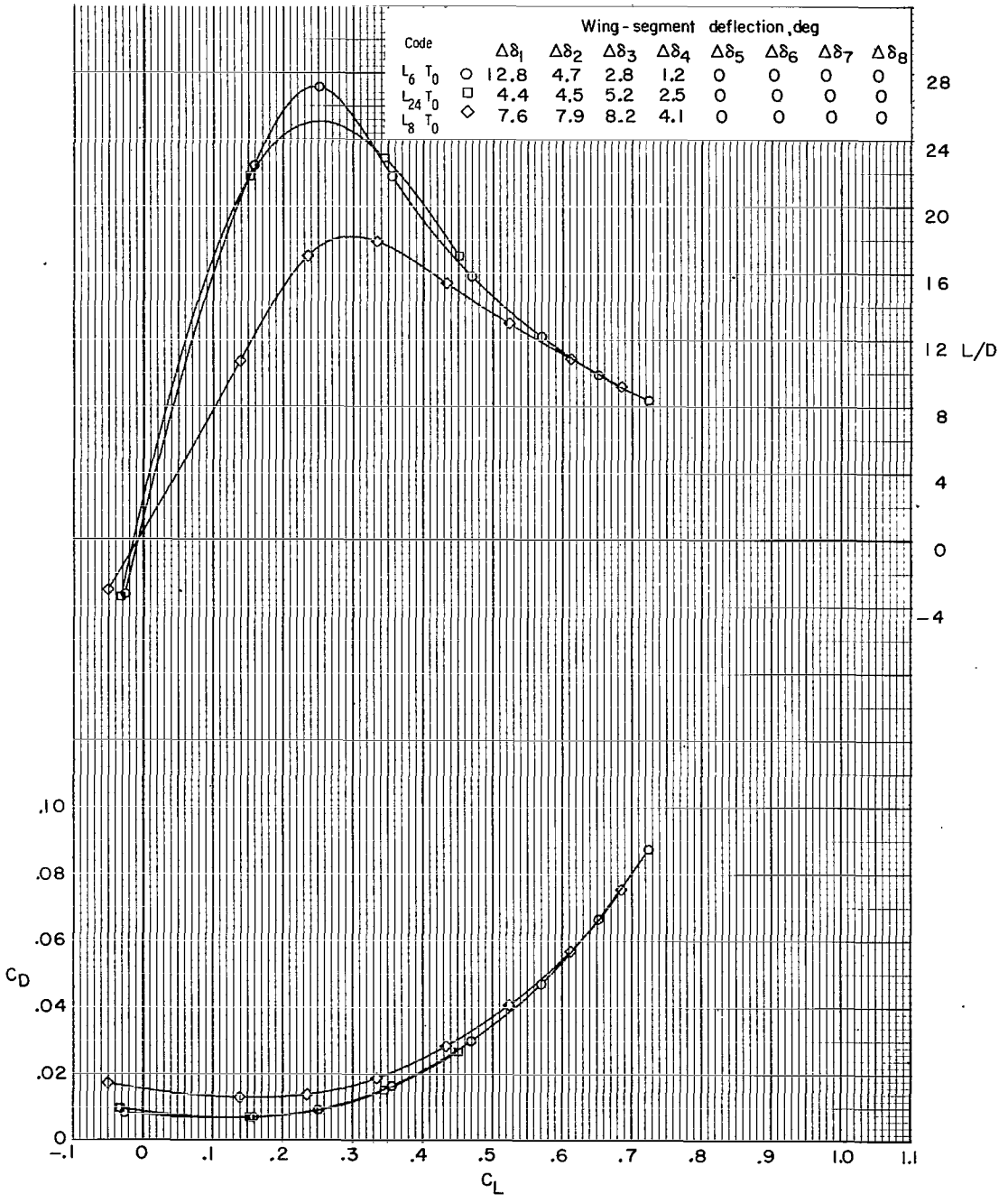

(c) Concluded.

Figure 8.- Concluded.

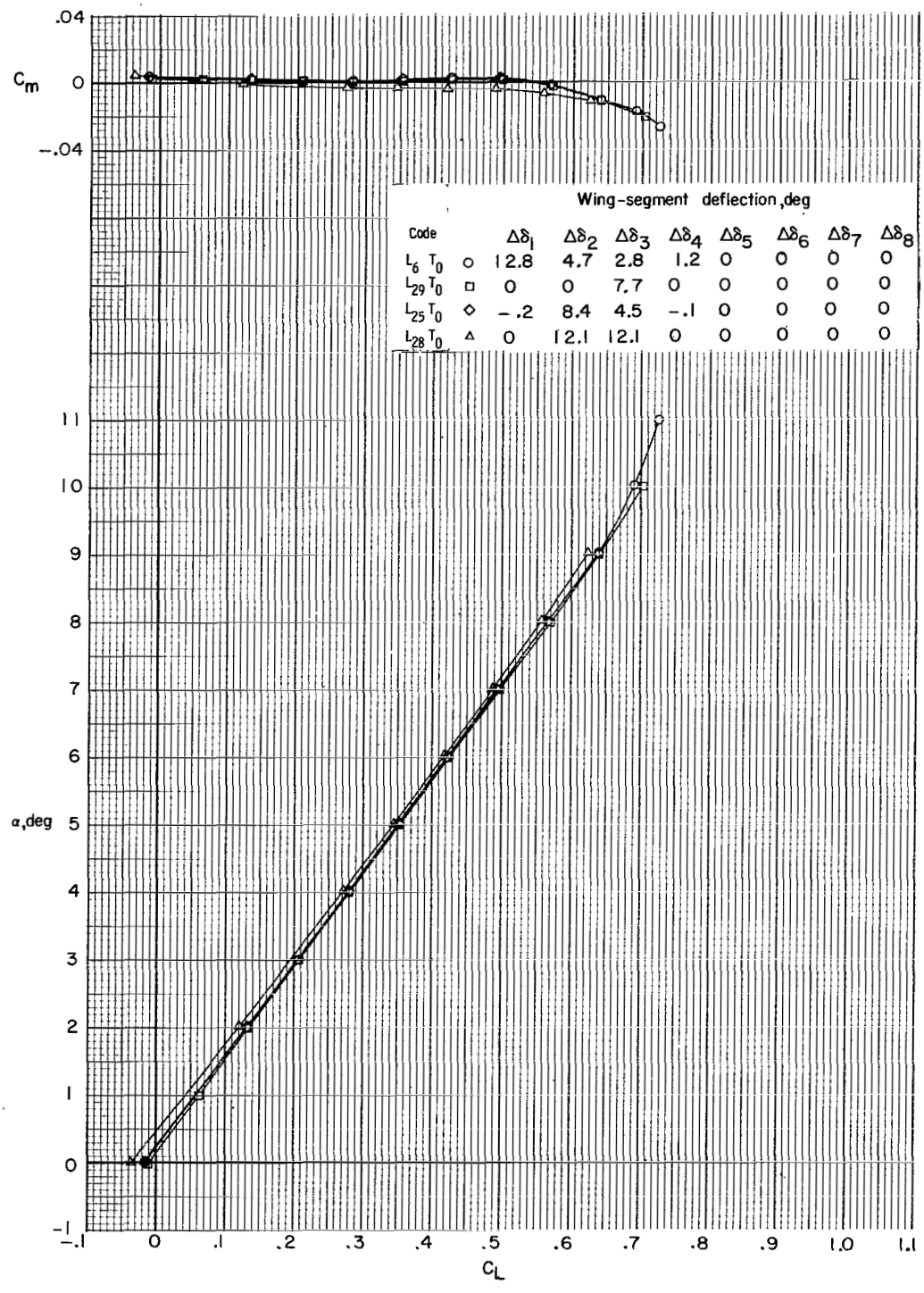

(a) M = 0.60; $R_{\bar{c}} = 6.2 \times 10^6$.

Figure 9.- Effect of simplified leading-edge camber on the longitudinal aerodynamic characteristics.

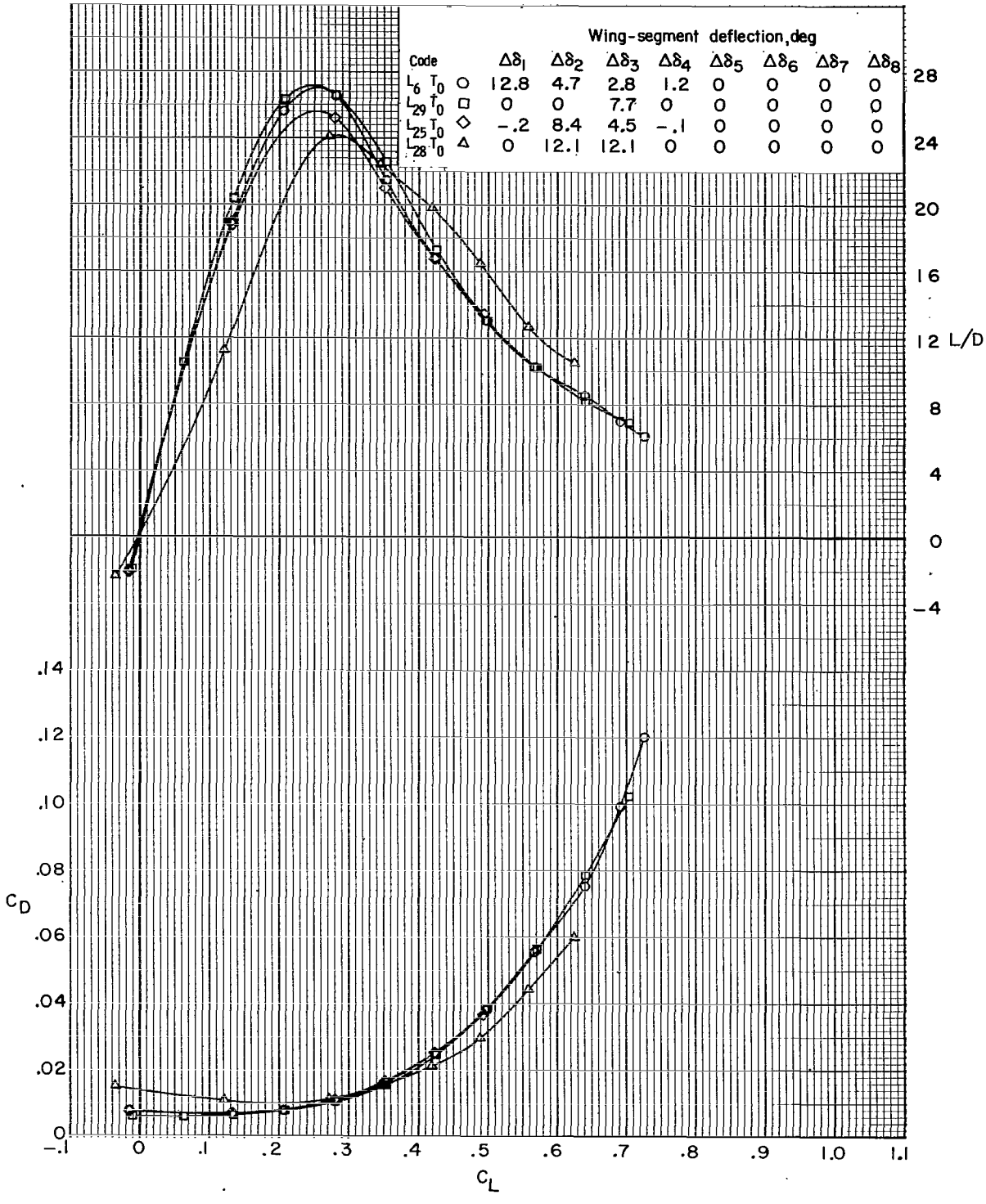

(a) Concluded.

Figure 9.- Continued.

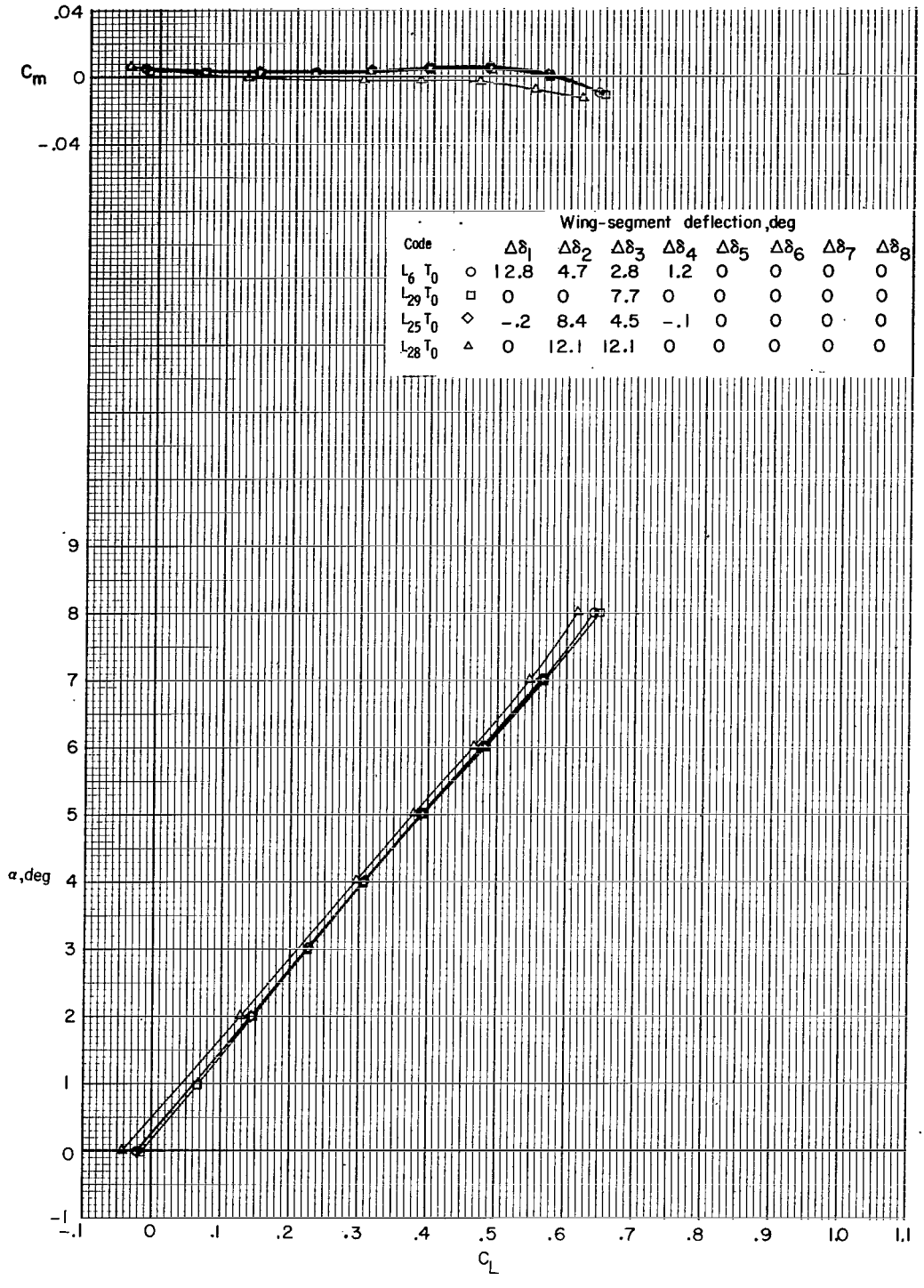

(b) M = 0.80; $R_{\bar{c}} = 7.4 \times 10^6$.

Figure 9.- Continued.

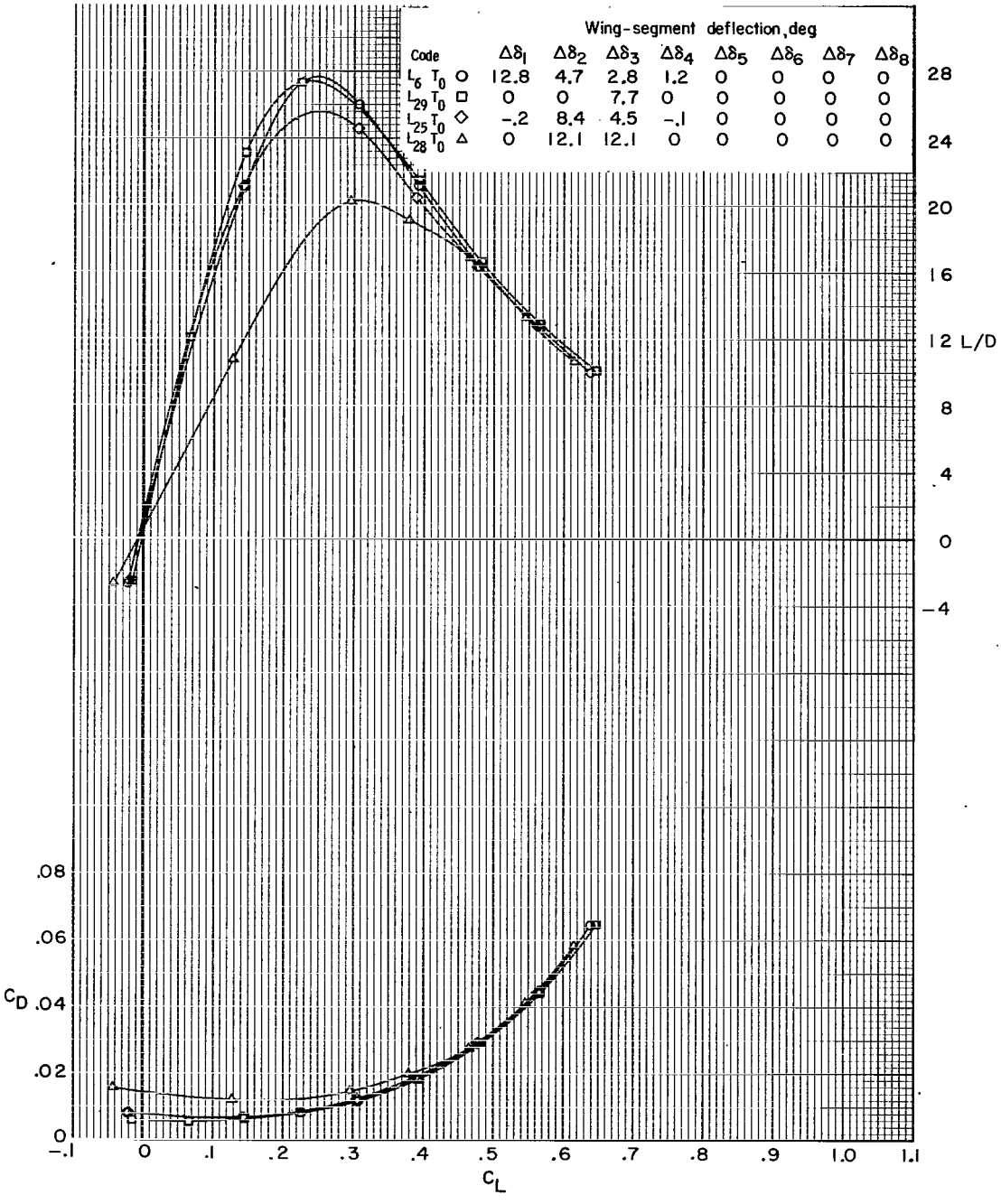

(b) Concluded.

Figure 9.- Continued.

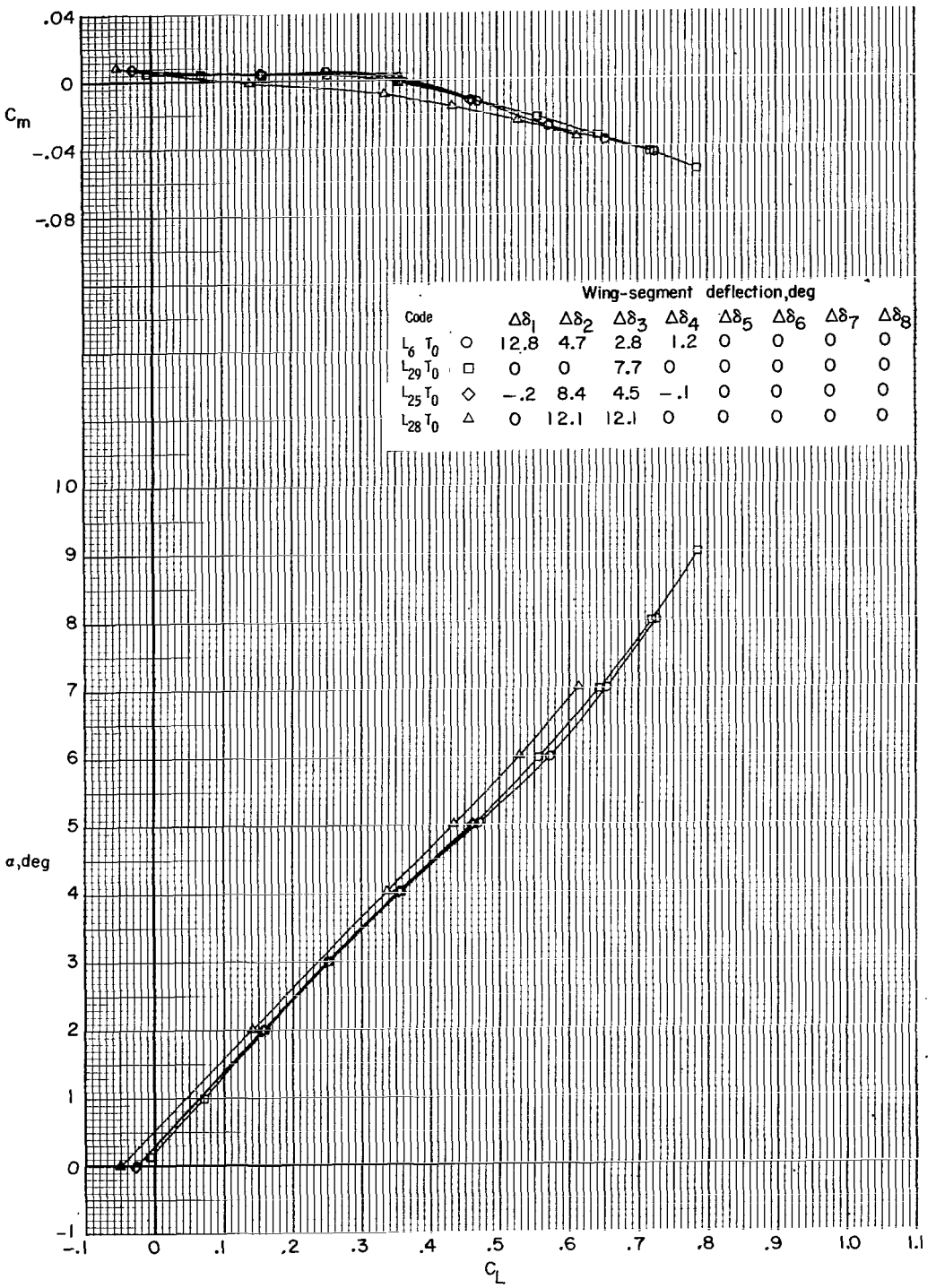

(c) M = 0.90; $R_{\bar{c}} = 7.6 \times 10^6$.

Figure 9.- Continued.

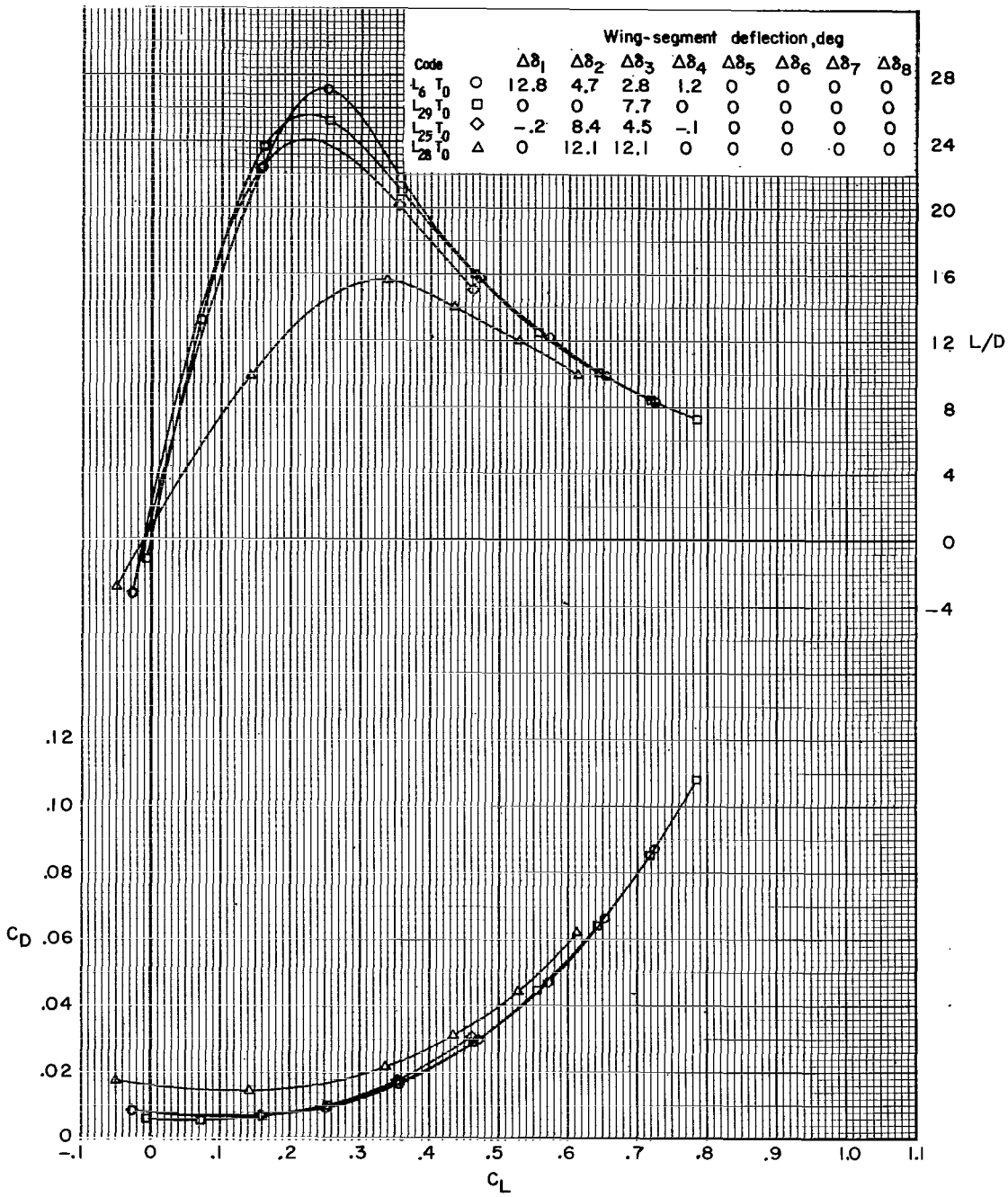

(c) Concluded.

Figure 9.- Concluded.

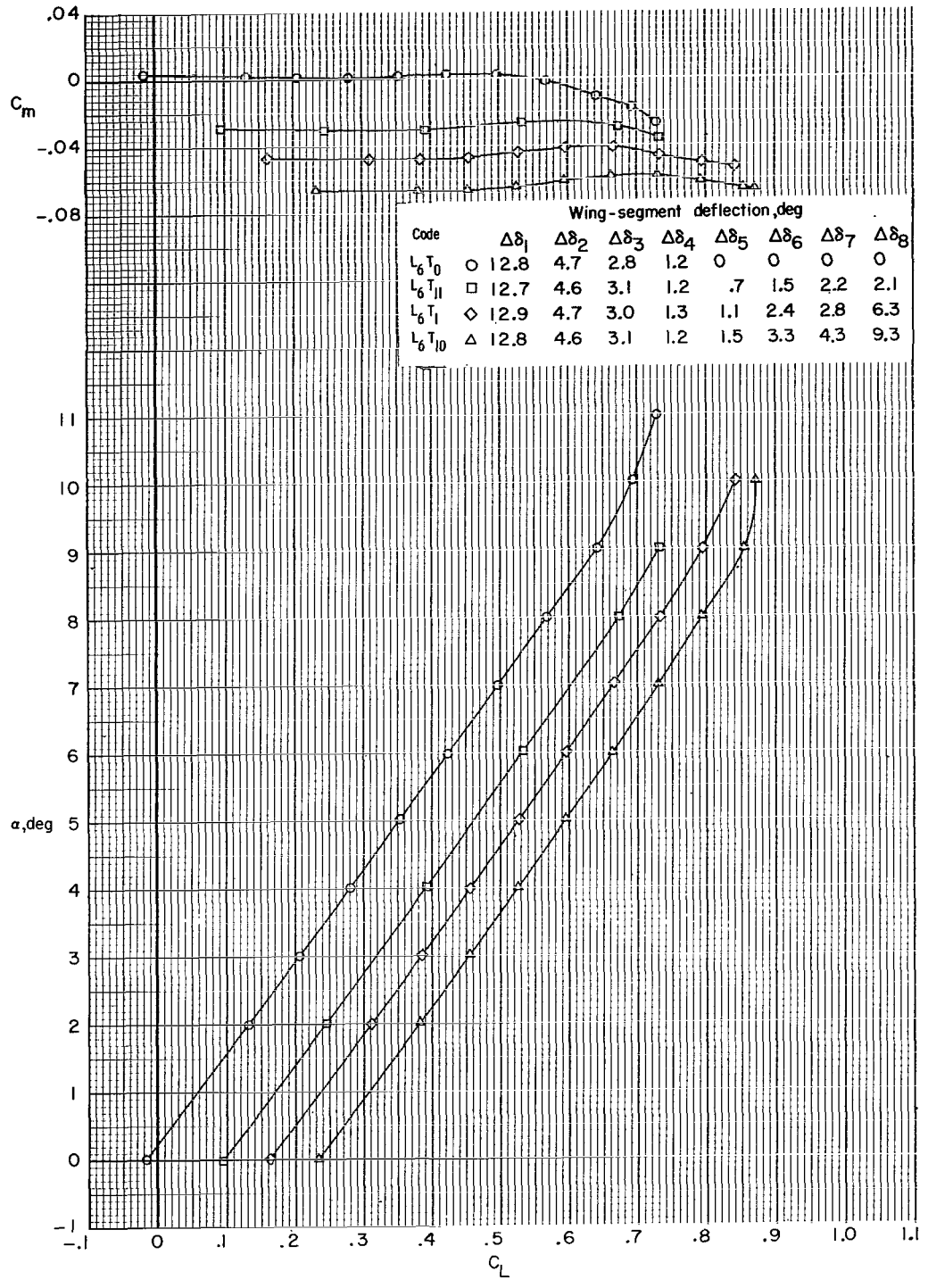

(a) M = 0.60; $R_{\bar{c}} = 6.2 \times 10^6$.

Figure 10.- Effect of elliptical trailing-edge camber on the longitudinal aerodynamic characteristics.

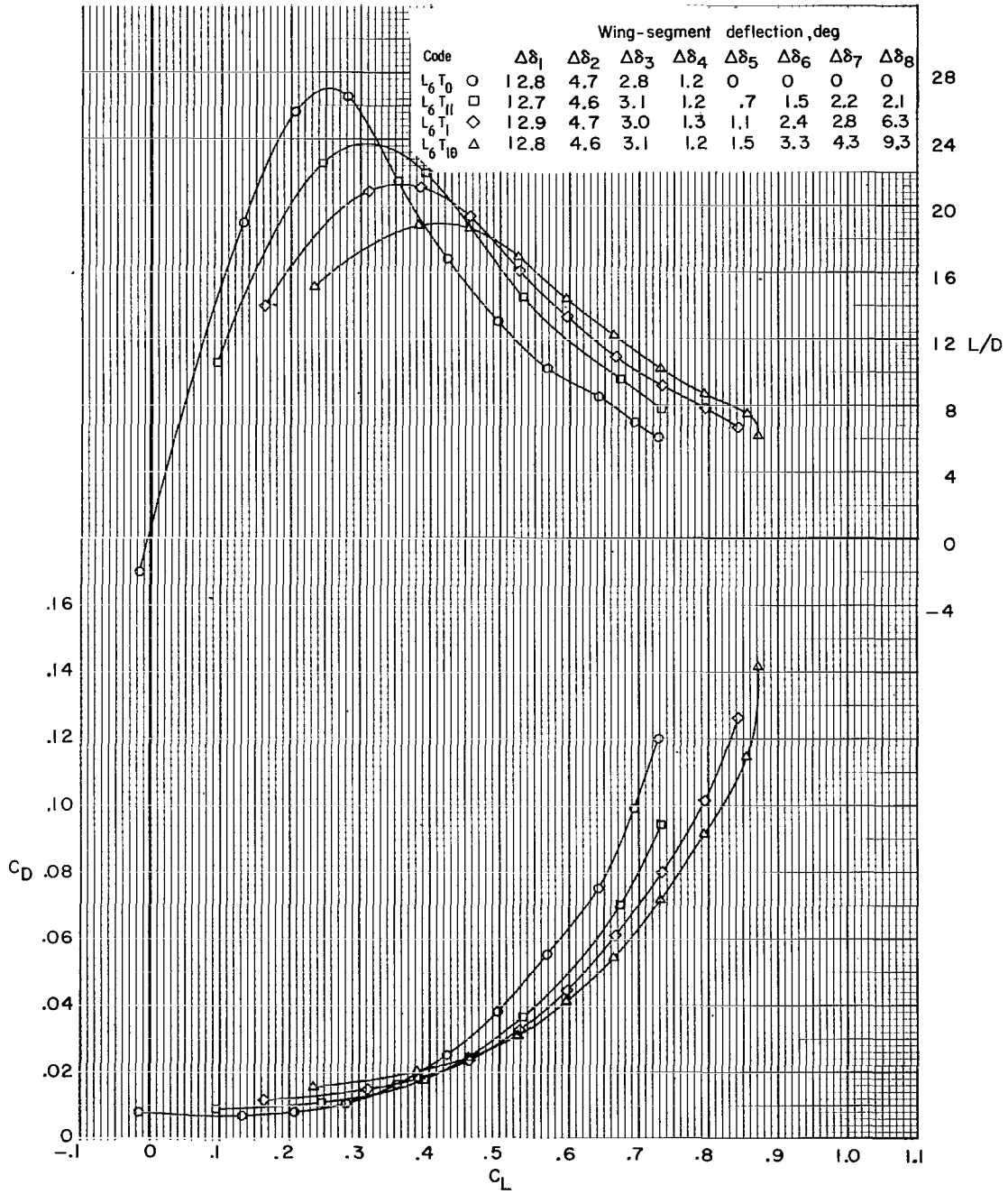

(a) Concluded.

Figure 10.- Continued.

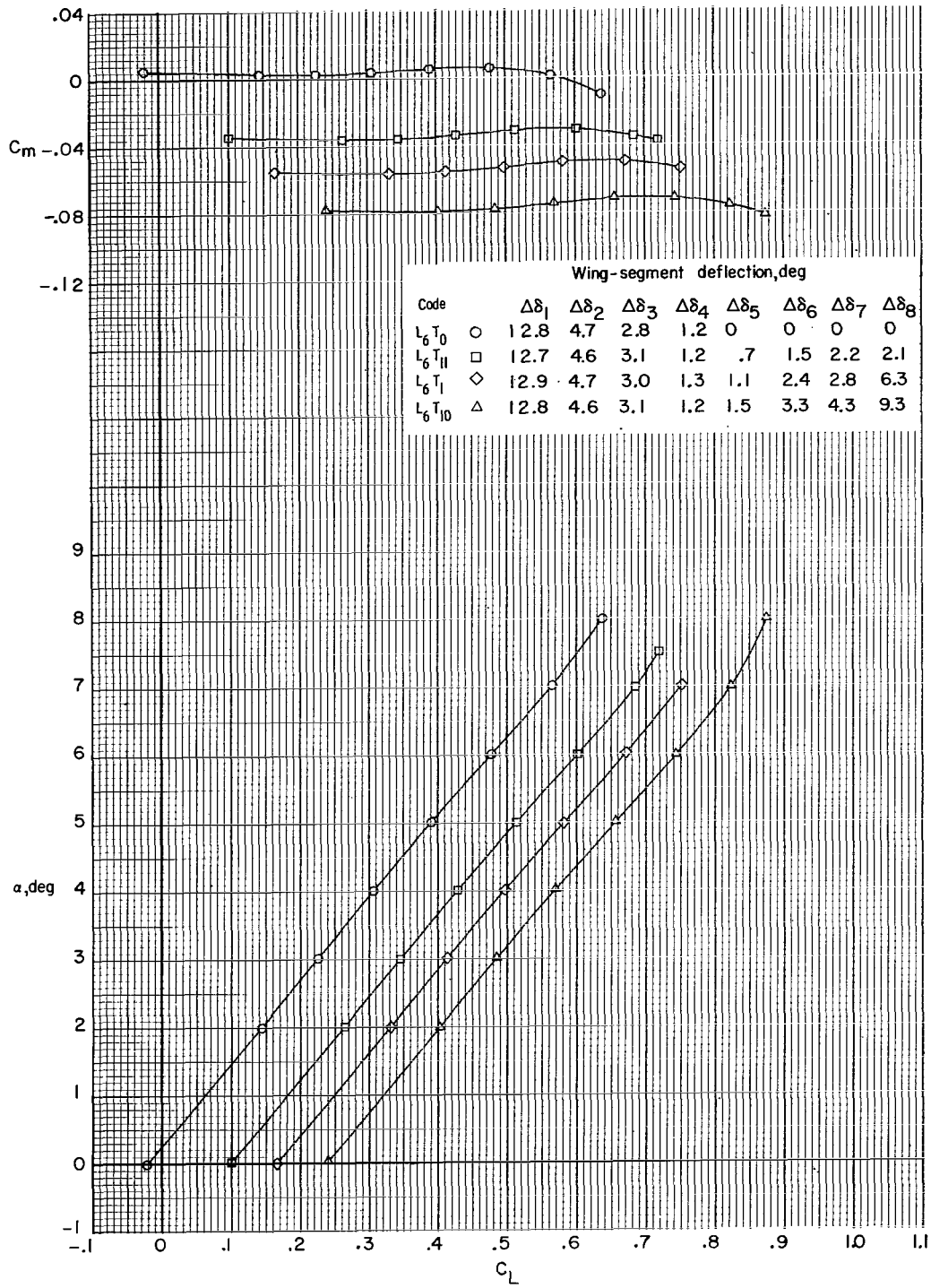

(b) M = 0.80; $R_{\bar{c}} = 7.4 \times 10^6$.

Figure 10.- Continued.

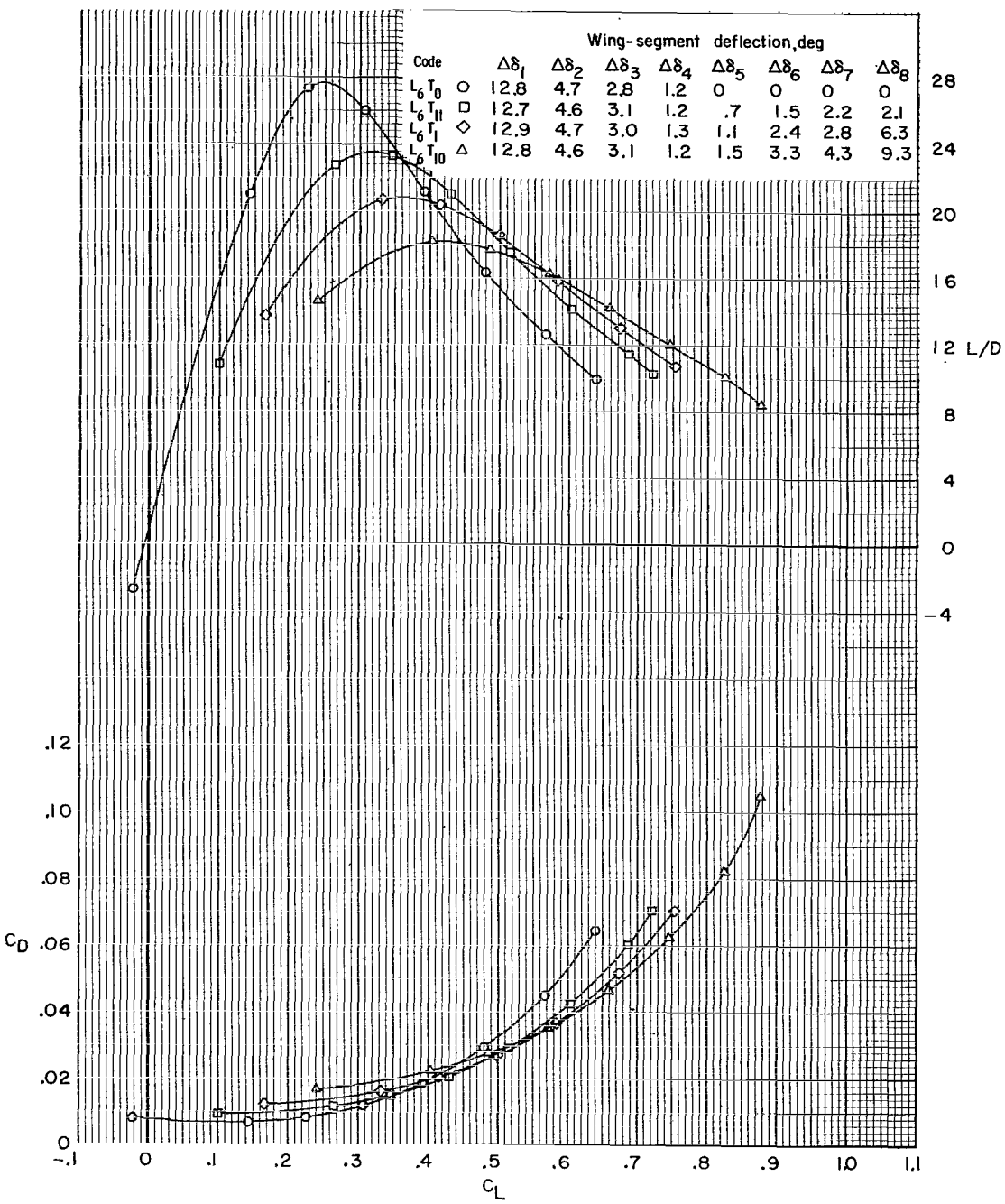

(b) Concluded.

Figure 10.- Continued.

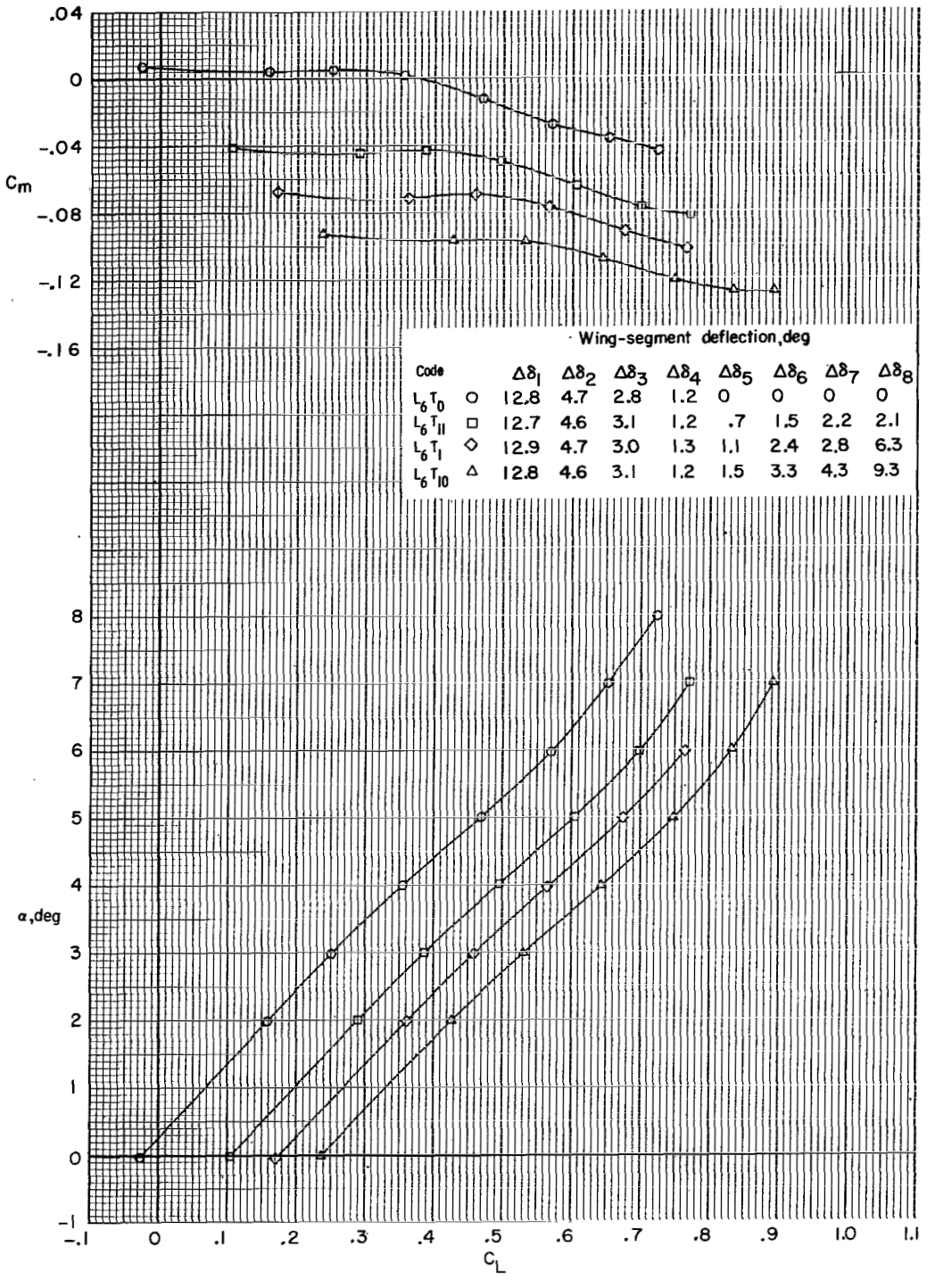

(c) M = 0.90; $R_{\bar{c}} = 7.6 \times 10^6$.

Figure 10.- Continued.

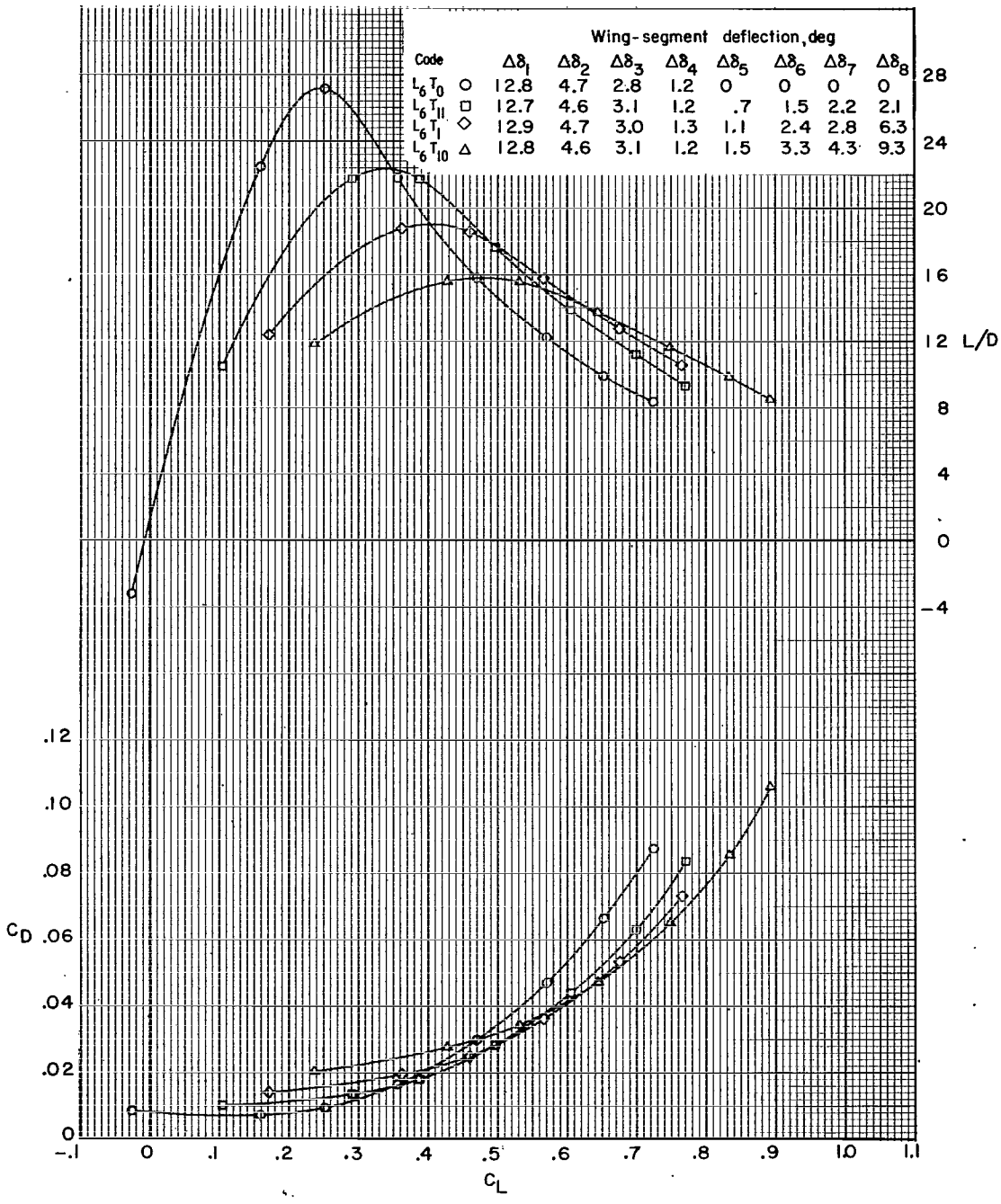

(c) Concluded.

Figure 10.- Concluded.

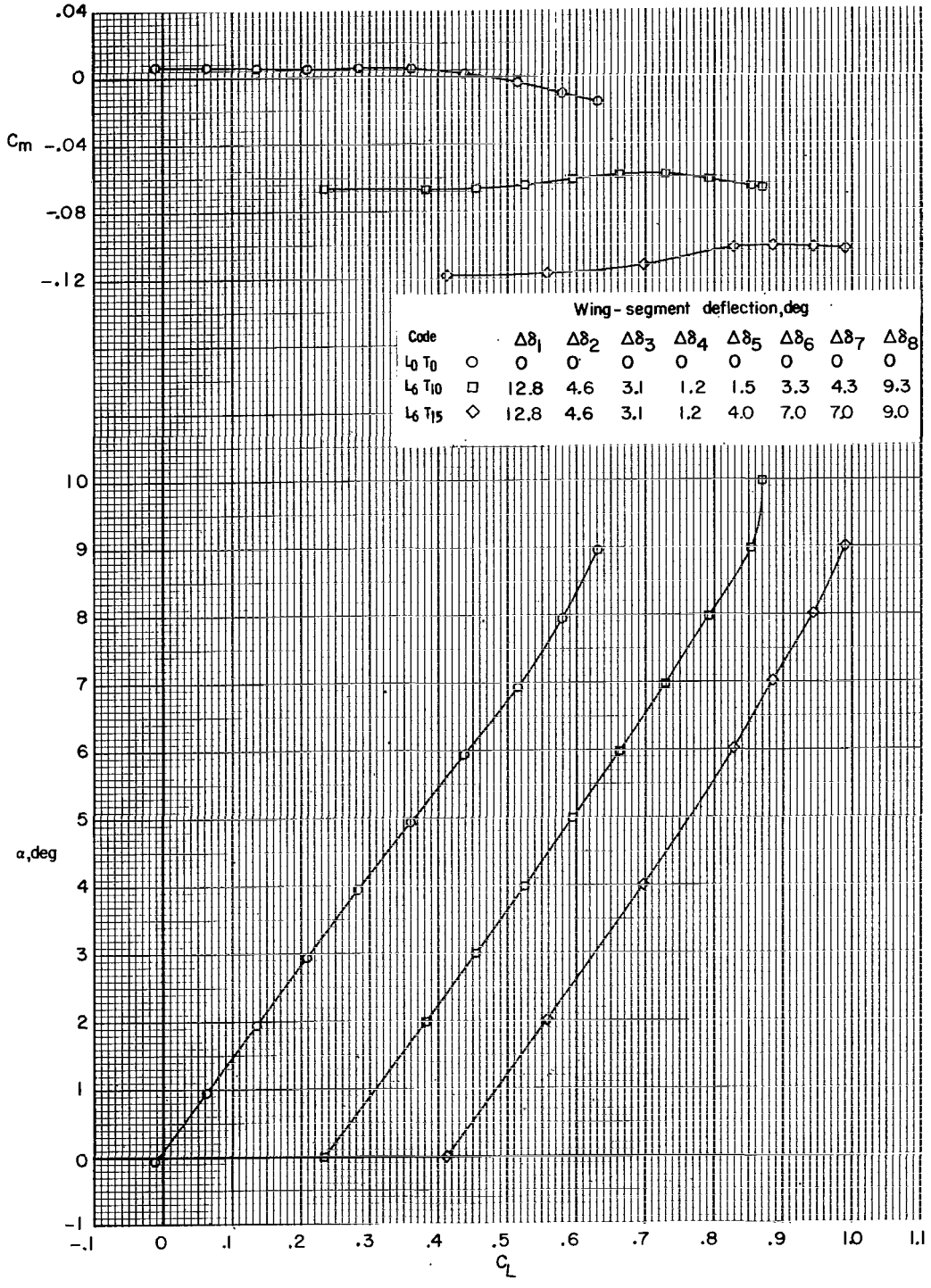

(a) $M = 0.60$; $R_{\bar{c}} = 6.2 \times 10^6$.

Figure 11.- Effect of a selective increase in trailing-edge camber on the longitudinal aerodynamic characteristics.

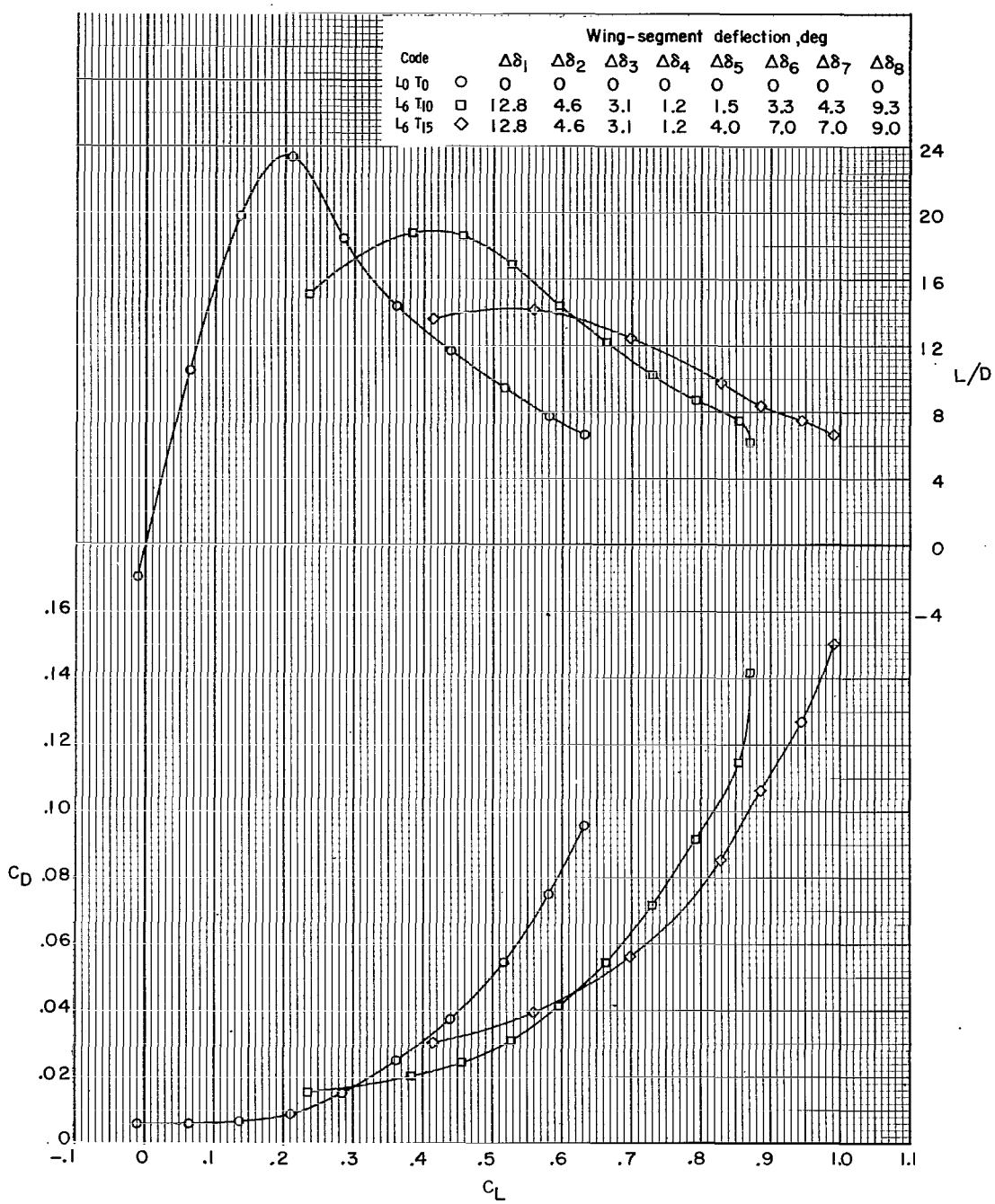

(a) Concluded.

Figure 11.- Continued.

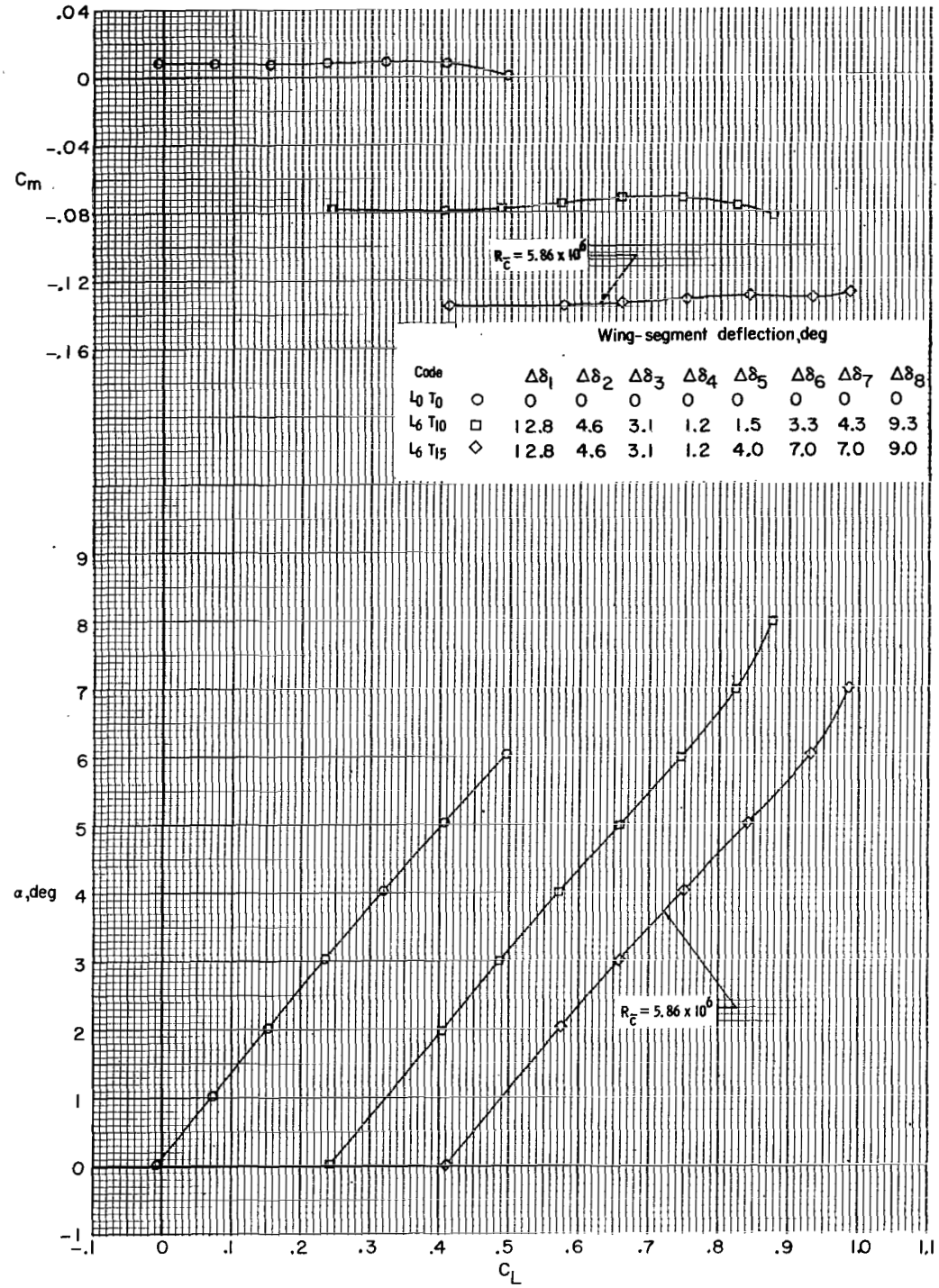

(b) M = 0.80; $R_{\bar{c}} = 7.4 \times 10^6$.

Figure 11.- Continued.

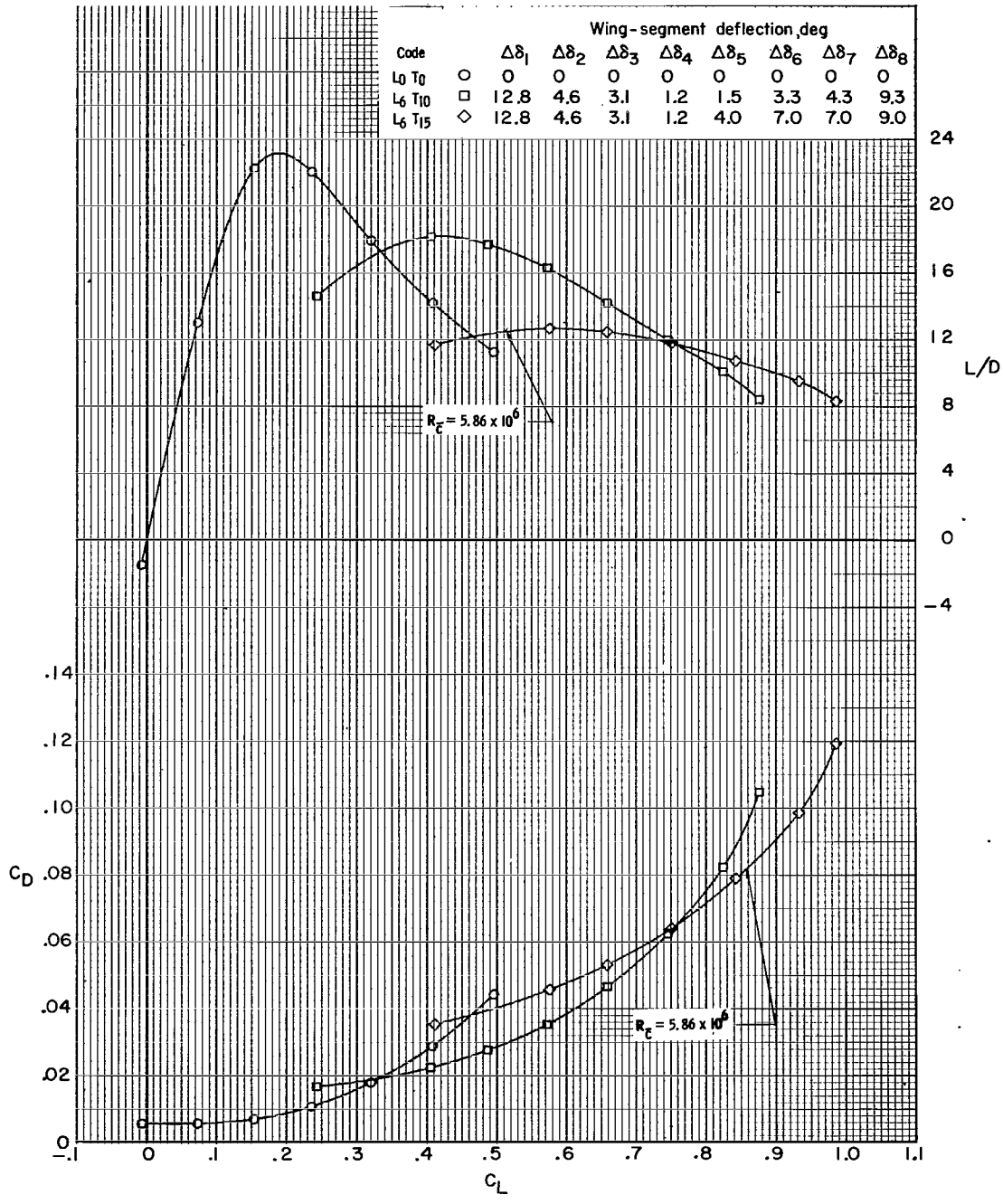

(b) Concluded.

Figure 11.- Continued.

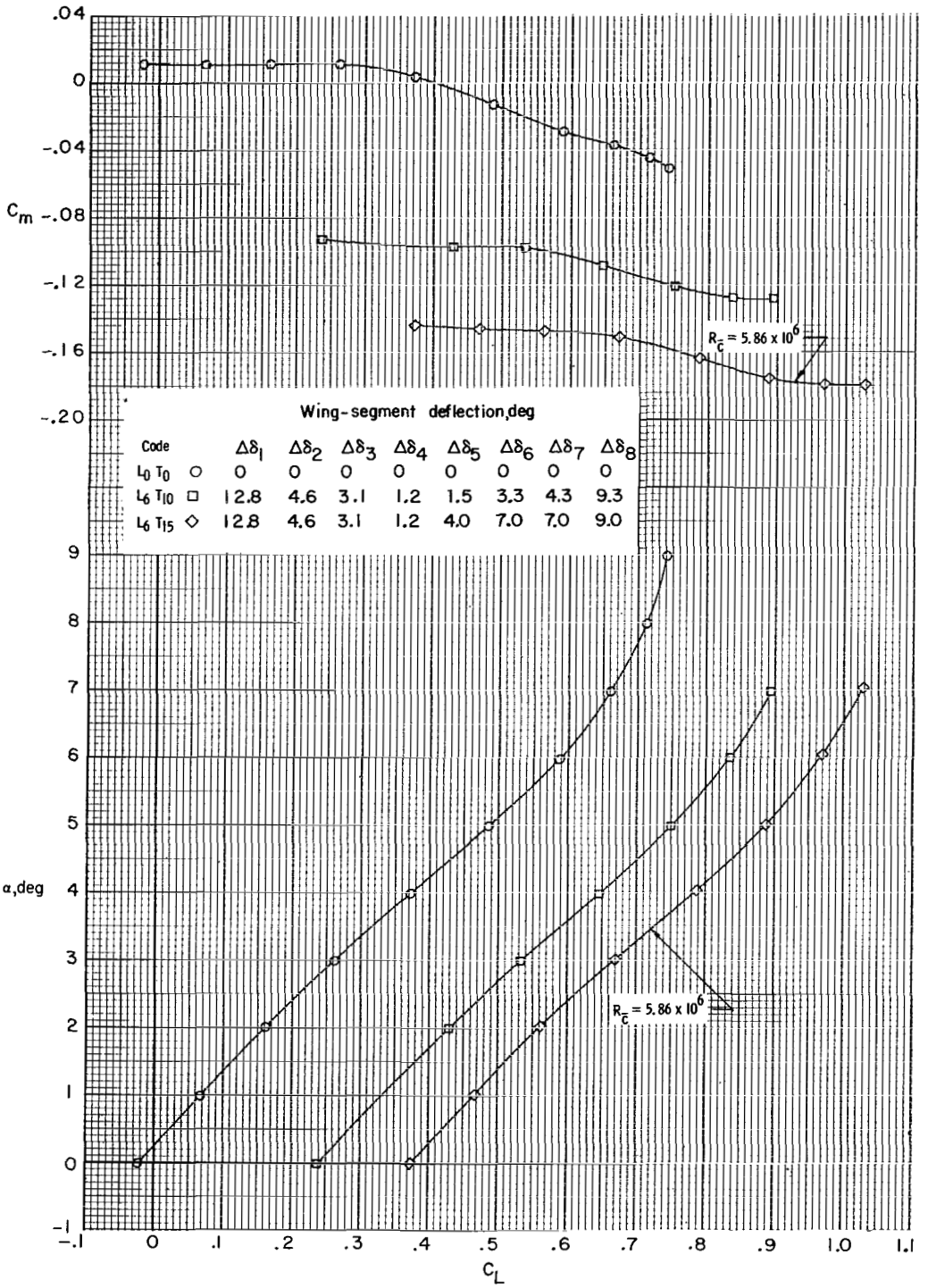

(c) M = 0.90; $R_{\bar{c}} = 7.6 \times 10^6$.

Figure 11.- Continued.

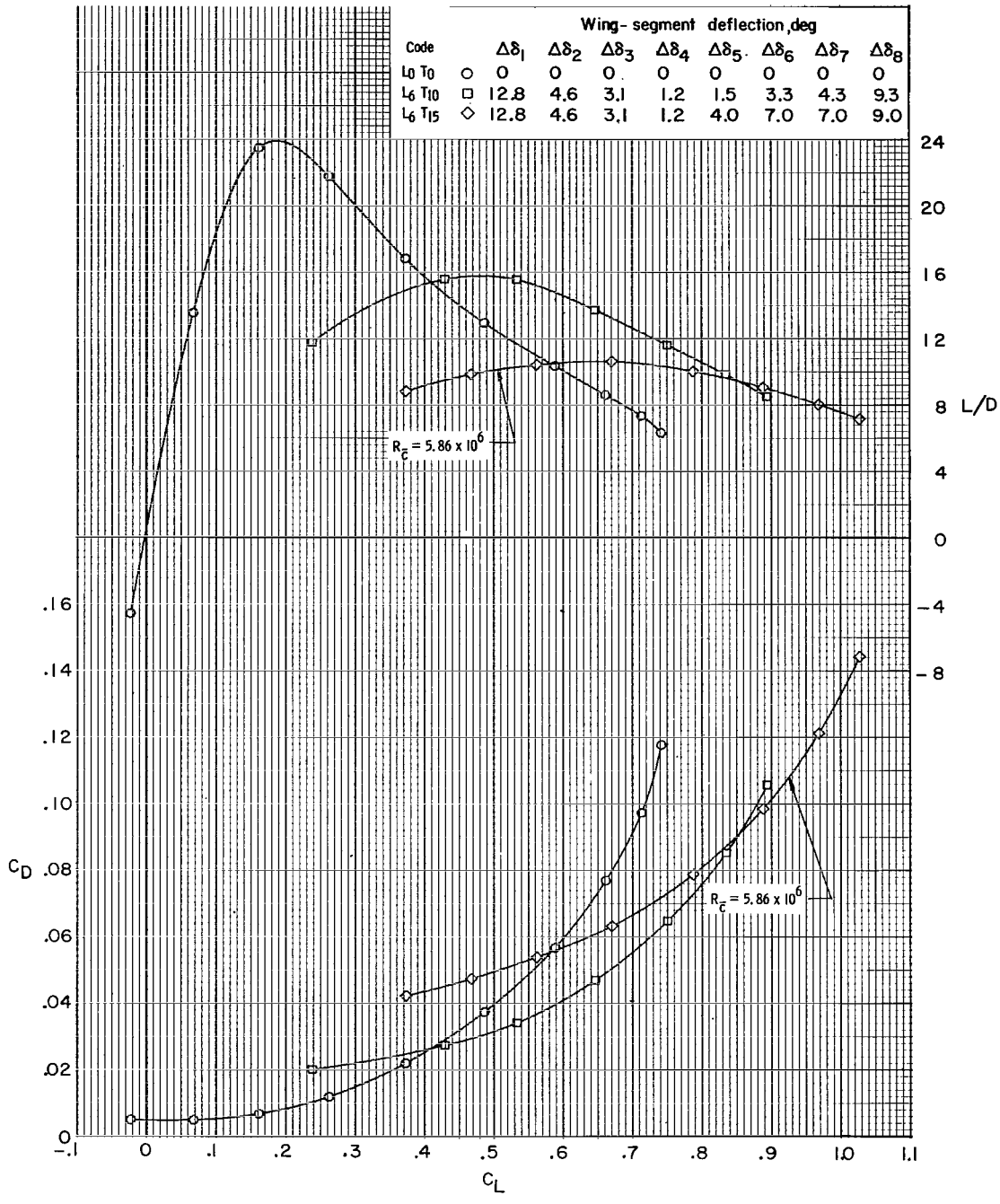

(c) Concluded.

Figure 11.- Concluded.

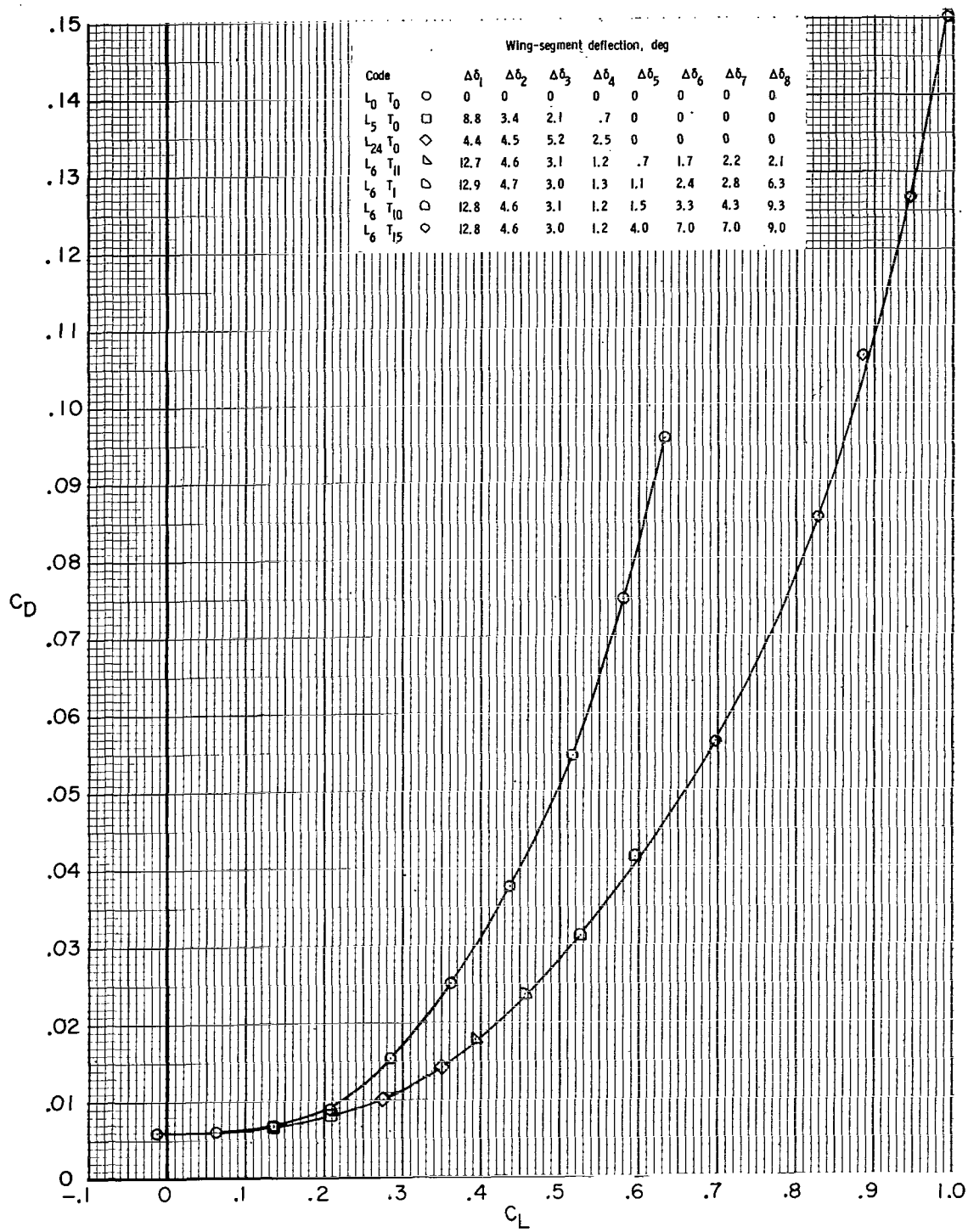

(a) M = 0.60.

Figure 12.- Optimum-camber aerodynamics.

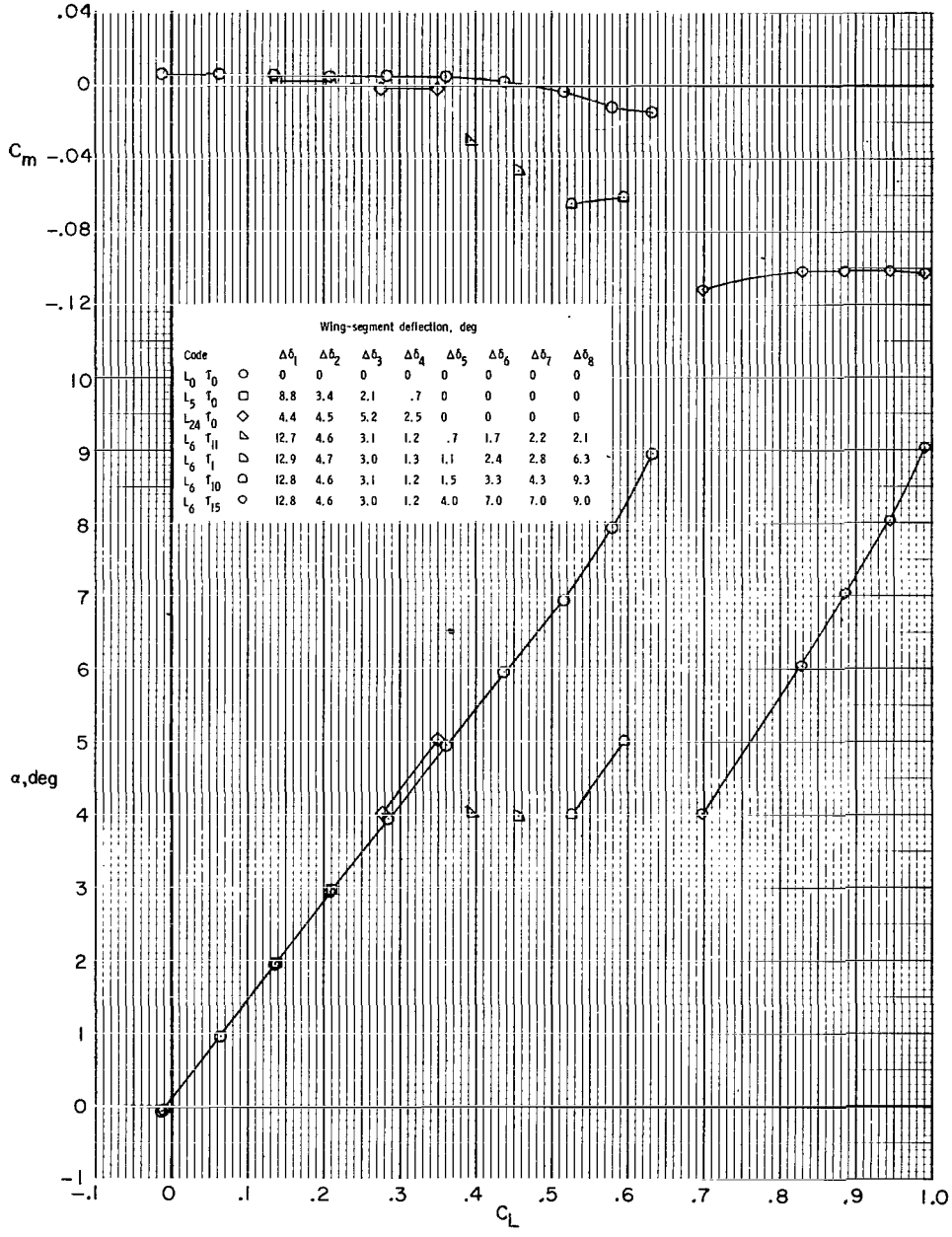

(a) Concluded.

Figure 12.- Continued.

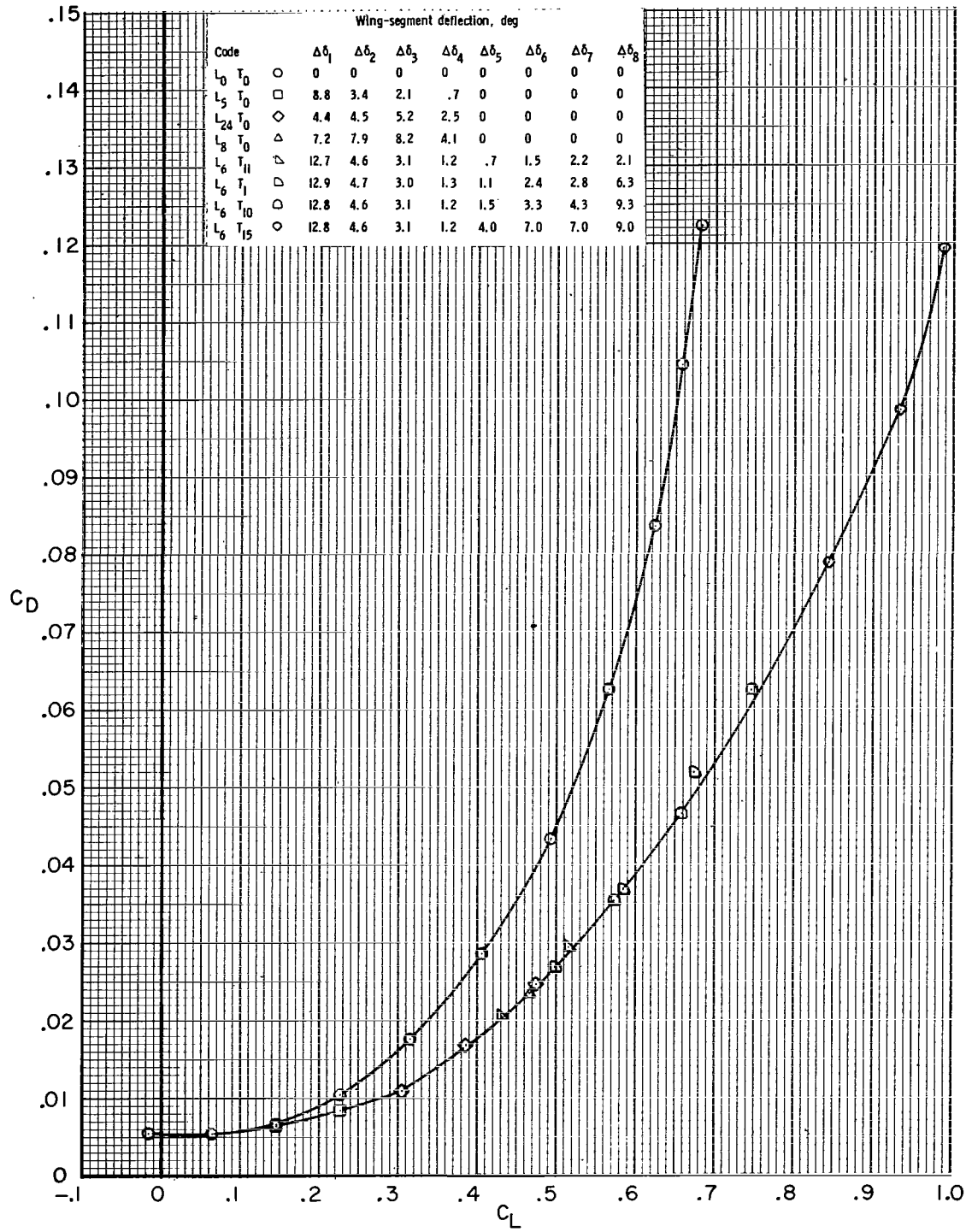

(b) M = 0.80.

Figure 12.- Continued.

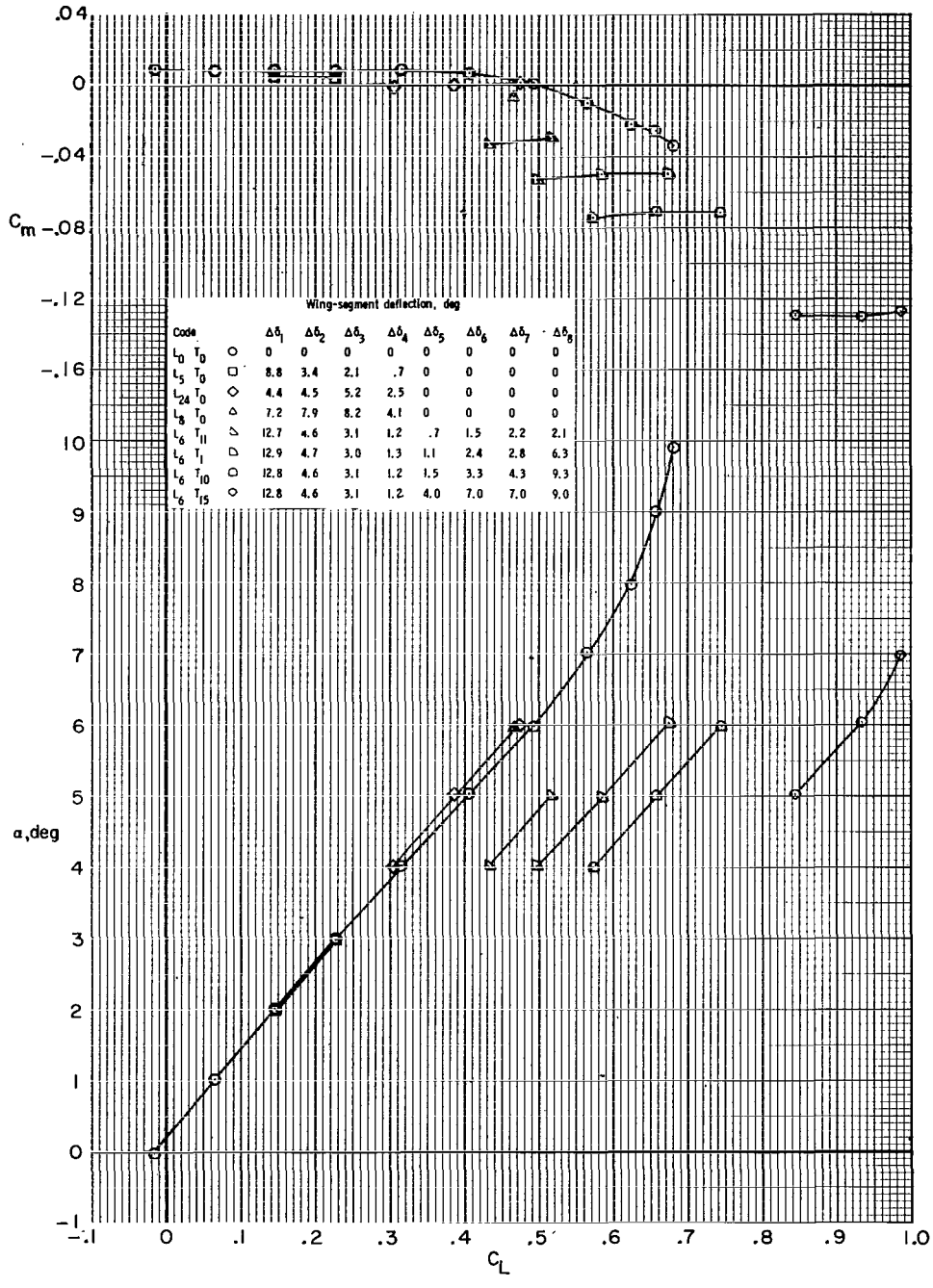

(b) Concluded.

Figure 12.- Continued.

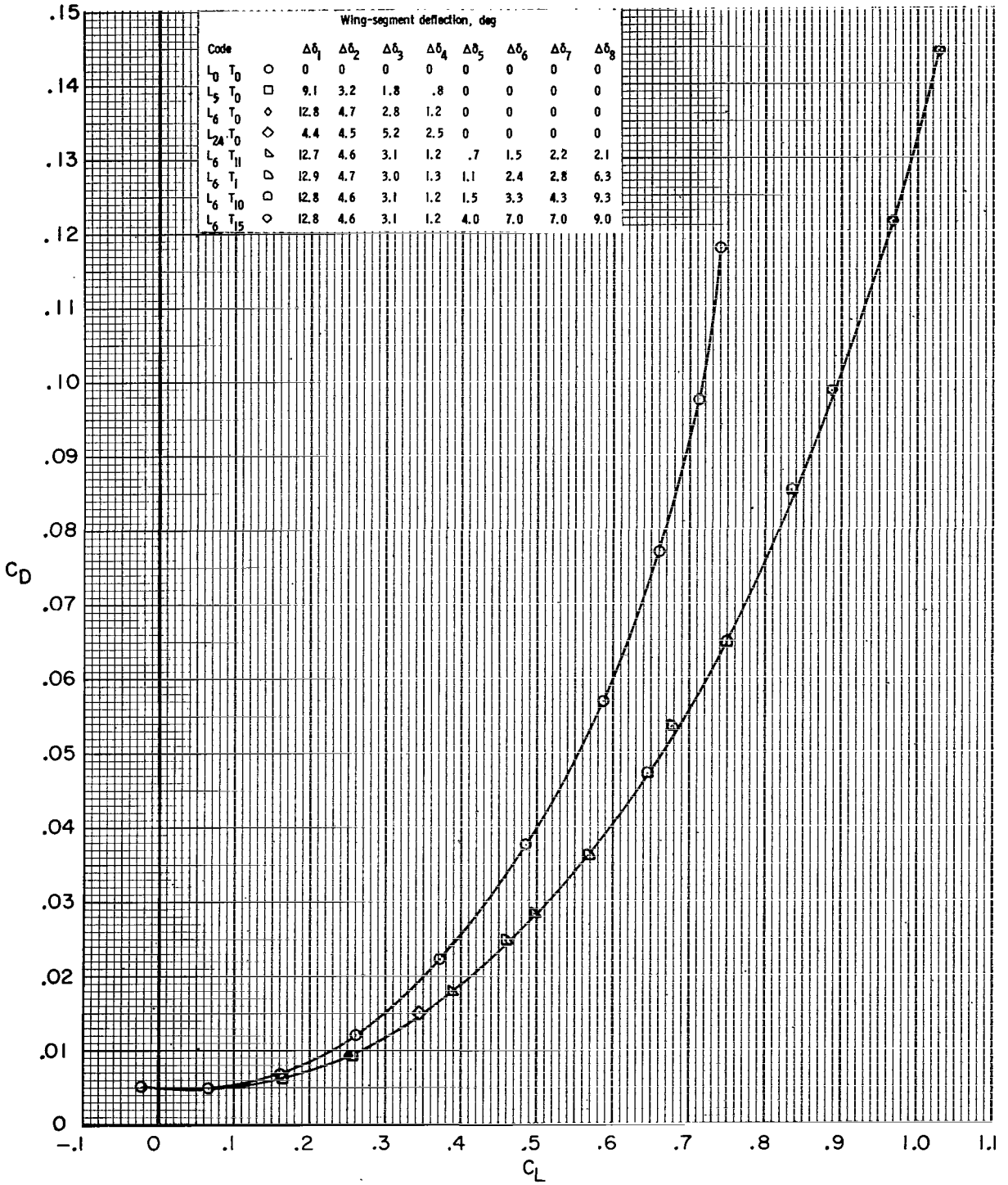

(c) M = 0.90.

Figure 12.- Continued.

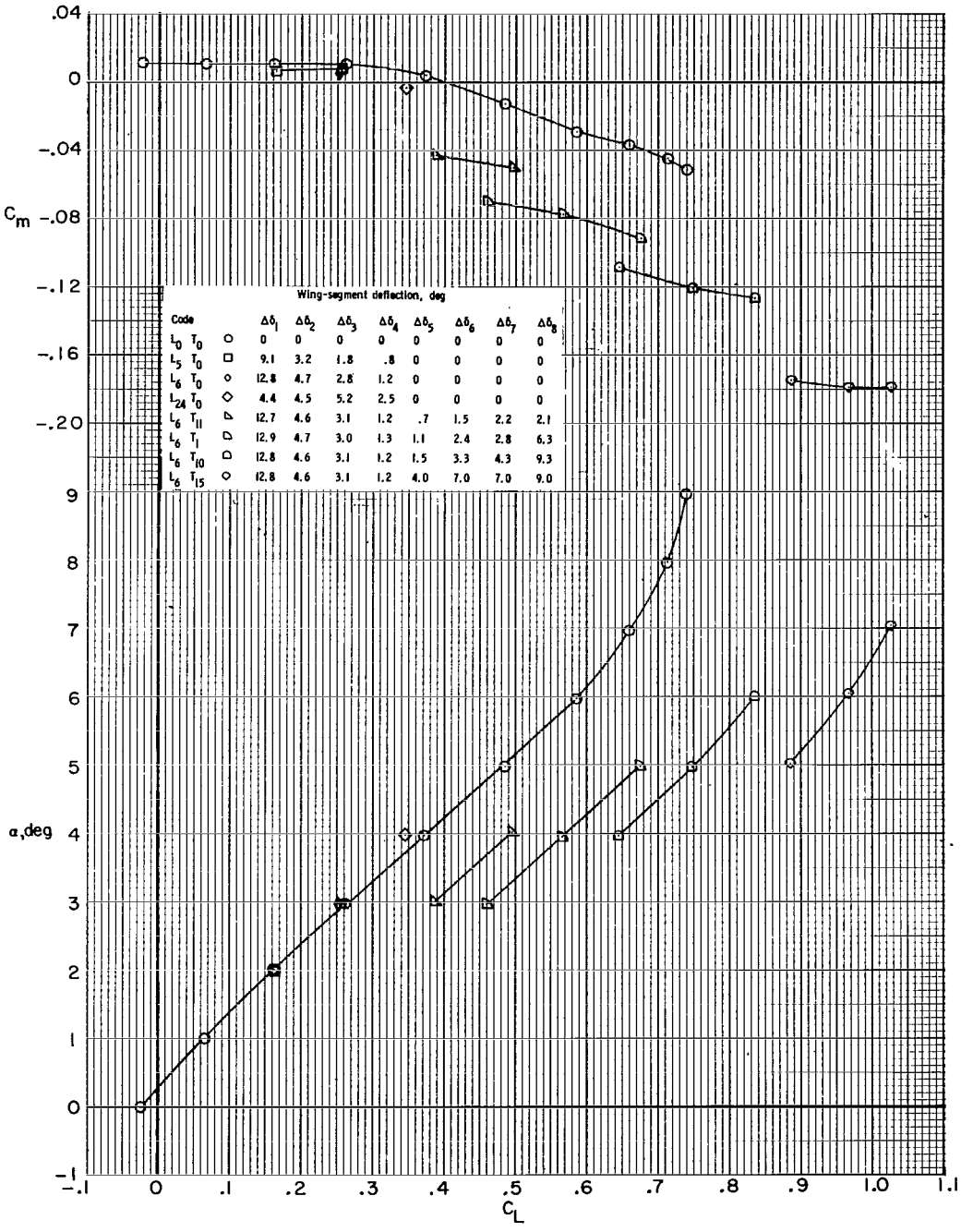

(c) Concluded.

Figure 12.- Concluded.

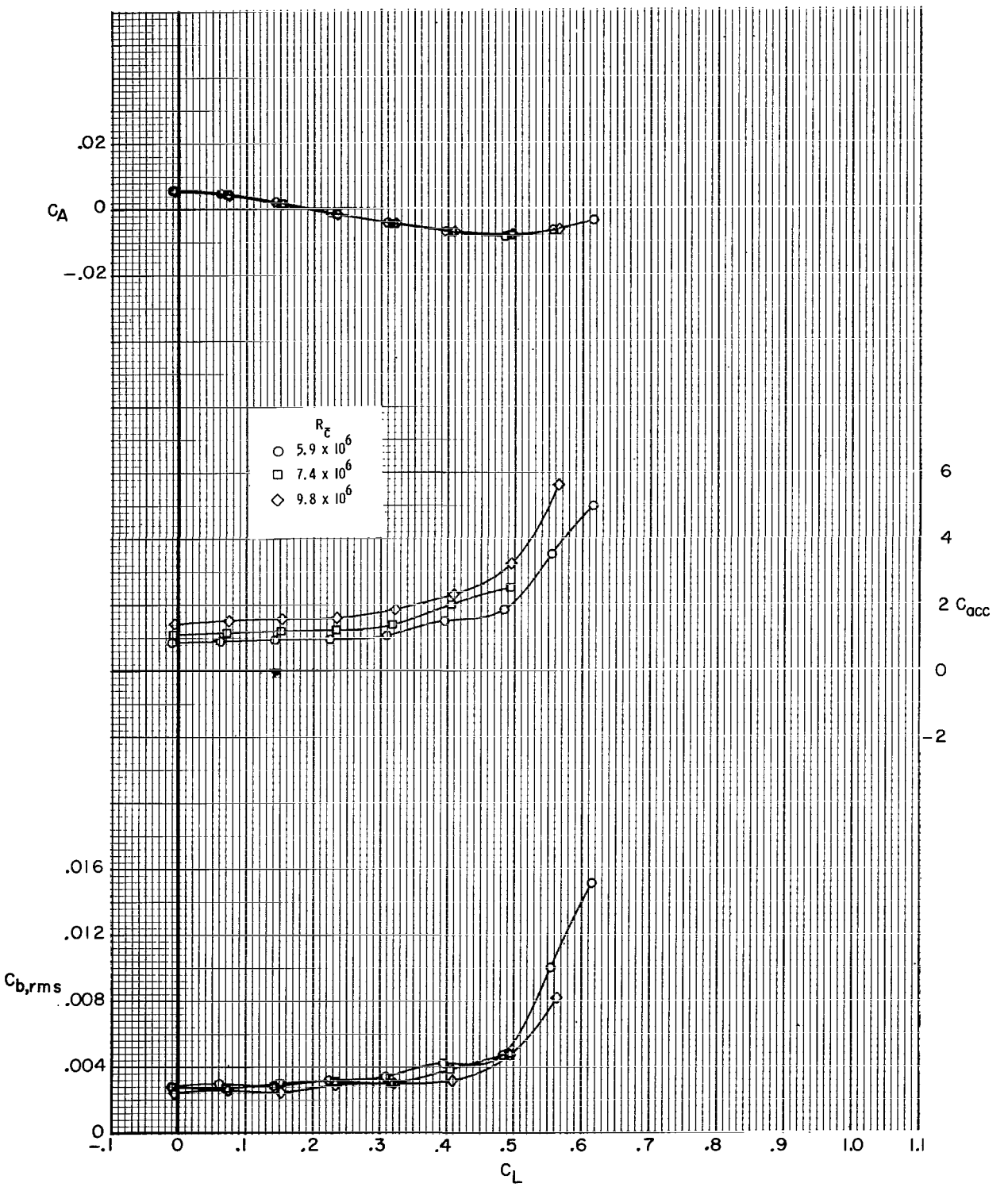

Figure 13.- Effect of Reynolds number on the buffet characteristics. M = 0.80.

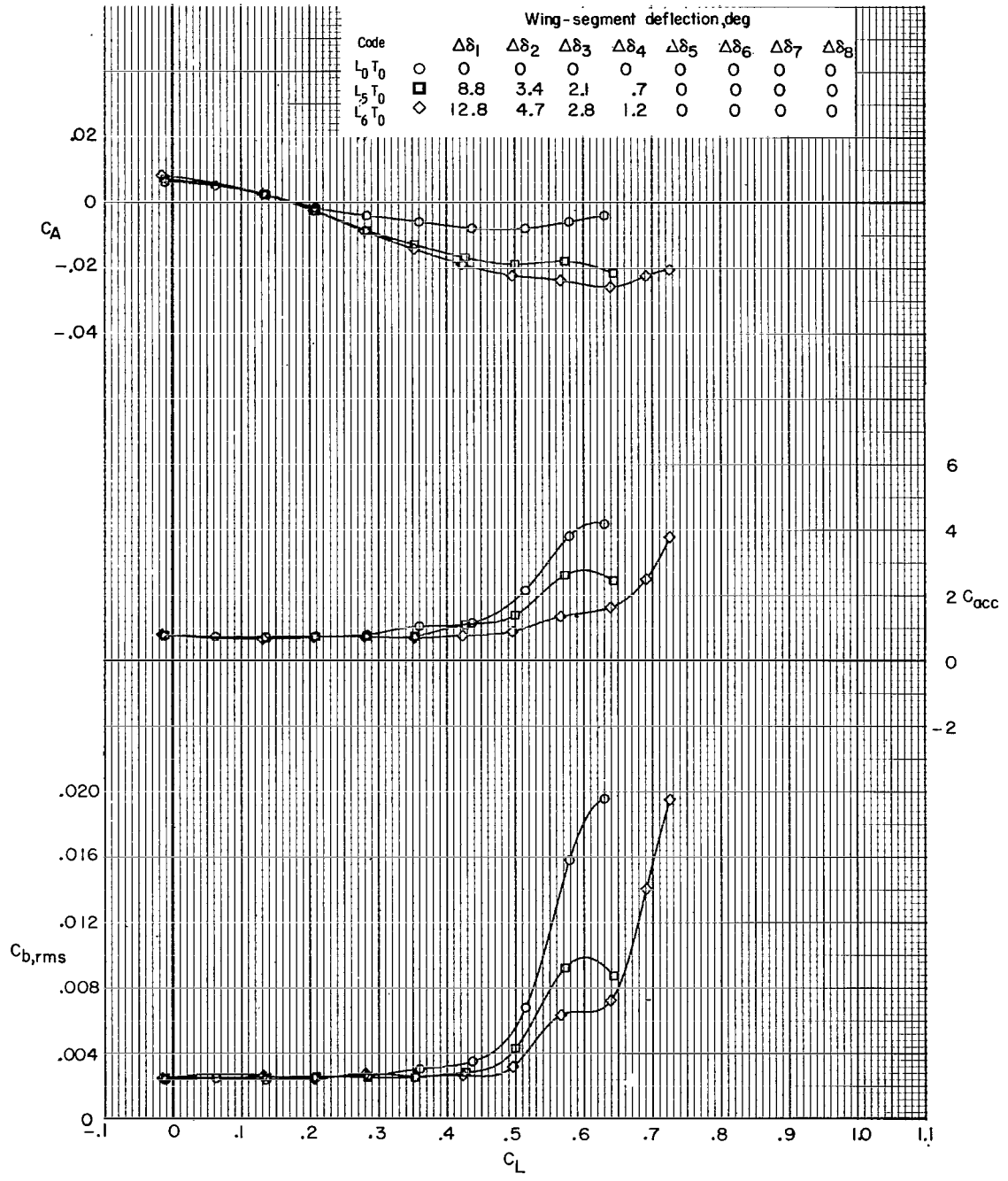

(a) $M = 0.60$; $R_{\bar{c}} = 6.2 \times 10^6$.

Figure 14.- Effect of elliptical leading-edge camber on the buffet characteristics.

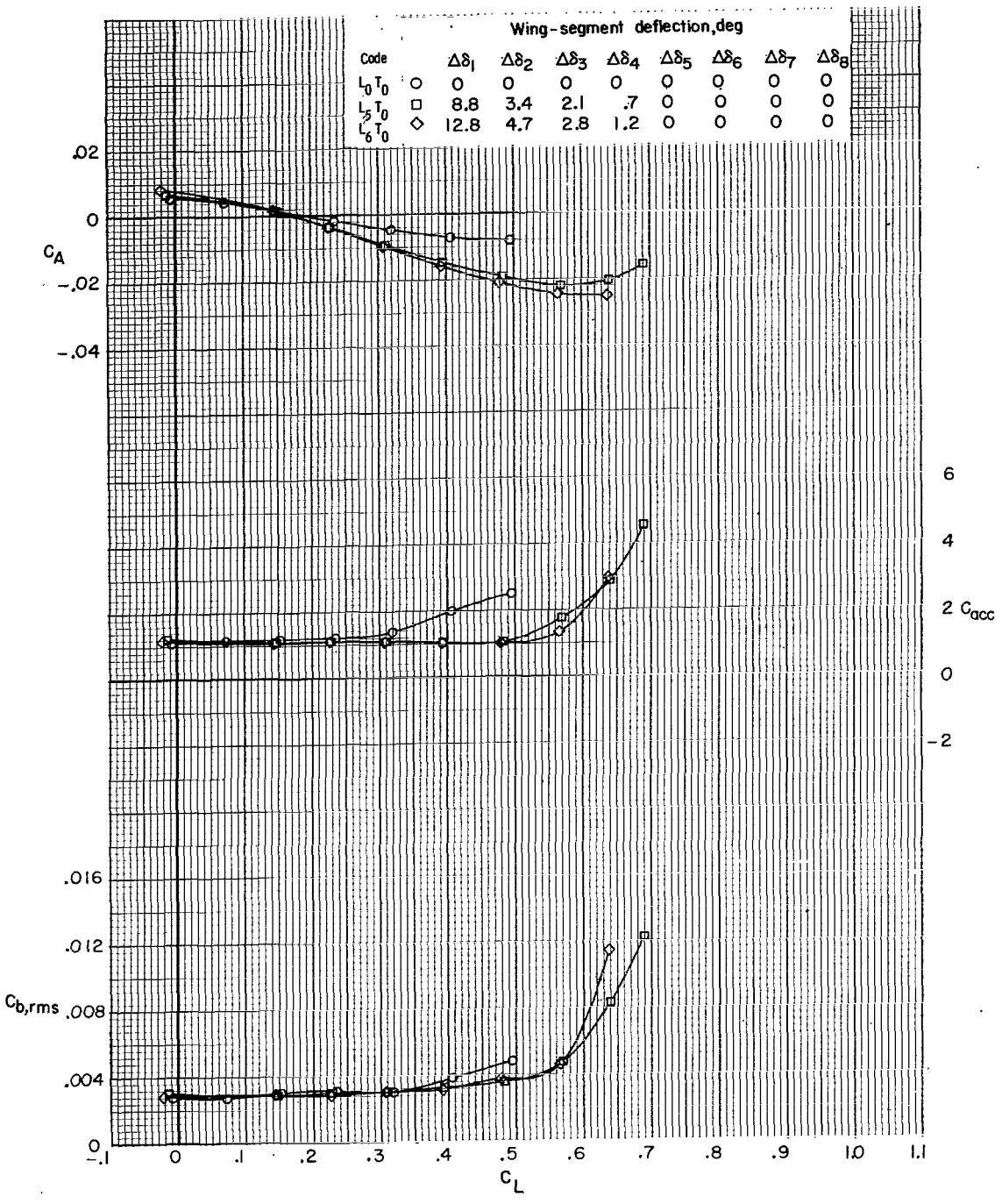

(b) M = 0.80; $R_{\bar{c}} = 7.4 \times 10^6$.

Figure 14.- Continued.

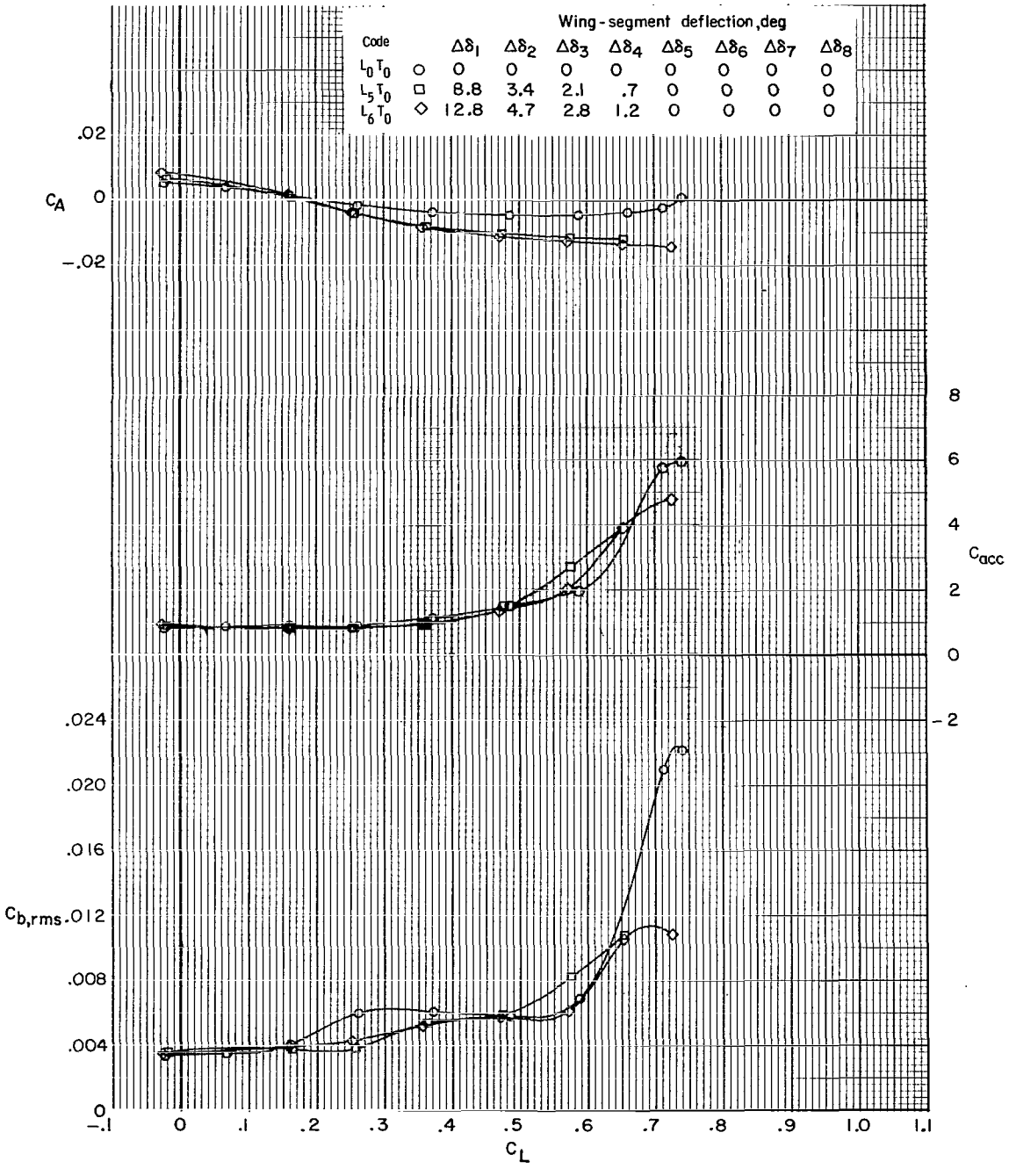

(c) M = 0.90; $R_{\bar{c}} = 7.6 \times 10^6$.

Figure 14.- Concluded.

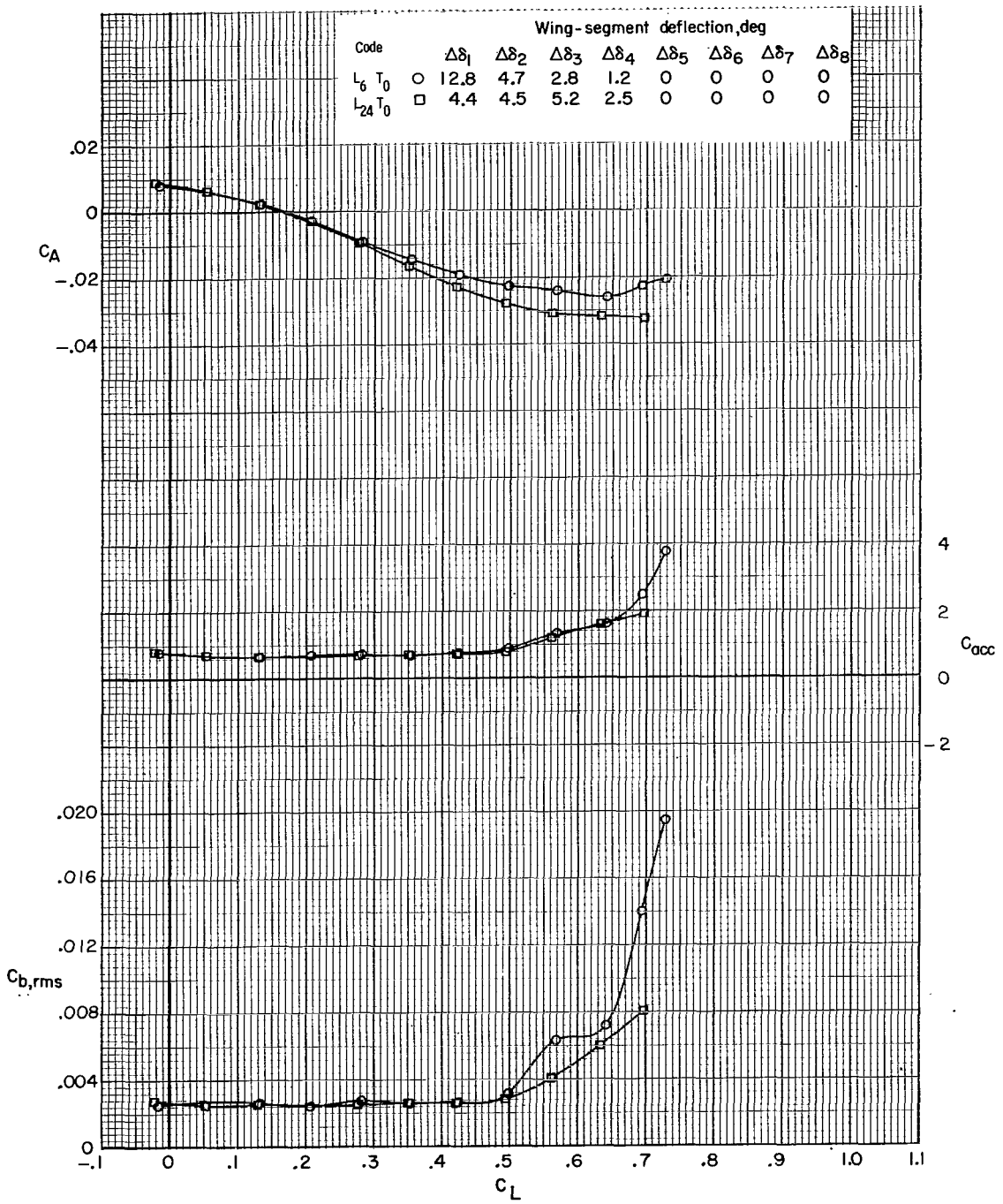

(a) $M = 0.60$; $R_{\bar{c}} = 6.2 \times 10^6$.

Figure 15.- Effect of circular leading-edge camber on the buffet characteristics.

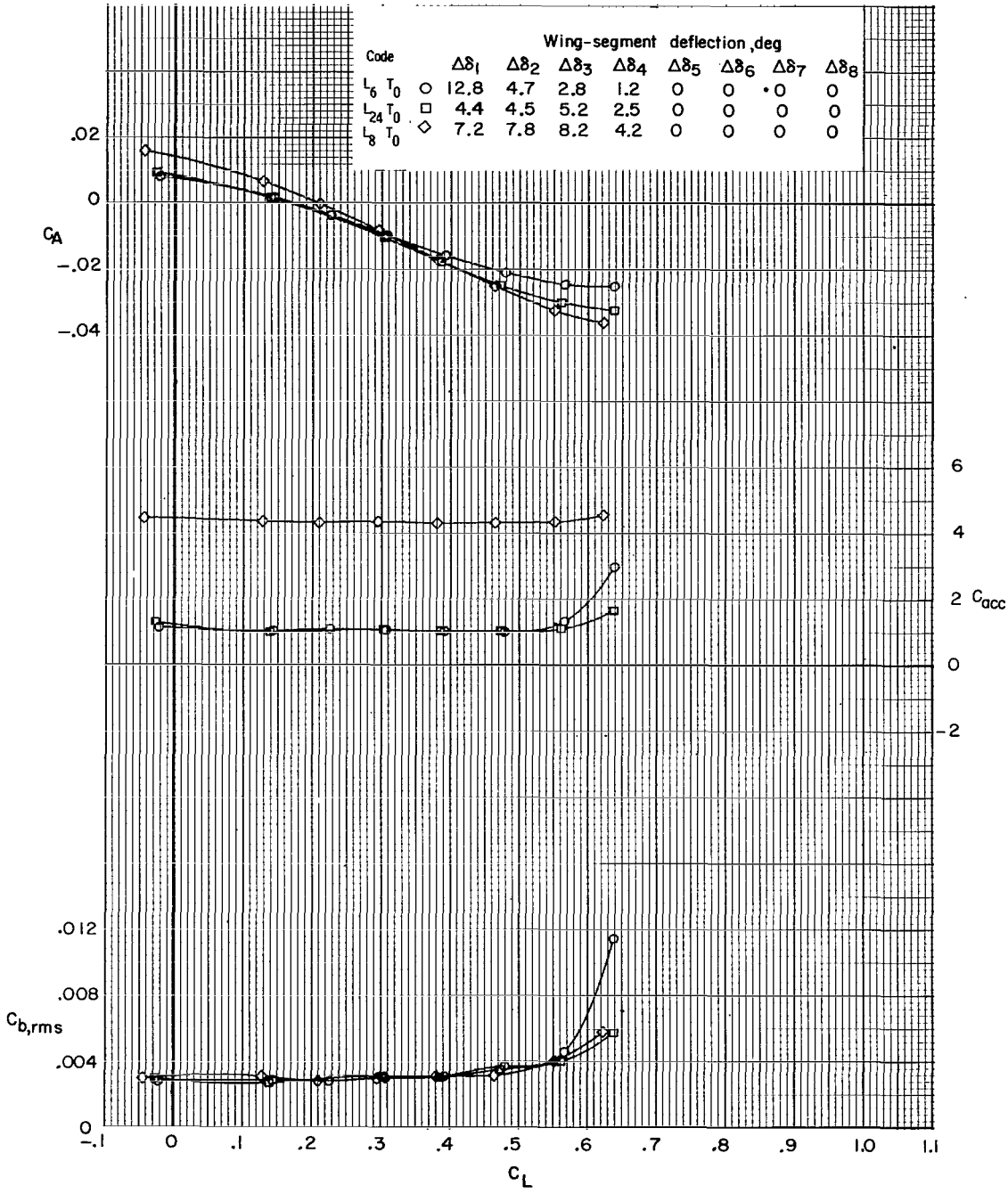

(b) $M = 0.80$; $R_{\bar{c}} = 7.4 \times 10^6$.

Figure 15.- Continued.

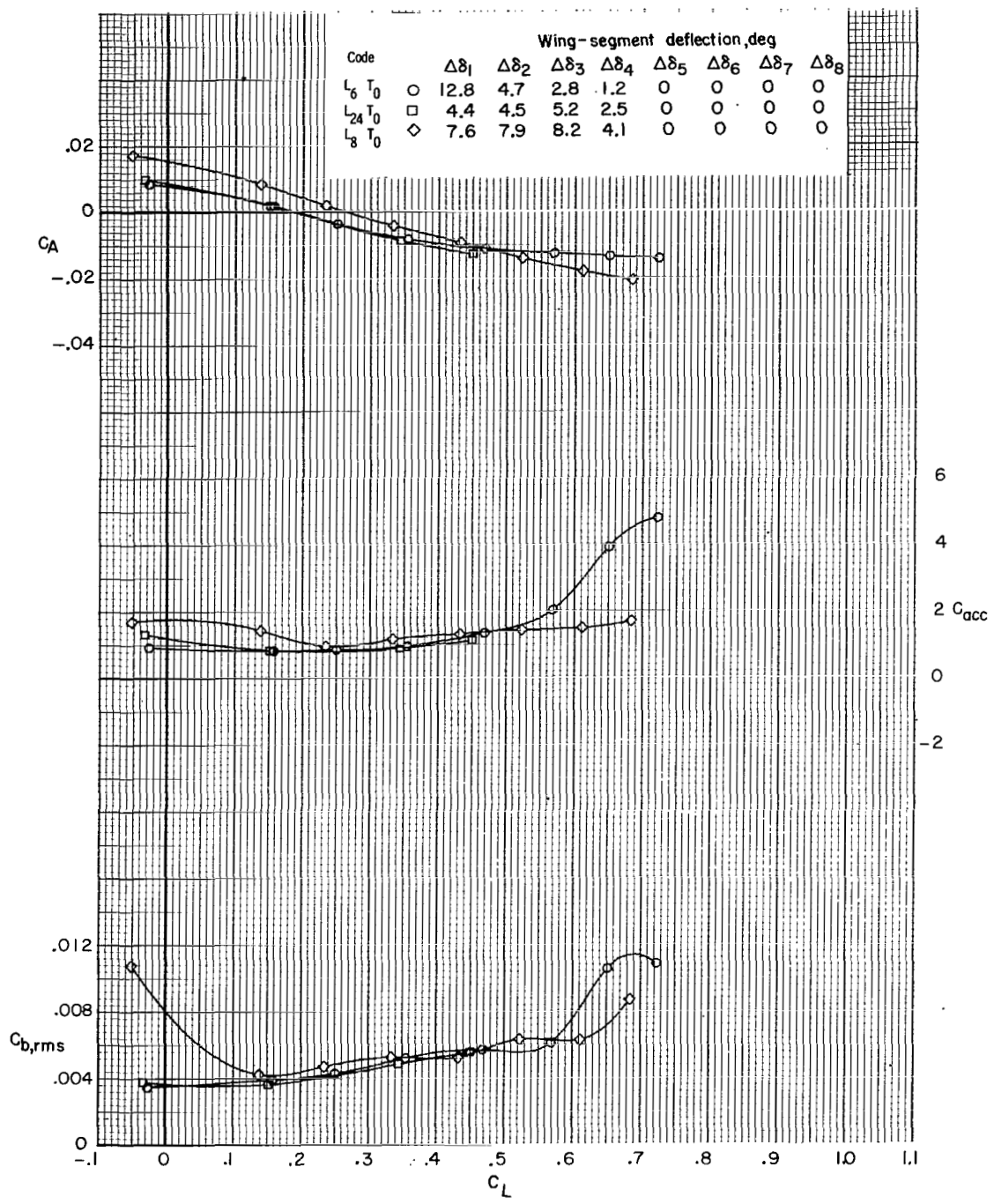

(c) M = 0.90; $R_{\bar{c}} = 7.6 \times 10^6$.

Figure 15.- Concluded.

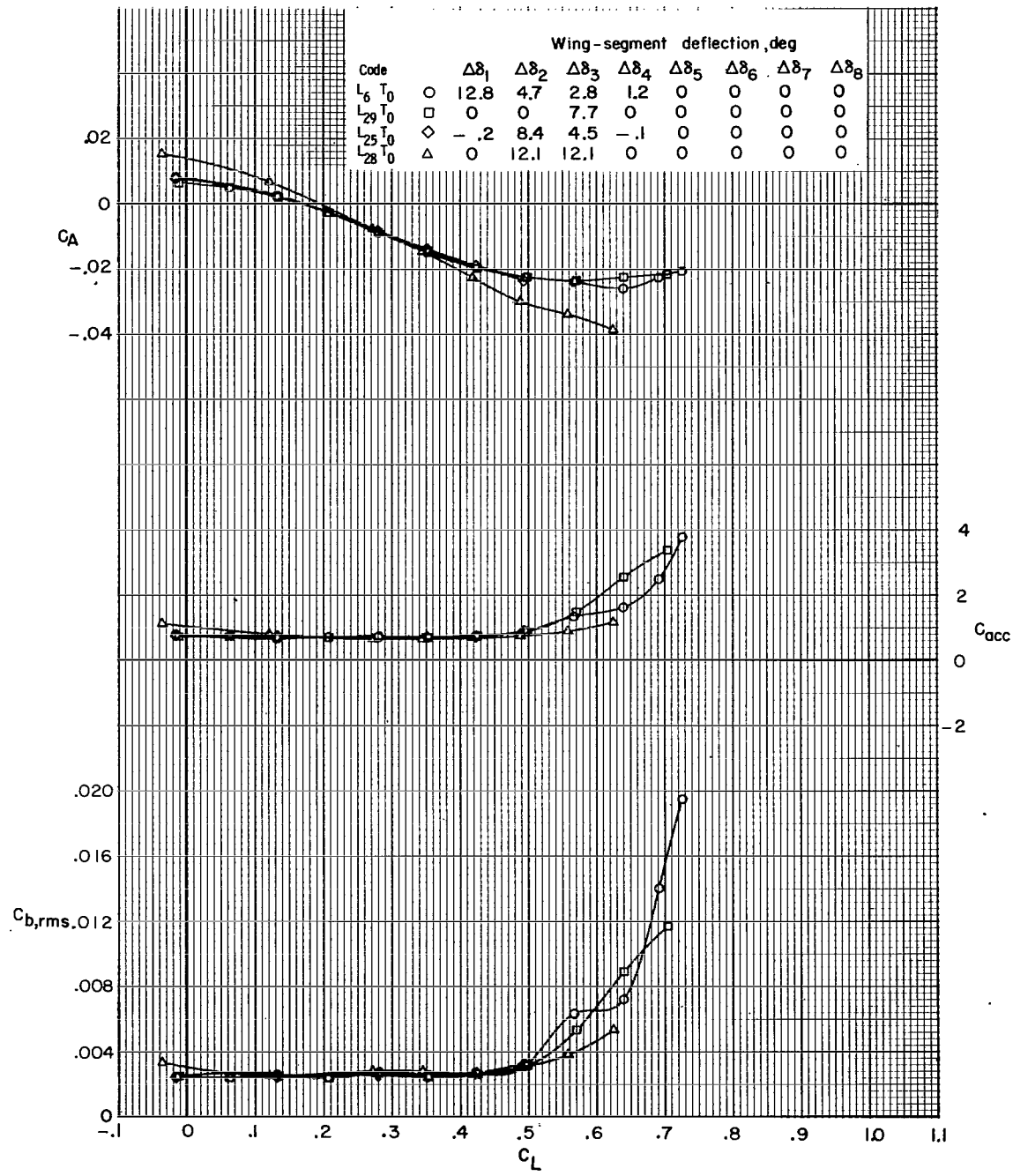

(a) $M = 0.60$; $R_{\bar{c}} = 6.2 \times 10^6$.

Figure 16.- Effect of simplified leading-edge camber on the buffet characteristics.

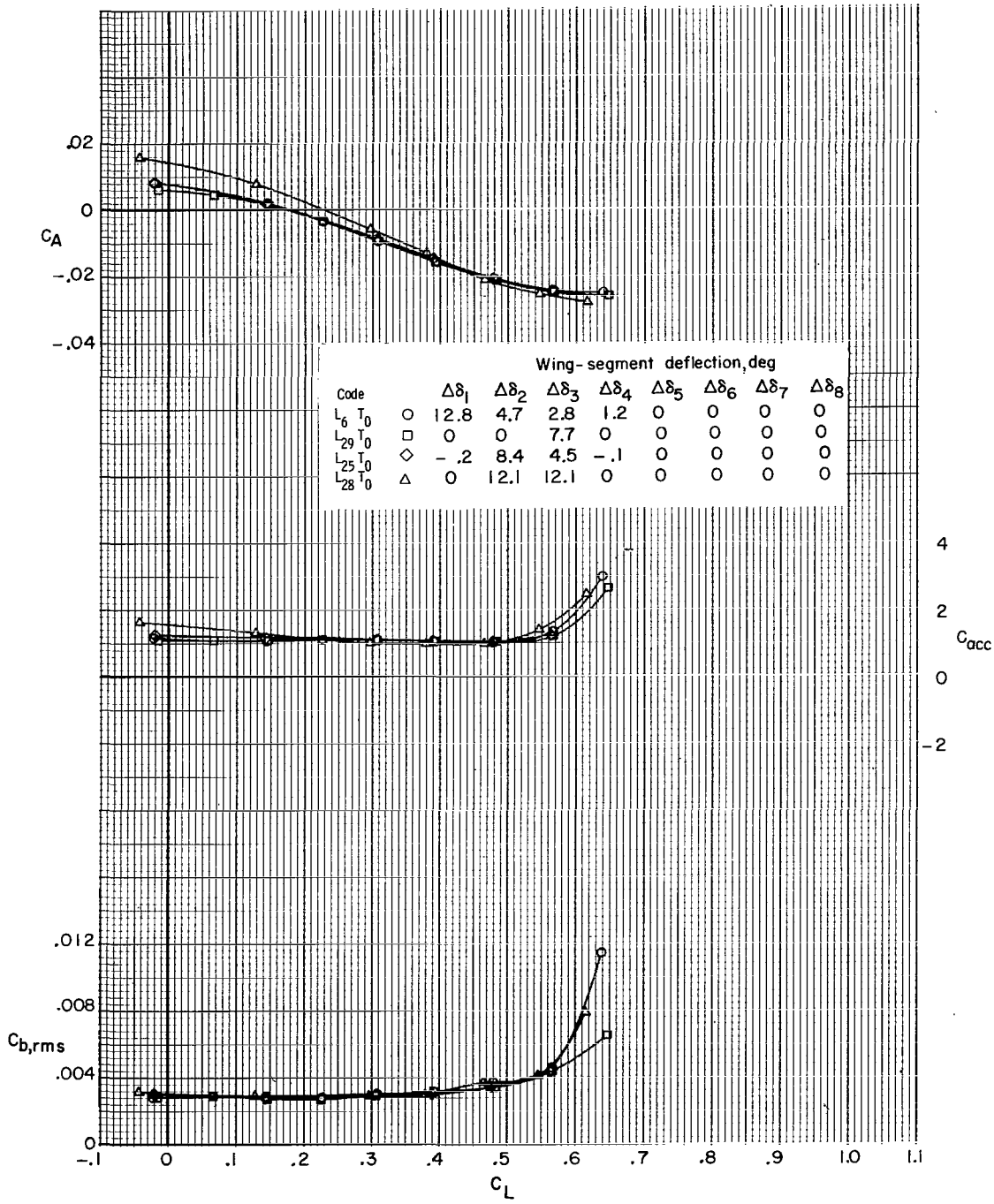

(b) M = 0.80; $R_{\bar{c}} = 7.4 \times 10^6$.

Figure 16.- Continued.

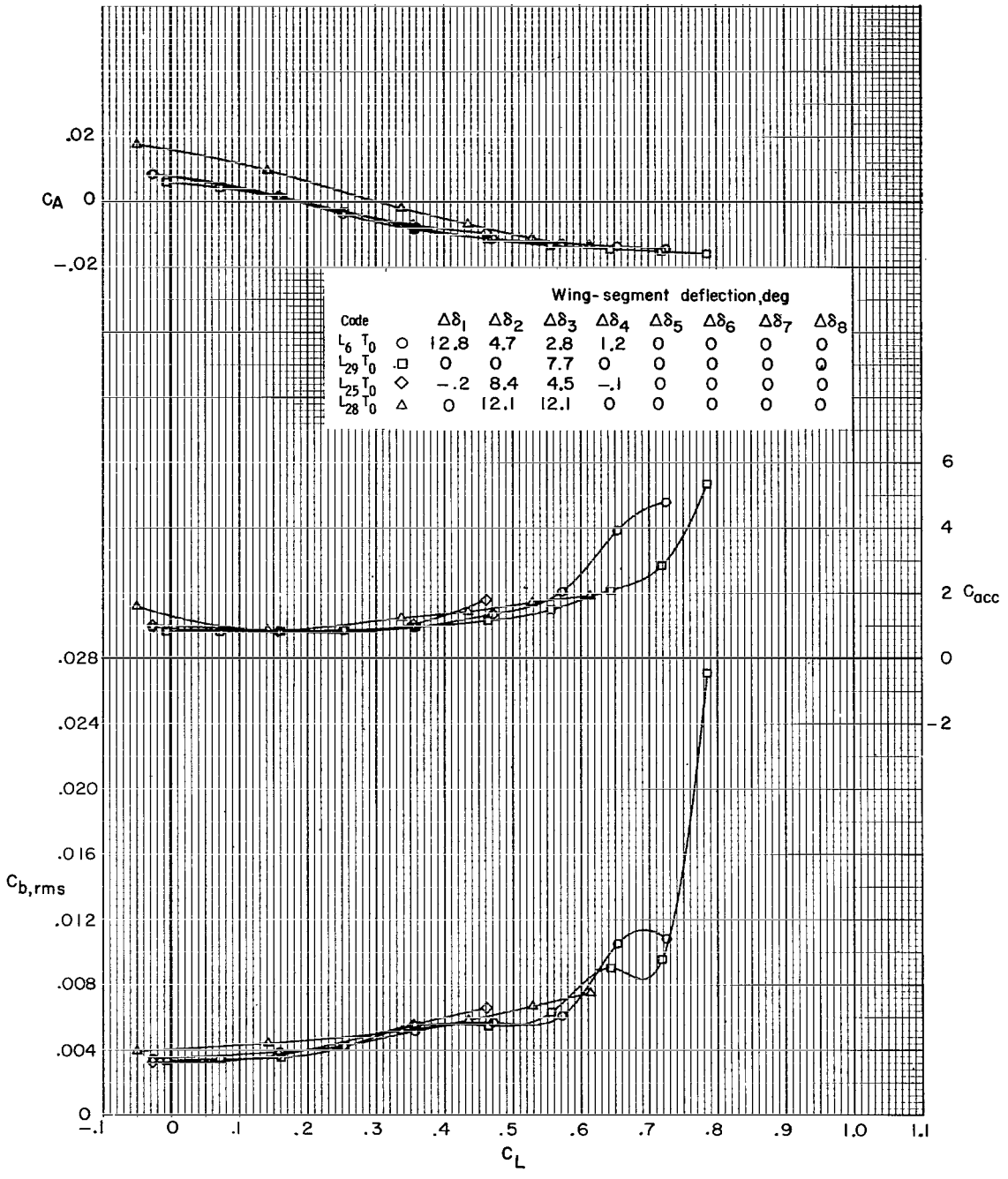

(c) M = 0.90; $R_{\bar{c}} = 7.6 \times 10^6$.

Figure 16.- Concluded.

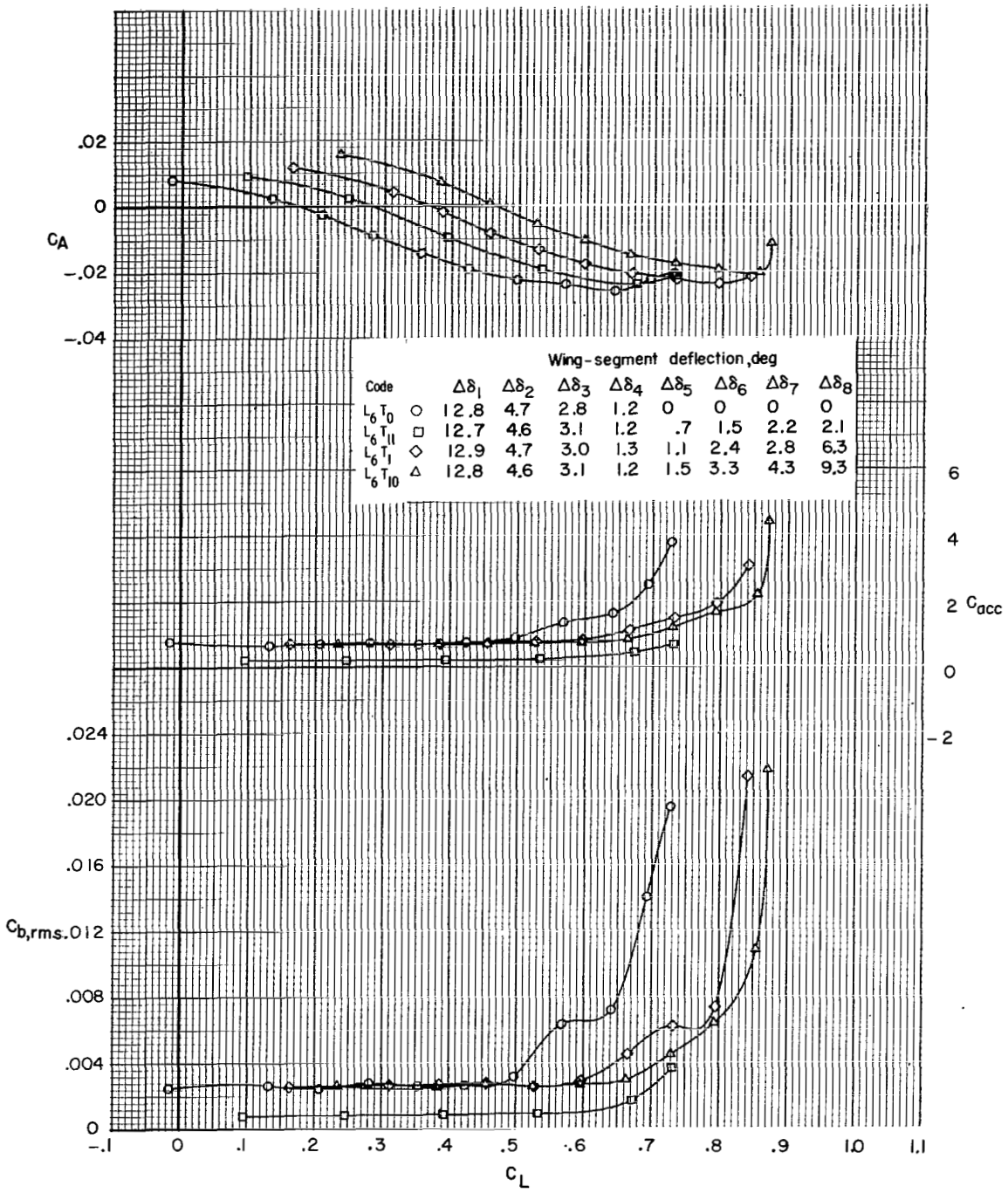

(a) M = 0.60; $R_{\bar{c}} = 6.2 \times 10^6$.

Figure 17.- Effect of elliptical trailing-edge camber on the buffet characteristics.

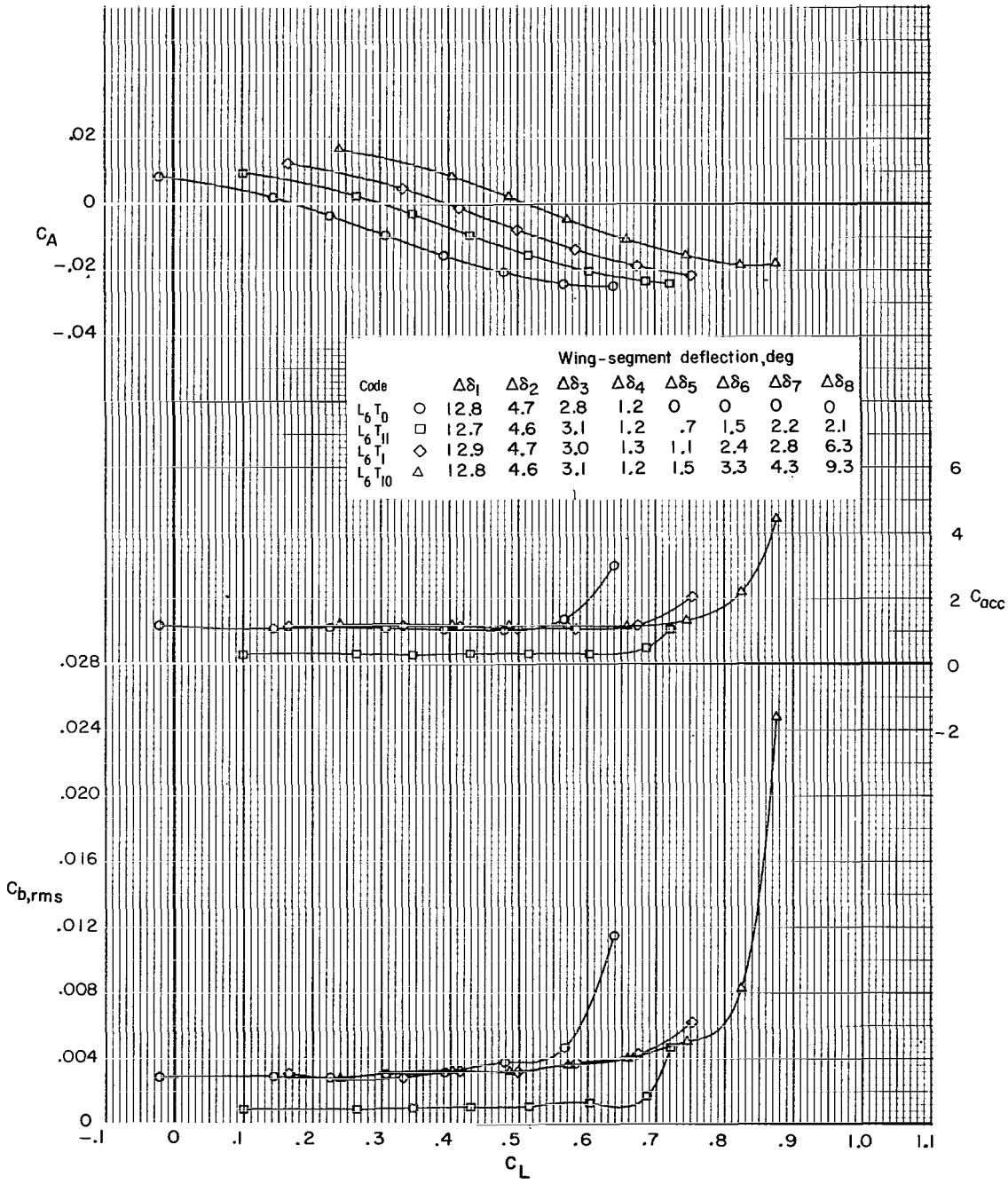

(b) M = 0.80; $R_{\bar{c}} = 7.4 \times 10^6$.

Figure 17.- Continued.

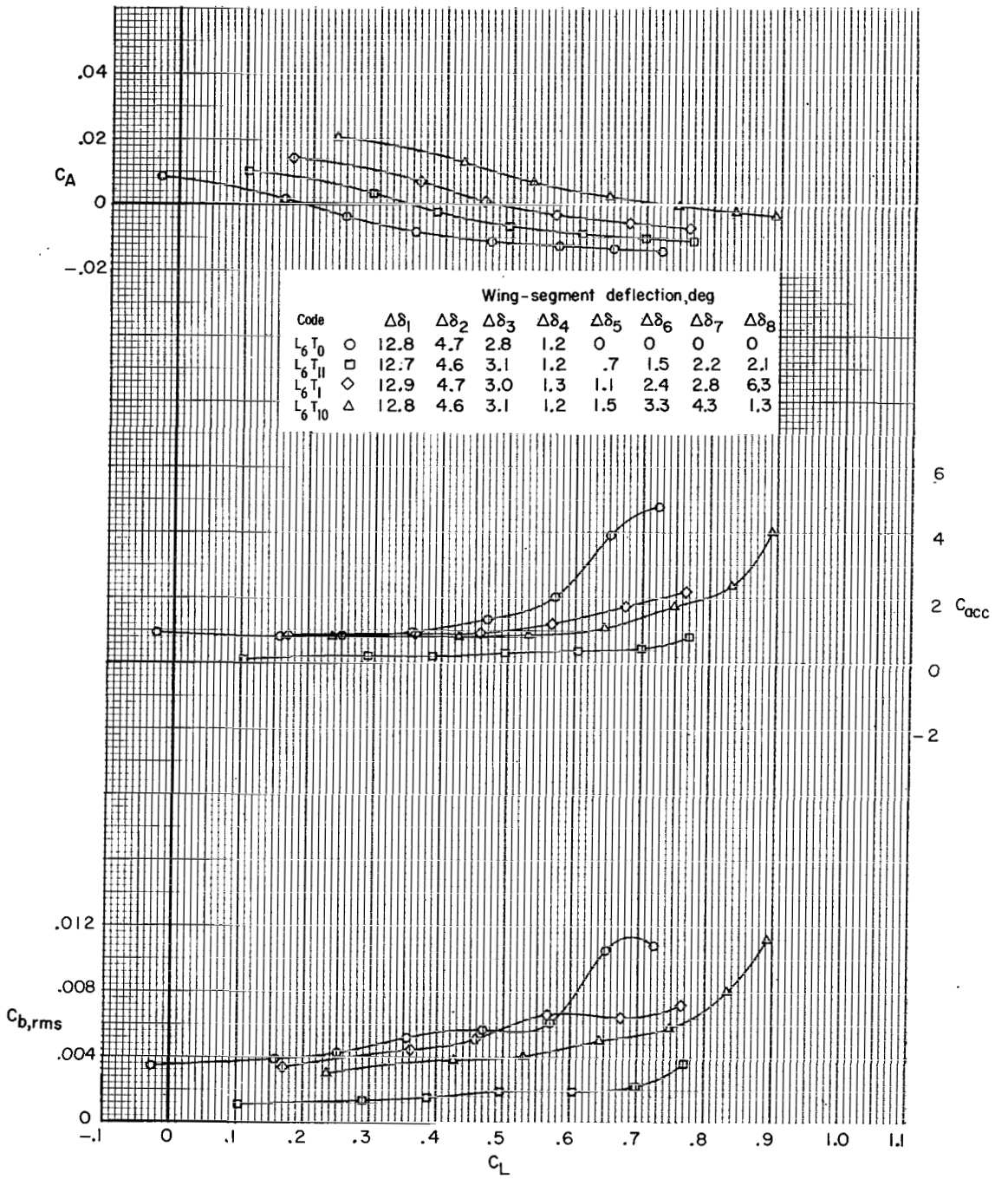

(c) M = 0.90; $R_{\bar{c}} = 7.6 \times 10^6$.

Figure 17.- Concluded.

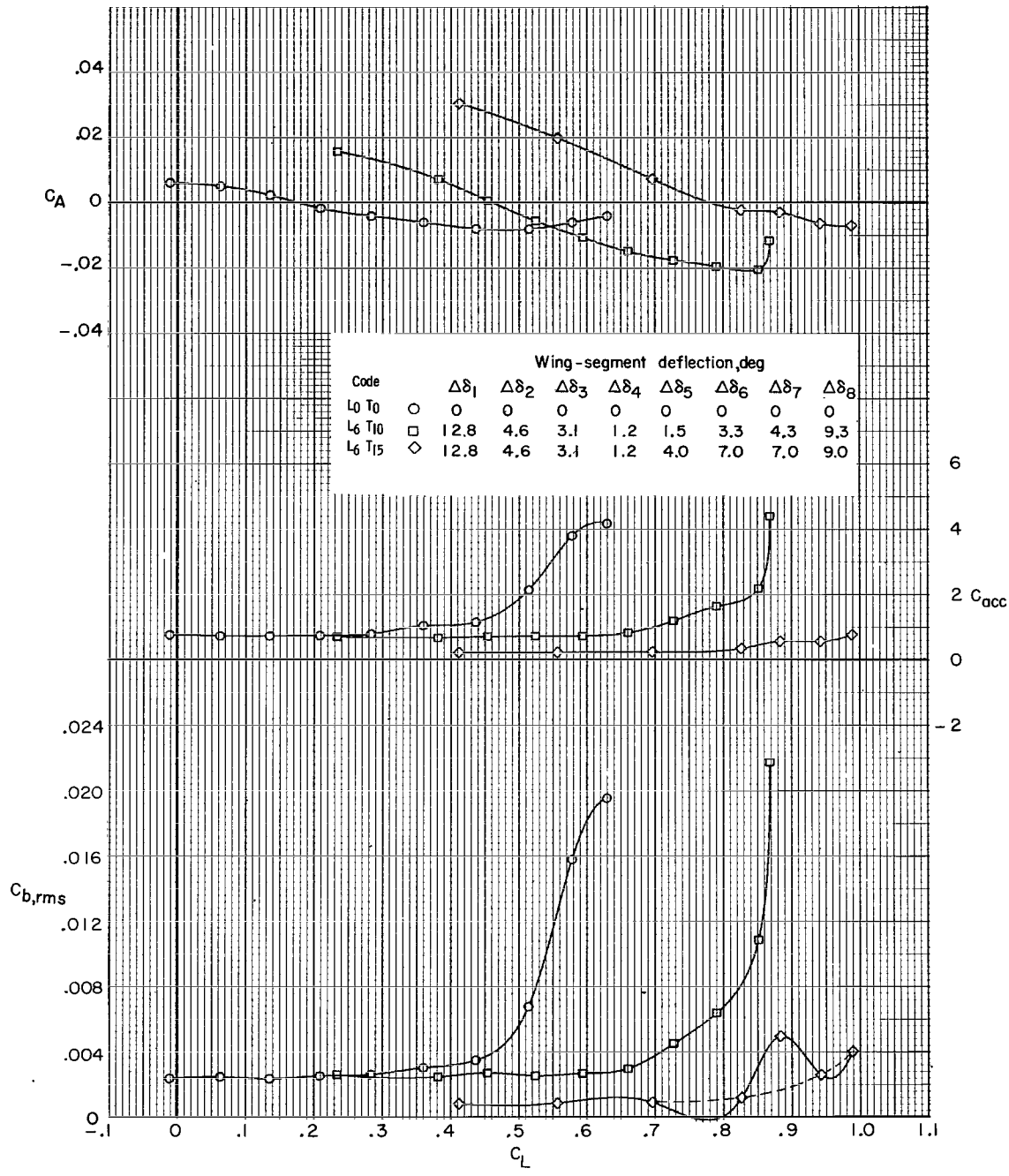

(a) $M = 0.60$; $R_{\bar{c}} = 6.2 \times 10^6$.

Figure 18.- Effect of a selective increase in trailing-edge camber on the buffet characteristics.

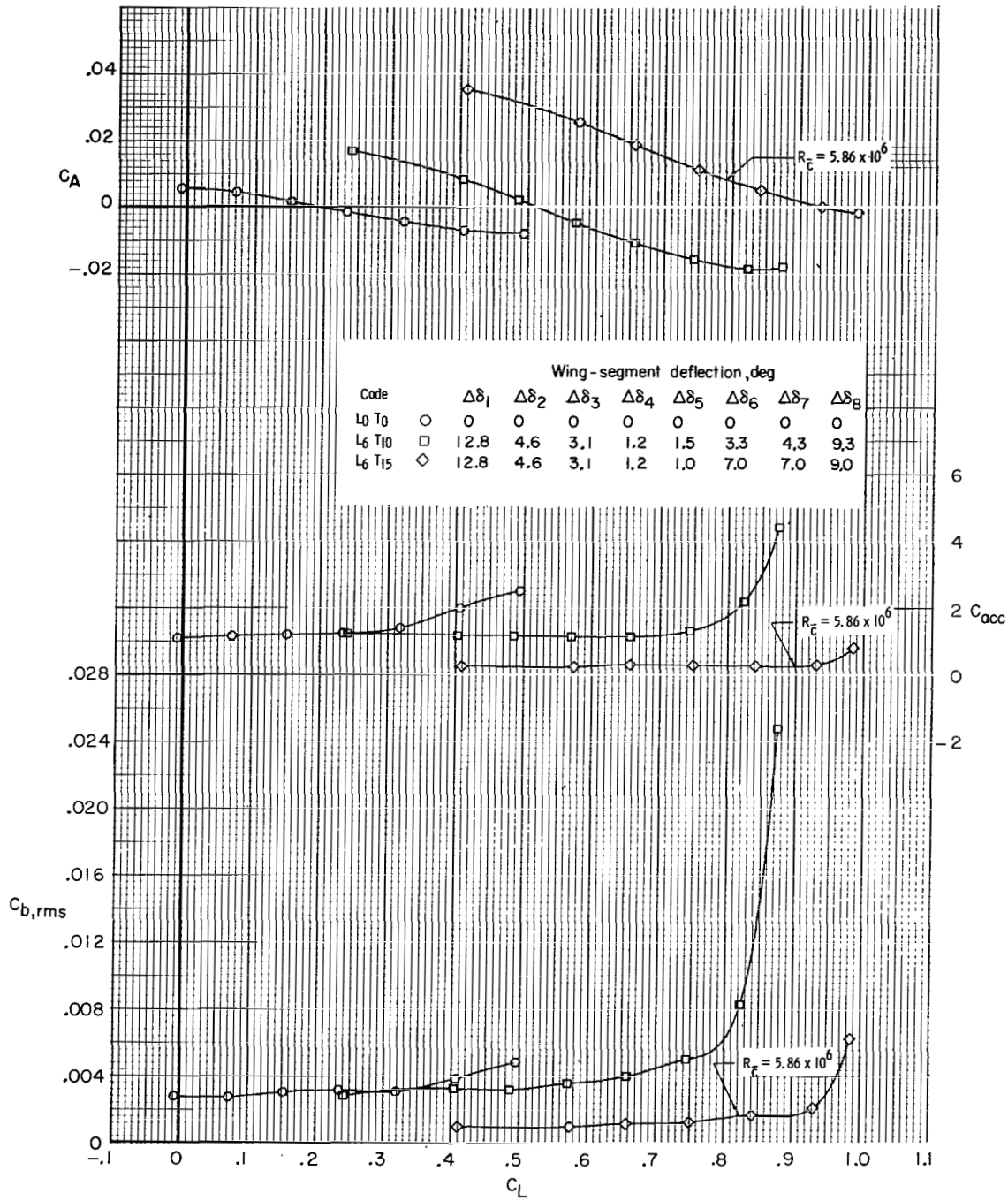

(b) M = 0.80; $R_{\bar{c}} = 7.4 \times 10^6$.

Figure 18.- Continued.

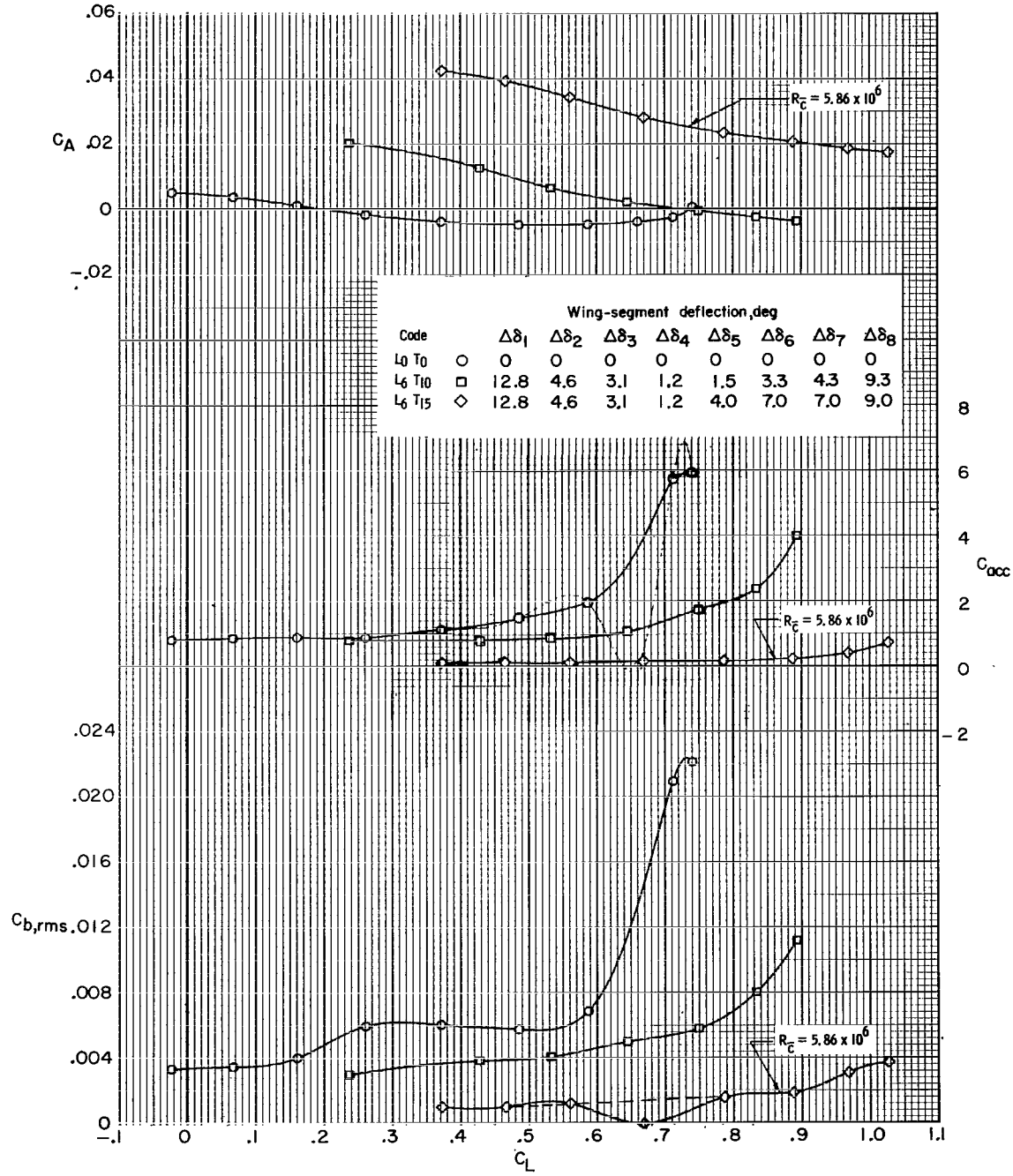

(c) M = 0.90; $R_{\bar{c}} = 7.6 \times 10^6$.

Figure 18.- Concluded.

"The aeronautical and space activities of the United States shall be conducted so as to contribute . . . to the expansion of human knowledge of phenomena in the atmosphere and space. The Administration shall provide for the widest practicable and appropriate dissemination of information concerning its activities and the results thereof."

—NATIONAL AERONAUTICS AND SPACE ACT OF 1958

NASA SCIENTIFIC AND TECHNICAL PUBLICATIONS

TECHNICAL REPORTS: Scientific and technical information considered important, complete, and a lasting contribution to existing knowledge.

TECHNICAL NOTES: Information less broad in scope but nevertheless of importance as a contribution to existing knowledge.

TECHNICAL MEMORANDUMS: Information receiving limited distribution because of preliminary data, security classification, or other reasons. Also includes conference proceedings with either limited or unlimited distribution.

CONTRACTOR REPORTS: Scientific and technical information generated under a NASA contract or grant and considered an important contribution to existing knowledge.

TECHNICAL TRANSLATIONS: Information published in a foreign language considered to merit NASA distribution in English.

SPECIAL PUBLICATIONS: Information derived from or of value to NASA activities. Publications include final reports of major projects, monographs, data compilations, handbooks, sourcebooks, and special bibliographies.

TECHNOLOGY UTILIZATION PUBLICATIONS: Information on technology used by NASA that may be of particular interest in commercial and other non-aerospace applications. Publications include Tech Briefs, Technology Utilization Reports and Technology Surveys.

Details on the availability of these publications may be obtained from:

SCIENTIFIC AND TECHNICAL INFORMATION OFFICE

NATIONAL AERONAUTICS AND SPACE ADMINISTRATION

Washington, D.C. 20546